# Analysis of Antenna and RF Front-End Topologies for Multi-Beam Systems

Salman Salman

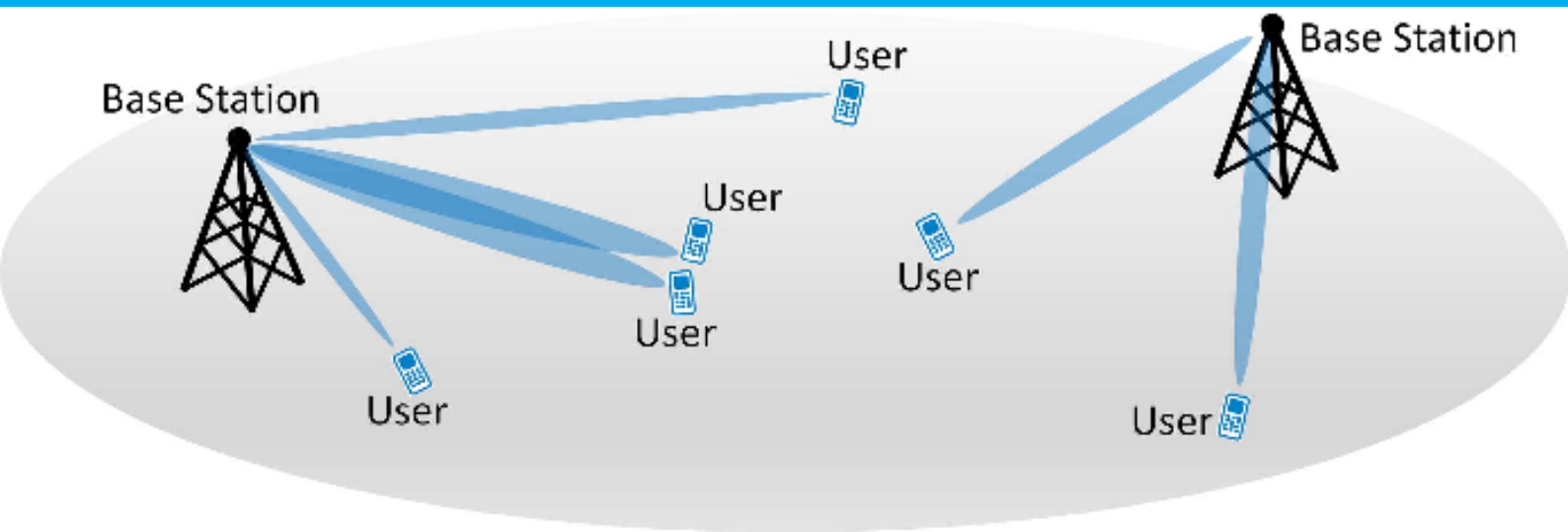


TU Delft

# Analysis of Antenna and RF Front-End Topologies for Multi-Beam Systems

by

Salman Salman

to obtain the degree of Master of Science
at the Delft University of Technology,
to be defended publicly on Monday August 27, 2018 at 13:00.

| | | |
|---|---|---|
| Student number: | 4593413 | |
| Project duration: | January 1, 2018 – August 27, 2018 | |
| Thesis committee: | Prof. dr. A. Yarovoy, | TU Delft, supervisor |
| | Dr. Oleg . A. Krasnov, | TU Delft |
| | Dr. Gerard Janssen, | TU Delft |
| | Dr. Jan Puskely, | TU Delft |

An electronic version of this thesis is available at `http://repository.tudelft.nl/`.

TU Delft

# Abstract

Traditionally, antenna design involves optimizing the design parameters such as gain, minimum sidelobe level, scan range, half power beamwidth, for a particular application. Since 5G systems are pushing the boundaries for cellular communications by introducing unique challenges such as multiple beam antennas, beamforming etc. in the field of antenna design. Although separate studies do exist on these challenges, the concept antenna synthesis using different disciplines is relatively new. This work presents a 5G simulation model using a recently proposed hybrid beamforming technique employing cosecant power flux equalization in elevation plane with digital beamforming in azimuth plane. Various beamforming algorithms in azimuth domain are investigated for concurrent users sharing same frequency spectrum and their impact on system performance such as signal to interference plus noise ratio (SINR) is statistically analyzed. Moreover, the impact of antenna sidelobe levels on system SINR performance is investigated in detail. The simulation results shows that the cosecant subarray hybrid beamforming performs better than traditional hybrid beamforming in terms of SINR for cell edge users. In addition to that, this work provides a unique perspective to system engineers for intuitively analyzing the impact of antenna system on communication link and to derive design requirements that would be crucial in the antenna system synthesis

# Contents

# 1 Introduction

Wireless communications have grown at a rapid pace in last three decades, evolving from simple voice communication to advanced cellular communication [75],[42],[50]. Almost every decade has brought a new generation of communication technology that has impacted human lives in unprecedented ways. It is predicted that by the year 2020, the number of mobile devices would exceed 100 billion due to this ever increasing demand and recently widespread concept of Internet of Things [1],[3]. Furthermore, due to great increase in connected devices along with data hungry and multimedia applications, the mobile data traffic is expected to surpass that by wired equipment by the end of 2018 [2], [64]. So the current fourth generation (4G) system which enables megabits per second (Mb/s) data transfer speeds, will not be able to cope up with gigabits per second requirements of the future. Therefore, academia and commercial wireless operators have started conducting research and surveys for the development of fifth generation (5G) system.

The capacity of a wireless link is determined by its bandwidth and spectral efficiency. It also depends on the cell size [84]. The cell sizes are getting smaller and the physical layer is already very close to Shannon capacity [20]. This implies that bandwidth needs to be explored for higher capacity. Currently most of the wireless communication systems operate in the frequency range of 300 MHz to 3 GHz band often referred as "sweet spot" [73], [14]. This band enjoys favourable propagation characteristics over long distances in diverse communication environments [10], [12]. Due to exploding data traffic and connectivity, its capacity to accommodate these requirements seems dubious [56]. The performance metrics for new generation wireless communication systems are extremely high data rates, low latency time on the scale of milliseconds, improved energy and spectral efficiency [31]. These revolutionary requirements which seemed impossible in previous generation of wireless communications require innovative measures. The technologies that are foreseen to enable 5G communications are massive MIMO (Multiple Input Multiple Output), new multiple access strategies, ultra-dense networking and many others [32], [45], [25]. However the realization of these technologies presents new challenges for the physical layer designers, especially to antenna and microwave engineers.

The Federal Communications Commission has allotted the frequency band of 27.5-28.35 GHz for 5G wireless communications. However unlike sub-millimetre wave frequencies, electromagnetic waves having wavelengths in the order of millimetres suffer severe free space propagation and shadowing losses which degrades the signal-to-interference plus noise ratio (SINR) [68]. In-order to overcome these shortcomings, directional antennas with high gain can be deployed at both transmitter and receiver ends. This can mitigate Doppler Effect, improve the overall link budget thus it is widely used in millimetre wave line of sight (LoS) communication [68], [66]. Although a single narrow beam provides high gain, it has a very limited spatial coverage area, making it not useable for multiuser spatially separated mobile communications. Moreover, for dynamic mobile users, a single directive static beam cannot establish a reliable communication link. Similarly for non-LoS communication, the beam needs to be steered (either electronically or mechanically) to find a substitute suitable link. The multibeam antennas at base station allow to generate concurrent independent beams directed towards the users providing high gain can be used to overcome the short comings of single directive beam. This idea serves as the foundation of massive MIMO which differs from conventional MIMO systems by deploying very large number of antenna elements that can be made to operate adaptively and coherently

[59], [46], [48].

Historically, multibeam antenna systems are quite large in size and expensive which limited there application to space communication and radar systems [88], [52]. However at millimetre wave spectrum, the smaller wavelengths allow to incorporate large number of antennas in the same physical aperture as compared to sub-6 GHz spectrum thus resulting in higher array gain and directivity. In addition to more number of users being served, the multibeam array enables to exploit the rich spatial channel information i.e. each spatially separated narrow beam is uncorrelated with the other thus resulting in higher reliability of link [26], [11], [40]. Due to these benefits, multibeam generation or beamforming is seen as the key enabling technology for 5G base stations and user terminals for high speed data transfers.

## 1.1. Motivation

Traditionally, antenna design involve optimizing the design parameters such as gain, sidelobe level, half power beamwidth etc. as shown in Figure 1.1(a) for a particular application. Since 5G systems pushes the boundaries for cellular communications, they introduce unique challenges in the field of antenna design. Therefore, antenna designing for 5G systems require to cater multiple disciplines and aspects as shown in Figure 1.1(b) to obtain high system capacity with limited resources.

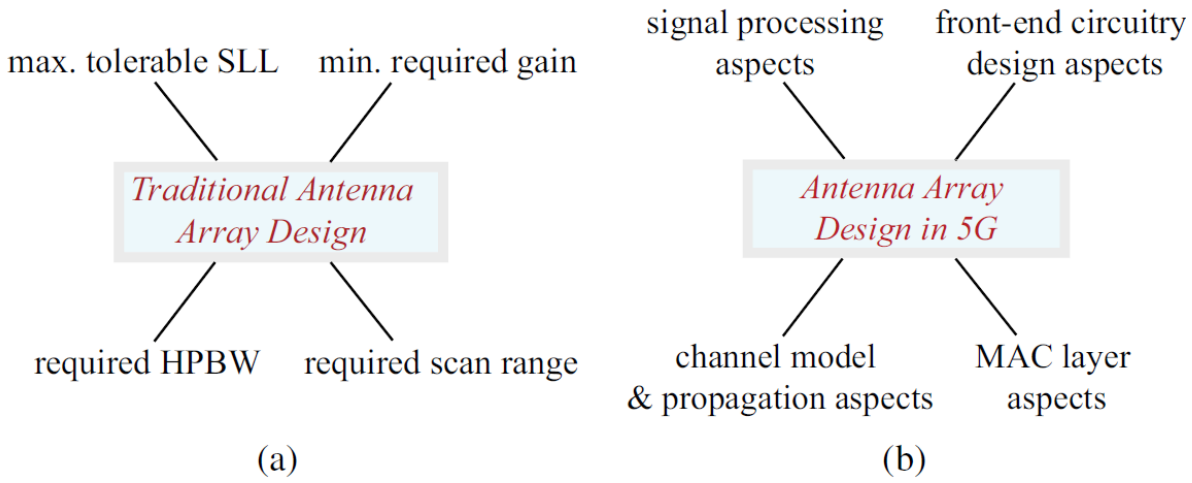


Figure 1.1: Antenna Design methodologies (a) Traditional approach (b) 5G perspective from [83]

Separate Studies are performed on the areas shown in Figure 1.1(b) (multiple beam antennas [51], beamforming algorithms [35], propagation models [74] etc.). However the concept antenna synthesis using different disciplines is relatively new. Some of the recent publication which links antenna array designing with other research domains is presented in Table 1.1. In these listed research domains, the signal processing aspect comprises of various beamforming algorithms such as linear, non-linear, narrowband, wideband, switched or adaptive beamforming. The issues such as power amplifier output and efficiency along with heat dissipation of the transceiver chain are covered in front end design aspect. The MAC layer aspect deals with designing efficient link between base station and users by optimizing medium access periods. In the end, channel modelling is related to the characterization of propagation environment between base station

Table 1.1: Recent publications on 5G antenna design combining different disciplines from [83]

| **Complementary Research domain** | **Reference #** |
|---|---|
| Signal processing & beamforming algorithms | [9],[10],[60],[55] |
| Front-end circuitry design & efficiency | [57],[76],[69],[15],[18],[17],[16] |
| MAC protocols | [27],[28],[29] |
| Channel modelling & propagation | [21],[22],[12],[86],[33],[13],[38],[43] |

and user under different conditions (Los, NLos etc.).

These examples indicate the importance of inter-disciplinary considerations in antenna design for 5G. Moreover, it also reflects that most of the current research work on 5G antenna system synthesis using multi-disciplines is done from signal processing perspective. Therefore, this provides the opportunity to explore and investigate issues like impact of inter user separation, multi-dimensional beamforming and antenna sidelobe levels on system performance.

## 1.2. Literature Review

As discussed earlier, Multiuser Massive MIMO systems are projected to play a vital role in 5G communication. The bandwidth requirements for 5G are expected to rise 100x times more than the current 4G systems. Traditional beamforming having one RF transceiver chain with single directive beam excludes the ability to communicate with multiple mobile users at the same time in same frequency domain. On the other hand, Digital beamforming (DBF) provides a very attractive alternative with infinite degree of freedom enabling to communicate with multiple users at the same time using a transceiver behind every antenna element. The signal processing algorithms provide means to mitigate inter and intra-cell interferences to achieve very high capacity. However, its high power consumption and cost requirements is a big concern for 5G application.

Active arrays with analog multiple beam forming, as developed and demonstrated at Ku-band in the 90's for space communications using MMIC technologies, have potential for line-of-sight communications and sensing.with frequency re-use [36]. Their applicability to high numbers of beams or for non-line-of-sight communications, with the complex time processing of signals required for multipath and MIMO, seems limited. Several multiuser MIMO downlink transmission signal processing techniques are discussed in [85]. The techniques compared are transmit zero forcing based on codebook feedback, Grid of Beam (GoB) approach, transmit zero forcing based on covariance matrix and beam steering on the basis of largest Eigen vector of downlink covariance matrix. The GoB method was implemented at RF level while the other techniques were implemented at baseband level shown in Figure 1.2. The results shows that using calibrated arrays, both the ZF methods perform better than GoB and Eigen beamforming with ZF with covariance matrix best among all.

In [23] the Massive MIMO digital beamforming implementation is presented using maximum ratio (MR) and Zero Forcing (ZF) combining and Minimum Mean Square Error (MMSE) techniques. The have shown that ZF suppresses inter-cell interference at the cost of decreasing array gain while MMSE provides a balance between amplifying signals and suppressing the interference. A similar analysis between conjugate beamforming (CB) also known as maximum ratio transmission (MRT) and ZF for digital beamforming is performed in [78]. They have proposed that in highly LOS environment, the ZF performs very close to CB. Additionally, [54] also provides the comparison of different digital beamforming techniques such as Matched Filtering (MF), Zero Forcing (ZF) and Minimum Mean Square Error (MMSE) from the receiver perspective. They evaluated the performance of beamforming algorithms for single input single output (SISO) and MIMO scenarios. It is concluded from their results that the MMSE performs better than ZF and MF for both SISO and MIMO with ZF closely following MMSE in MIMO system. In addition to that, MF performs better in case of SISO system. However due to very large number of antenna are being considered for mmWave 5G systems, the high power consumption of DBF (due to transceiver behind every antenna element and high speed A/D or D/A converters) makes hybrid beamforming a more attractive alternative for 5G systems.

The authors in [47] presents a comparison between two popular hybrid beamforming (HBF) techniques as shown in Figure 1.3. In the configuration shown in Figure 1.3(a), the transceiver is connected to all antenna elements such that the N data streams goes thru NM RF paths where M is the number of antenna elements. The analogue beamforming (ABF) is performed over NM paths and the digital beamforming is performed over N transceivers. This configuration provides high beamforming gain but has very high complexity. In the architecture shown in Figure 1.3(b), each transceiver is connected to M antenna elements instead of all antennas. The ABF is performed over M paths instead of NM. Although the beamforming gain of this arrangement is less than fully connected one, but its reduced complexity makes it more practical for base station deployment in current cellular systems. The paper [82] presents a comparison between fully digital zero-forcing beamforming and a fully connected hybrid beamforming. The authors assumed perfect channel state information (CSI) at the base station. They found out that if the number of RF chains is twice the number of

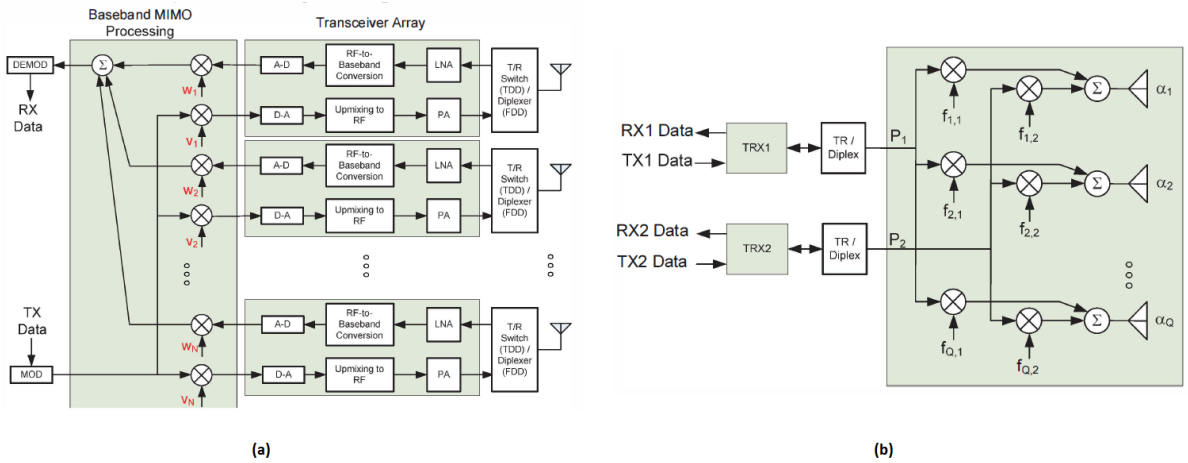


Figure 1.2: (a) Baseband MIMO architecture (b) RF MIMO architecture from [85]

data streams, hybrid beamforming performs similarly to digital beamforming. They concluded the paper by analyzing the impact of low resolution phase shifters on hybrid beamforming.

A detailed survey for mmWave beamforming techniques was conducted in [58]. Their report presents different requirements for indoor and outdoor mmWave beamforming. For indoor, adaptive beamforming, the codebook approach is preferred as it relies more on direction of arrival than on channel state information (CSI). Until now, analog beamforming is the mainstay for indoor mmWave communication. For outdoor mmW communication, they suggest hybrid beamforming instead of digital beamforming due to its lesser complexity and power consumption. Furthermore, the interest in digital beamforming as a possible contender for 5G systems is not completely over. There are recent researches which indicates the possibility of deploying digital beamforming for 5G systems. In [34] and [77] present an analytical method to evaluate the performance of digital beamforming for mmWave 5G system using low resolution ADCs. Their model shows that the quantization has the effect of saturation on maximum achievable SINR. However, low quantization levels have much less effect on high gain beamforming. These quantization levels are realizable with current state of the art ADCs. These results indicate that for multi-user/multi-stream cases, fully digital beamforming with low quantization provide comparable performance to that of analog or hybrid beamforming with similar or even lower power consumption. In [4] the power consumption comparison between analog, digital and hybrid beamforming is performed from the receiver perspective. The authors have shown that analogue beamforming performs better in low SNR conditions but have only single RF chain that implies to limited degree of freedom. Moreover the popular belief that digital beamforming is always less power efficient than hybrid is not universally correct. Rather it depends on the number quantization bits in digital beamforming, on the components used in hybrid beamforming and on the number of parallel users in the system. They have also presented an example where digital beamforming with low quantization levels has better energy efficiency than hybrid beamforming for similar spectral efficiency. Furthermore they also concluded that a similar power efficiency argument can be made for downlink digital beamforming with low quantization levels in comparison to hybrid beamforming.

The literature discussed up-till now mainly focuses on different beamforming architectures and signal processing methods of multiple beam generation for 5G systems. Recently, combining channel propagation aspects system performance metrics for multibeam antenna array synthesis has gained attention. An impedance matrix model approach to derive base station antenna requirement for the given beamforming algorithm and channel model is presented in [13]. The impact of base station antenna array on system performance metrics (such as SINR and capacity) is studied in [21], [22], [38] respectively. The research in [86] deal with the effect of inter-user angular spacing on interference reduction has been presented. In [43], it has been argued that conventional antenna designing criteria's such as sidelobe level and directivity cannot fully represent the channel capacity for 5G system and even normally undesired grating lobes can be used for increasing channel gain. It has been shown in [33] that directing a single beam towards the strongest multipath outperforms directing multiple beams (with reduced EIRP) in terms of carrier to interference plus noise ratio

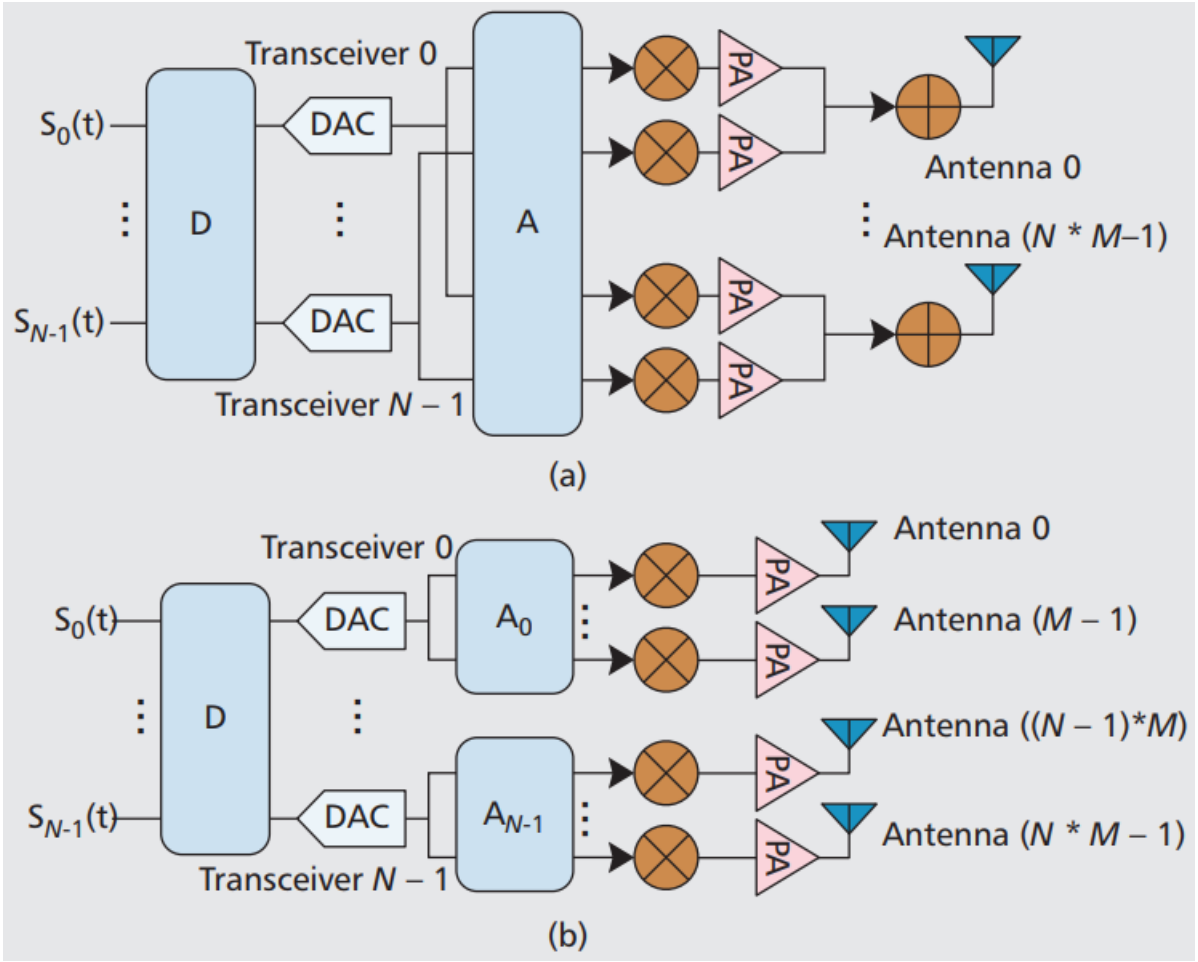


Figure 1.3: Hybrid Beamforming Architectures from [47]

unless there are more than one equally strong multipaths.

## 1.3. Aim of Research

The literature review shows that a lot of focus has been on improving the overall system performance by introducing new or modifying the beamforming algorithms. Traditionally, antenna synthesis falls in the analog domain while the parameters use to gauge the system performance (such as SINR or BER) are describe in digital domain; thus are dealt by system engineers as two distinct entities. This makes it harder for the system designer to intuitively see the impact of antenna on system performance. Some recent studies as presented earlier in section 1.2 have shown the potential of realizing the 5G multibeam generation antenna systems using inter-disciplinary approach. However, these studies are limited to system performance evaluation with respect to antenna array elements periodicity, beamforming architectures and improvement in certain beamforming algorithms.

Therefore, the main goal of this thesis is to reduce the gap between antenna design, signal processing and channel modelling for 5G systems. This would enable to derive the antenna system design parameters that are optimized for a certain user requirement encompassing signal processing and channel propagation effects. The second goal of this thesis is to analyze the impact of recently introduced concept of cosecant radiation pattern in the elevation plane [69] and digital beamforming in the azimuth plane for 5G base station antenna arrays. The objective is to study the effect of several digital beamforming techniques in azimuth domain (such as adaptive beamforming, constant sidelobe levels, zerofrocing (ZF), minimum-mean-square-error (MMSE)) with cosecant radiation pattern in the elevation plane on system performance metrics. More-

over, performance of Grid of Beam (GoB) approach with cosecant radiation beamforming technique is also investigated. In addition to that, a statistical performance comparison between cosecant radiation beamforming (with its all variants) and traditional hybrid beamforming (with orthogonal matching pursuit algorithm) is performed using signal to interference plus noise ratio (SINR) and bit error rate (BER) via Monte Carlo simulations.

The analysis is performed by considering only one dominant path (LoS or NLoS) between base station and randomly distributed user equipment. Each user has a single omnidirectional antenna and is served with a separate beam. The effect of mutual coupling between antenna elements at base station is not taken into account and the power per beam is limited. The channel state information and the user position is known at the base station.

## 1.4. Outline

The remainder of the thesis is organized as follows:

- Chapter 2 presents the overview of various beamforming architectures. The chapters begins with the description of some antenna basics and terminologies used in antenna designing. Thereafter, analog, digital and hybrid beamforming schemes along with their advantages and disadvantages are discussed. In the end, hybrid beamforming with a cosecant shaped beam in elevation and digital beamforming in azimuth is presented.3
- Chapter 3 describes the signal model Multiuser MIMO system used for creating the simulation environment. The assumptions for the channel model formation based on Saleh-Vanezula model is also presented. The MIMO digital beamforming algorithms from uplink and downlink perspective are described in detail. Afterwards, the orthogonal matching pursuit algorithm for fully connected hybrid beamforming is derived in detail.
- Chapter 4 shows the analysis that performed using the system model presented in the previous chapter. The parameters used in the development of simulation environment are listed with their corresponding values. Thereafter the results obtained by performing Monte Carlo simulation for various simulation scenarios are shown.
- Chapter 5 summarizes the entire thesis and discusses the conclusion drawn from the results presented in chapter 4. This chapter concludes with recommendation for the future work.

# 2

# Beamforming Architectures

The frequency spectrum sub-3 GHz has become very crowded due to ever increasing demand for mobile devices and data communication [67]. Therefore the existing cellular systems have a very narrow frequency band of operation (around 600 MHz currently in use). In order to cope up with the existing high demands of spectral efficiency (in bits/second/Hertz/cell), the present 4G systems are employing advance technologies such as multiuser diversity, OFDM, link adaption, MIMO, hybrid automatic repeat request (HARQ) and turbo codes. Since 5G communication systems aims for unprecedented high data rates, it is quite evident that the current frequency spectrum for cellular communication won't be able to fullfill that demand. One of the solution that has been proposed that is to utilize the un-used spectrum available in range of 3-300 GHz called as millimetre wave band (wavelength lies in the range of 1 mm-100 mm) as shown in Figure 2.1.

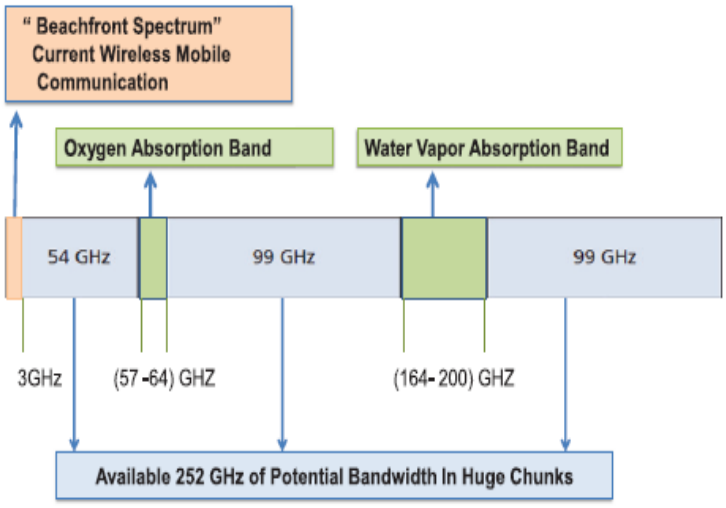


Figure 2.1: Millimetre-wave band spectrum from [7]

So a potential 252 GHz of bandwidth is available which also suitable for mobile communication. The attenuation to RF signal occurs due to oxygen molecules of up to 15 dB/km and because of water molecules of about tens of dBs/km is observed in the frequency range of 57-64 GHz and 164-200 GHz respectively. Since this high attenuation limits the communication range of a system, these frequency bands are excluded for cellular applications. The major difference between microwave and millimetre wave communication is that the millimetre wave suffers high losses while propagating through obstacle like wall which also causes blockages. According to the experimental results presented in [72] (at 28 GHz and 38 GHz in temporal resolution of 2.3 ns), the path loss exponent value of 2 was recommended for Line of Sight (LoS) propagation and 4 for non-line of sight (NLoS) propagation. The atmospheric attenuation for the range of 200 meters is mentioned to be 0.012 dB@28GHz, 0.016 dB@38 GHz, 4 dB@60 GHz and 0.060 dB @73 GHz in [71]. The rain attenuation for the same frequencies over the range of 200 meters is given as 1.2 dB @28 GHz and 2 dB @73 GHz in [70]

respectively.

As the frequency goes up or wavelength goes down, the antenna size decreases. Therefore, it is possible to pack more element on similar antenna arrays size as of for the microwave arrays. This allows making narrow focused beams towards the intended receiver. Since, a typical 5G millimetre wave environment will be based on a 100 meters to 300 meters cell typically comprised of highly dense urban streets. This requires compensating the atmospheric losses, rain attenuation penetration and low efficiency of power amplifiers. Creating high gain narrow beams with large antenna arrays at base station are envisioned as way to overcome above mentioned short coming for 5G systems.

## 2.1. Antenna Basics

In order to fully understand different beamforming techniques, essential antenna parameters needs to be defined. The most critical parameters that describes antenna are gain, radiation pattern, efficiency and polarization. The antenna radiation pattern shows the radiated field pattern in space coordinate system. The radiation pattern gives the field strength and directivity of the radiated electromagnetic signal. The radiation pattern can be created by plotting the received electric field at constant radius with respect to azimuth or elevation angle. This pattern is termed as amplitude filed pattern [63]. A similar kind of plot can be constructed for received power density would be called as power pattern. The Figure 2.2 shows a typical antenna radiation pattern in linear and log scale respectively. The radiation pattern as shown in Figure 2.2 is divided into several parts such as main lobe, side lobes and back lobes. The main lobe contains the maximum energy radiated from the antenna pointing towards the receiver. Side lobes are any other radiation lobes except the main lobe and a back lobe is a side lobe which points in the opposite direction of the intended user. The radiation pattern are generally seen in logarithmic scale for the ease of view. In order to specify the radiated energy in the direction of intended users, a parameter called as beam width is defined. The beamwidth of a radiation pattern is describe as the angular separation between two same points on the either side of the maxima of main lobe. Generally, the beam width is calculated is called as half power beamwidth as it's the difference of angles at the opposite points of main lobe where the radiated power is half of its maximum value.

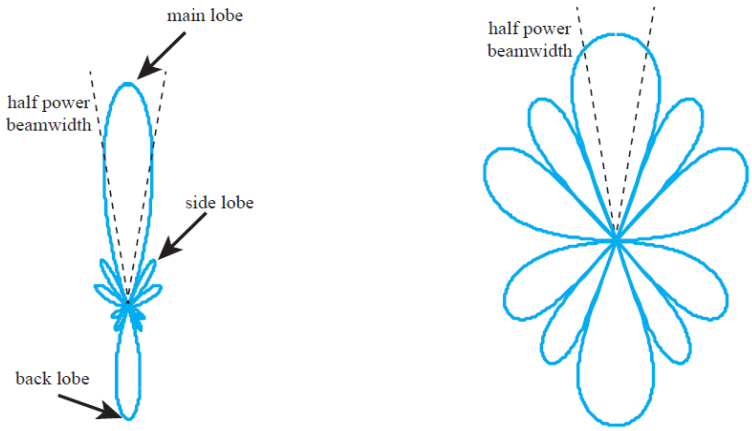


(a) Linear scale (b) Log scale

Figure 2.2: Antenna radiation pattern in polar domain

The directivity of the antenna is defined as the ratio between the radiation intensity in the maximum direction with respect to the radiation intensity of an isotropic radiator. The isotropic radiator is a radiator which radiates equally in all direction.

$$D(\theta,\phi) = \frac{U(\theta,\phi)}{U_0} = \frac{4\pi U(\theta,\phi)}{P_{rad}} \tag{2.1}$$

$$D_{max}(\theta,\phi) = \frac{U_{max}}{U_0} = \frac{4\pi U_{max}}{P_{rad}} \tag{2.2}$$

Where $U(\theta,\phi)$ is the radiation intensity of an antenna which is non-isotropic at certain solid angle (W/unit solid angle), $U_{max}$ is the maximum radiation intensity of this antenna (W/unit solid angle), $U_0$ is the radiation intensity of ideal isotropic antenna (W/unit solid angle) and $P_{rad}$ is the total power radiated (W).

The directivity of an antenna describe how well antenna can radiate in a particular direction. The maximum value of directivity is usually greater than unity since the directivity of anisotropic radiator is always unity. There exist a trade-off between high directivity and large beamwidth. higher the directivity lower would be the beamwidth and vice versa. In addition to that, there are also some internal losses in the antenna which dissipates some energy. These losses comprises of conductive and dielectric losses. The radiation efficiency is described as

$$\eta_{rad} = \frac{P_{rad}}{P_{in}} \tag{2.3}$$

By taking into account the efficiency of the antenna, the antenna gain can be described as

$$G(\theta,\phi) = \eta_{rad} D(\theta,\phi) \tag{2.4}$$

## 2.2. MIMO

Various diversity techniques are used to make the radio communication link more robust and reliable. These methods comprises of frequency diversity (spread spectrum, OFDM etc), time diversity (assigning separate time slots and channel coding techniques), and spatial diversity (space division multiple access). The spatial diversity can be achieve using multiple antennas either at transmitter or at receiver. Therefore multiple antenna systems are called as Multiple Input, Multiple Output (MIMO) system. In addition to that, multiple antennas can also be deployed to increase the system capacity by creating multiple channel paths that increases the amount of data transfer.

### 2.2.1. Single Antenna Systems

The traditional communication system comprises of one antenna at transmitter and one at the receiver as shown in Figure 3. Therefore these systems are called as single input single output (SISO) systems


Figure 2.3: Conventional SISO system

The shannon capacity theorem implies that the capacity of the channel C depends on the bandwidth B and signal to noise ratio S/N. The capacity for the SISO system can be given as:

$$C = B\log(1+\frac{S}{N}) \tag{2.5}$$

### 2.2.2. Multi-Antenna Systems

A typical MIMO system comprises of m transmit antenna and n receive antennas as shown in Figure 2.4. This creates multiple propagation paths using the same channel. Therefore, the receiver not only gets the direct signal component but also the indirect components coming from other antennas. For time independent narrow band channel matrix H, h11 represents the direct transmission path from antenna 1 to 1 as shown in Figure 2.4. While the cross transmission path h21 represents an indirect transmission path from antenna 1 to

2. So the number of independent data stream will always be less than or equal to the number of antennas in case of asymmetrical system. For instance, a 4x4 systems could have 4 or fewer transmit streams while a 3x2 system could have 2 or fewer data streams. The increase in the system capacity C for a MIMO system using M independent data streams can be given as :

$$C = M.B\log(1+\frac{S}{N}) \tag{2.6}$$

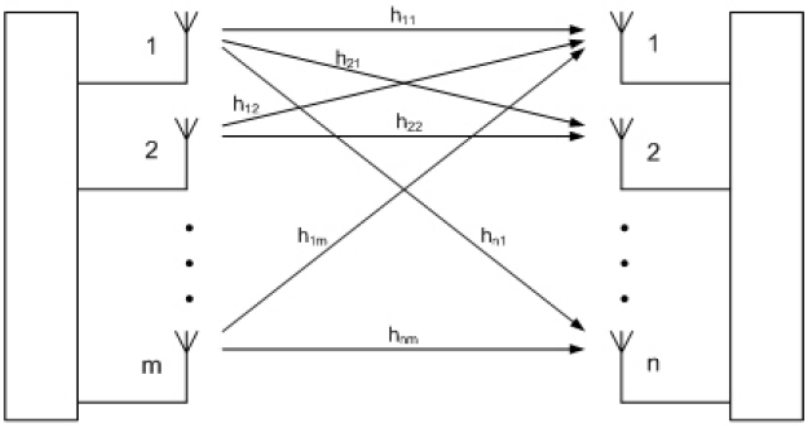


Figure 2.4: MIMO system diagram

#### 2.2.2.1. SU-MIMO

The MIMO system deployed to increase the data rate or robustness of a system for single, is called as single user MIMO (SU-MIMO) as shown in Figure 2.5.

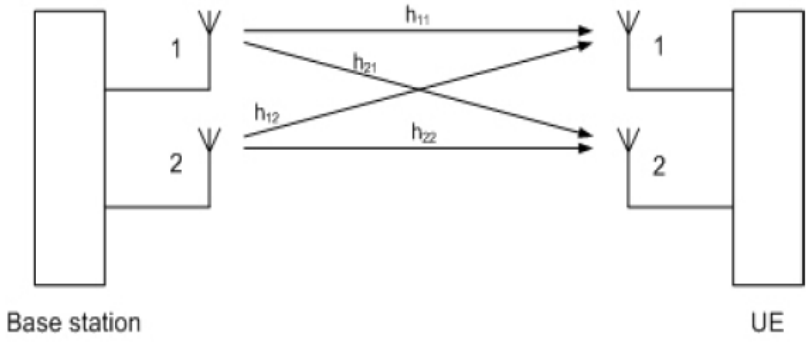


Figure 2.5: Single User MIMO system-SU-MIMO

#### 2.2.2.2. MU-MIMO

The systems where there are multiple users and a single transmitter with multiple antennas is called as Multiuser-MIMO system (MU-MIMO) as shown in Figure 2.6. This scenario is particularly useful in cellular communication where base station having an antenna array can communicate with multiple users in a cell.

#### 2.2.2.3. Massive MIMO

Massive MIMO is a derivative of MU-MIMO in which the number of base station (BS) antenna are quite large. This creates more number of communication paths between BS and the user thus creating favourable

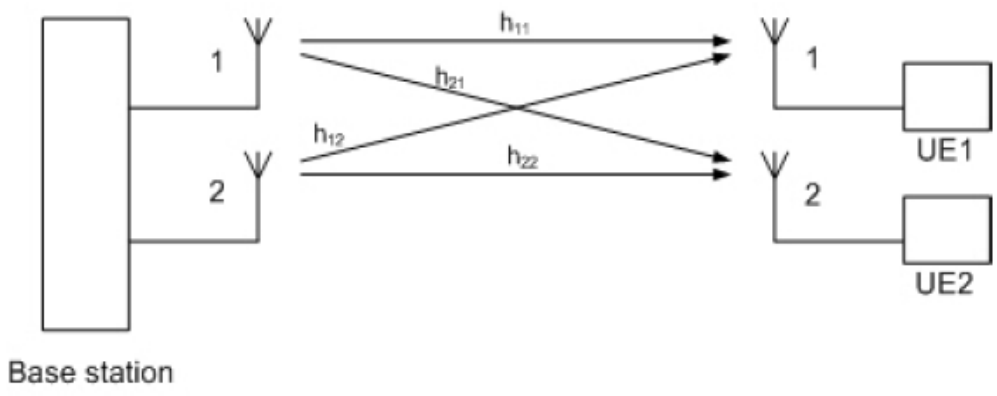


Figure 2.6: Multiuser MIMO-MU-MIMO

propagation conditions. The large number of antennas at base station allow the use of simpler linear signal processing techniques as the becomes optimal [63]. This also enables to take advantage of multiplexing gain and array gain via simple linear processing. Moreover, by increasing the number of antennas at BS; higher throughput for the system is also achieved. Though the massive MIMO is useful at centimetre wave frequencies also but it is crucial for millimetre wave frequencies. Since the high propagation losses for millimetre wave frequencies requires large array gains in order to achieve sufficient signal to interference plus noise ratio (SINR) at the receiver.

However, large number of antennas in massive MIMO creates new challenges such as large number of RF chains for each antenna element which would then increase the implementation cost and energy consumption of the entire system. Therefore, different beamforming architectures are used to generate multiple beams in massive MIMO each with having its own trade-off between performance and complexity.

## 2.3. Beamforming Fundamentals

In high directivity systems, the antenna beam is needed to be steered to cover a large area for communication. The electrical beam steering is realized by using antenna arrays with multiple antenna elements having control over the signal coming to each of them as shown in Figure 2.7. The beam steering to a certain angle $\theta$ away from the centre can be achieved by delaying the signal to individual elements in such a manner that they add constructively in the intended direction $\theta$. Let's assume the signal in the nth element is delayed by (n-1)$\tau$. with antenna element spacing d, the signal transmitted by all the elements would have different delays among them. The free space delay between any nth antenna element signal and the last antenna element ($N^{th}$) signal is given as

$$t_n = \frac{(N-n)d\sin\theta}{c} = (N-n)\,t_0 \tag{2.7}$$

$$t_0 = \frac{d\sin\theta}{c} \tag{2.8}$$

The electric field vector (E) from a nth antenna at the wavefront is

$$E_n = e^{j\omega_0[t-t_n-(n-1)\tau]} \tag{2.9}$$

$$E_n = e^{j\omega_0[t-(N-n)t_0-(n-1)\tau]} \tag{2.10}$$

$$E_n = e^{j\omega_0[t-(N-n)t_0]}e^{j\omega_0[(n-1)\tau]} \tag{2.11}$$

Summing the E-field vector for all the N antenna elements, we have

$$E_{array} = \sum_{n=1}^{N} E_n \tag{2.12}$$

$$E_{array} = e^{j\omega_0[t-(N-1)t_0]} \sum_{n=1}^{N} e^{j\omega_0[(n-1)(t_0-\tau)]} \tag{2.13}$$

$$E_{array} = e^{j\omega_0[t-(N-1)t_0]} \sum_{n=1}^{N-1} e^{j\omega_0[n(t_0-\tau)]} \tag{2.14}$$

$$E_{array} = e^{j\omega_0[t-(N-1)t_0]} e^{j\omega_0 \frac{(N-1)(t_0-\tau)}{2}} \frac{\sin[\frac{1}{2}N\omega_0(t_0-\tau)]}{\sin[\frac{1}{2}\omega_0(t_0-\tau)]} \tag{2.15}$$

Therefore the magnitude of the summed E-field vector is

$$\left|E_{array}\right| = \left| \frac{\sin[\frac{1}{2}N\omega_0(t_0-\tau)]}{\sin[\frac{1}{2}\omega_0(t_0-\tau)]} \right| \tag{2.16}$$

The magnitude of the summed E-filed can be maximized for an angle $\theta$ by setting $t$=$t_0$,

$$\tau_{opt} = t_0 = \frac{d\sin\theta}{c} \tag{2.17}$$

Using this condition, the E-field obtained via summing is N times larger than the E-field of a single antenna element. Since power is proportional to the square of electric field, therefore the radiation intensity of an antenna array would be $N^2$ times greater than of single antenna. This also implies that the Effective Isotropic Radiated Power (EIRP) of an antenna array is $N^2$ times greater than of single antenna. The E-field for spatial angle $\theta$ using a fixed delay $\tau$ is given as ,

$$\left|E_{array}\right| = \left| \frac{\sin[\frac{1}{2}N\omega_0(\frac{d\sin\theta}{c}-\tau)]}{\sin[\frac{1}{2}\omega_0(\frac{d\sin\theta}{c}-\tau)]} \right| \tag{2.18}$$

The maximum directivity of an N-element is given as

$$D_{array,max} = \frac{U_{max}}{U_0} = \frac{E_{max}^2}{E_0^2} = \frac{\frac{1}{N}N^2}{1} = N \tag{2.19}$$

The factor of $\frac{1}{N}$ in the numerator of $D_{array,max}$ is because that each antenna element receives the $\frac{1}{N^{th}}$ of the total input power. Therefore, the maximum directivity of N element antenna array is also N times greater than the single antenna element.

The programmable time delays at RF frequencies are relatively difficult to implement in a compact form [63]. In addition to that, for narrow band signal; time delays can be approximated by phase shifts. Therefore, the beamforming and steering is achieved by using N element phased array antenna as shown in Figure 2.8. The signal in applied to each element in phased array antenna are progressively phase shifted. The signal to $n^{th}$ element in an array has a phase shift of $(n-1)\phi$. The E-field vector from the nth antenna is given as

$$E_n = e^{j\omega_0[t-t_n-(n-1)\frac{\phi}{\omega_0}]} \tag{2.20}$$

$$E_n = e^{j\omega_0[t-(N-1)t_0]} e^{j\omega_0[(n-1)(t_0-\frac{\phi}{\omega_0})]} \tag{2.21}$$

The sum for all the E-fields of the array is given as,

$$E_{array} = e^{j\omega_0[t-(N-1)t_0]} e^{j\omega_0[\frac{(N-1)(t_0-\frac{\phi}{\omega_0})}{2}]} \frac{\sin[\frac{1}{2}N(\omega_0 t_0-\phi)]}{\sin[\frac{1}{2}(\omega_0 t_0-\phi)]} \tag{2.22}$$

Similarly, the magnitude of the E-field vector for an array is given as

$$\left|E_{array}\right| = \left| \frac{\sin[\frac{1}{2}N(\omega_0 t_0-\phi)]}{\sin[\frac{1}{2}(\omega_0 t_0-\phi)]} \right| \tag{2.23}$$

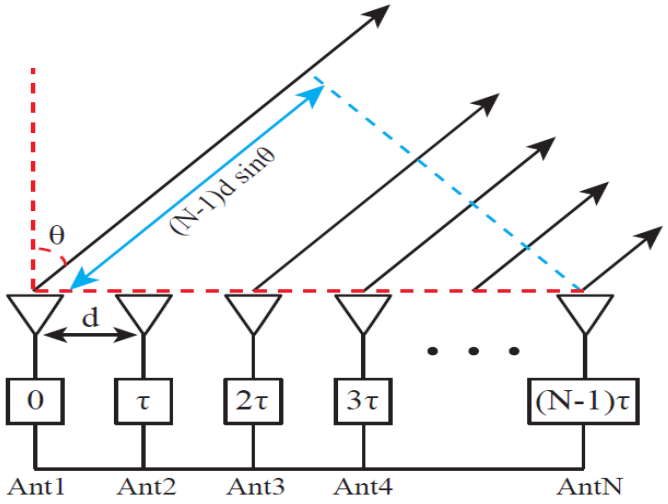


Figure 2.7: N-element timed Antenna array

The maximum magnitude for the summed E-field can be obtained for an angle $\theta$ by setting $\omega_0 t_0 = \phi$

$$\phi_{opt} = \omega t_0 = \frac{\omega_0 d \sin\theta}{c} \tag{2.24}$$

The E-field radiation pattern at angle $\theta$ for a fixed phase shift of $\phi$ is given as

$$\left|E_{array}(\theta)\right| = \left| \frac{\sin\left[\frac{1}{2}N(\omega_0 \frac{d\sin\theta}{c} - \phi)\right]}{\sin\left[\frac{1}{2}(\omega_0 \frac{d\sin\theta}{c} - \phi)\right]} \right| \tag{2.25}$$

The antenna radiation pattern is also effected by the inter-element spacing of the antenna array “d”. when the spacing exceeds by half wavelength, multiple radiation lobe with similar magnitude as of main lobe appears in the radiation pattern. These un-intended radiation lobes are called as grating lobes. These grating lobes are undesired as the transmits energy in un-wanted direction which results in loss of signal but also it can cause interference signal of another users.

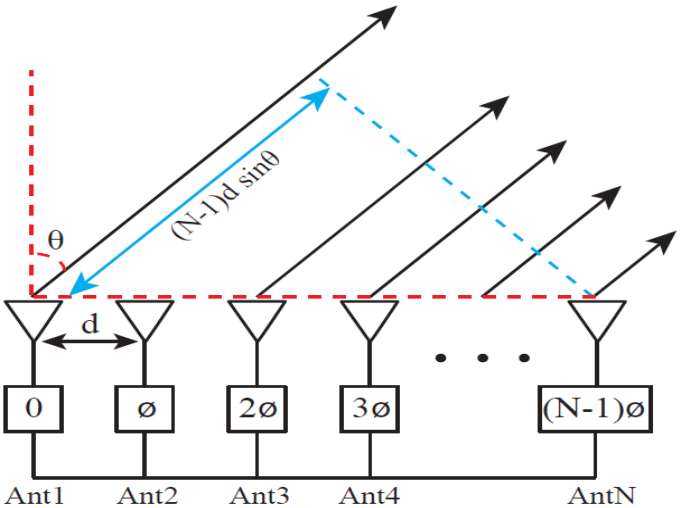


Figure 2.8: N element Phased Antenna Array

## 2.4. Beamforming Architectures

The beam formation in the desired direction can be achieved via multiple ways depending on where the phase shifts takes place in the signal path. The beamforming architecture can be broadly divided into three domains: Analog Beamforming, Digital Beamforming and Hybrid beamforming. The analog beamforming can be performed via phase shifting at RF or LO level. The digital beamforming is performed in baseband (BB) domain. The hybrid architectures divides the beamforming process in analog and digital domain.

### 2.4.1. Analog Beamforming

#### 2.4.1.1. RF Phase shifting

The most popular and widely used beamforming architecture is RF phase shifting network. A typical passive RF phase shifting network is shown in Figure 2.9(a) consists of uniform linear array (ULA) of M elements with inter-element separation of d and N RF channels. The transceiver for each data stream is connected to all elements of an array via switch or duplexer and phase shifter to control the magnitude and phase of each beam. Since each antenna element is connected to all "N" RF chains via phase shifter, thus total amount of phase shifter require are the product of number of beams and the antenna elements i.e. N x M [5].

Let's assume phase shift between mth antenna element and nth phase shifter as $\phi_{mn}$, where m=1,…., M and N=1,…. N. To direct the beam at angle $\theta_n$ which is off broad side for wavelength of $\lambda_0$, the required phase shift for the corresponding elements would be

$$\phi_{nm} - \phi_{n(m-1)} = \frac{2\pi d \sin\theta_n}{\lambda_0}, \qquad m = 2, ..., M. \tag{2.26}$$

As the inter-element spacing "d" increases, the beam gets narrower at the cost of scanning range. Because as the inter-element distance increases, the grating lobe appears in the radiation patterns which limits the scanning range. In order to avoid the grating lobes the inter-element distance "d" must fulfills

$$\frac{\lambda_0}{d} > 1 + max|\sin\theta_n|, \qquad n = 1, ..., N. \tag{2.27}$$

The RF phase shifting can also be achieved using active phase shifter instead of passive phase shifters as shown in Figure 2.9(b). The RF phase shifter are positioned between low noise amplifier (LNA), power amplifier (PA) and mixers. This type of system architecture improves receiver sensitivity, noise figure and also allows to generate high power levels. The efficiency of active RF phase shifting networks is better as compared to passive as the number of beams increases.

#### 2.4.1.2. LO Phase shifting

Despite the ease of implementation, RF phase shifting network has several disadvantages such as poor isolation, amplitude variation due to increase temperature which results in the degradation of beam accuracy and radiation pattern. In addition to that, the manufacturing of precise phase shifter at higher frequencies particularly at millimetre wave is quite challenging. Moreover, due to wire bonding length for connection at high frequency with switches and power amplifiers also induces large insertion losses.

In order to avoid these problems related to high frequency, phase shifting is being proposed at Intermediate Frequency (IF) [61] or even at baseband (BB) [6]. This enables the user of low cost components at lower frequencies in addition to reducing insertion losses. However, implementation of a phase shifter or a time delay circuit at lower frequency would require longer delay lines. Therefore rather than using a phase shifting network or a time delay circuit, virtual phase shift can be obtained at local oscillator (LO) by modifying its phase [49]. As the system architecture for LO phase shifting network is shown in Figure 2.10, the beam direction can be modified by applying phase shifts at LO. So, for M number of elements generating N beams, in total N x M mixers along with N distribution circuits would be required. The phase control circuits can be realized by high frequency clock divided [44], variable gain amplifier with phase rotators [53] or digitally via direct digital synthesis [30] to achieve fine beams with high precision.

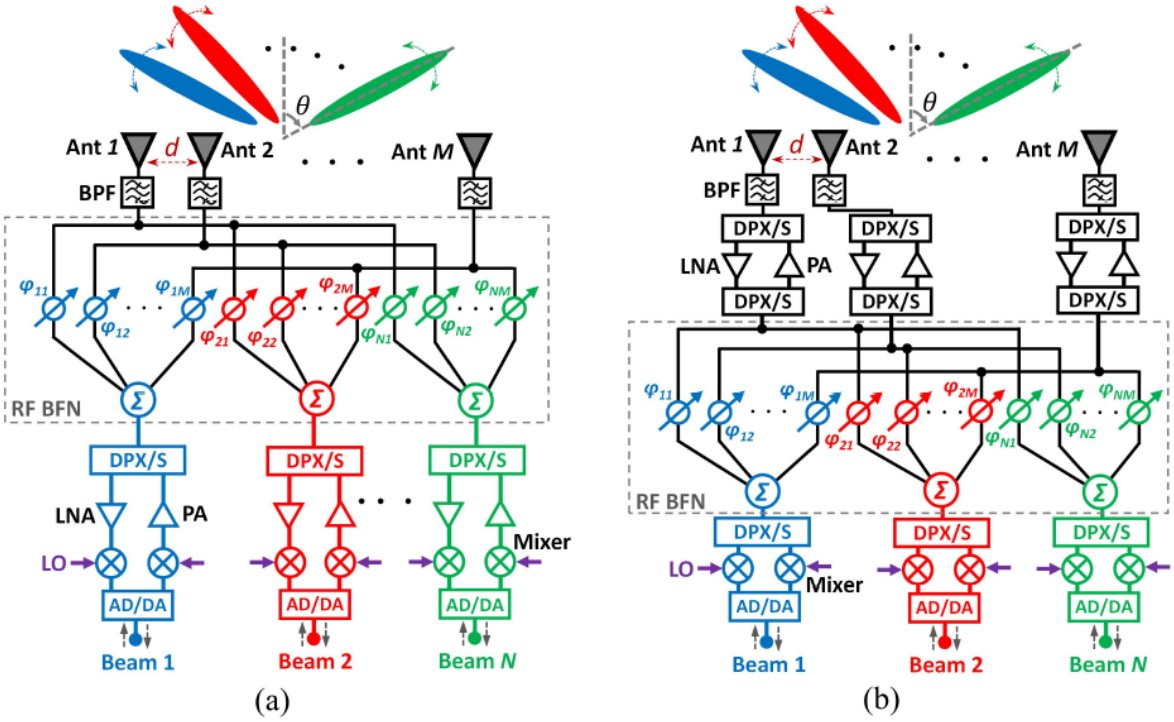


Figure 2.9: System Architecture for RF Phase Shifting Network from [51] (a) Passive (b) Active

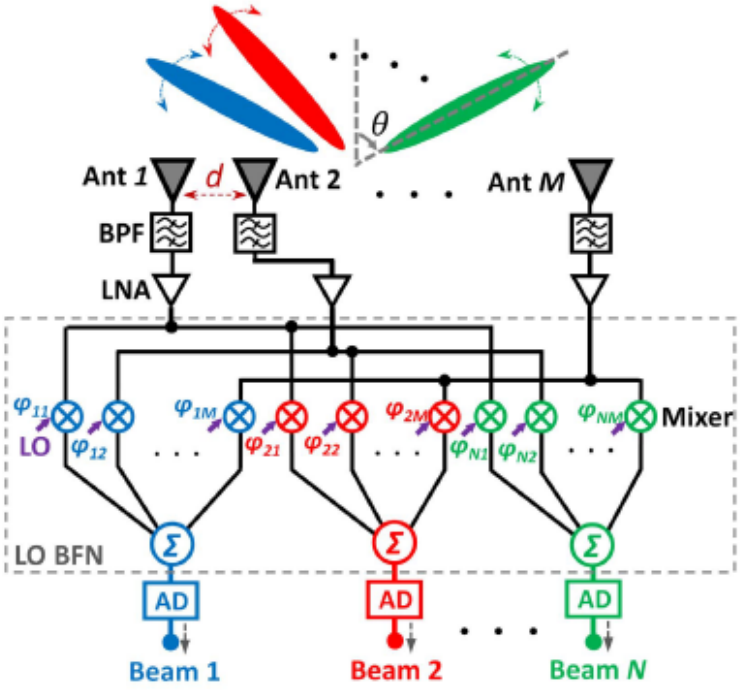


Figure 2.10: System Architecture for LO phase shifting from [51]

### 2.4.2. Digital Beamforming

The digital beamforming provides a more versatile and flexible approach to generate multiple independently controlled beams as compared to analog phase shifting techniques such as RF phase shifting and LO phase shifting. It also provide robustness against the failure of one or more antenna elements. The system architecture of M element ULA capable of generating N beams using digital beamforming is shown in Figure 2.11. There is a transceiver consists of power amplifier, low noise amplifier, mixer, analog to digital converter (A/D), digital to analog converter (D/A) behind each element. However unlike analog techniques, there are no phase shifters and attenuators.

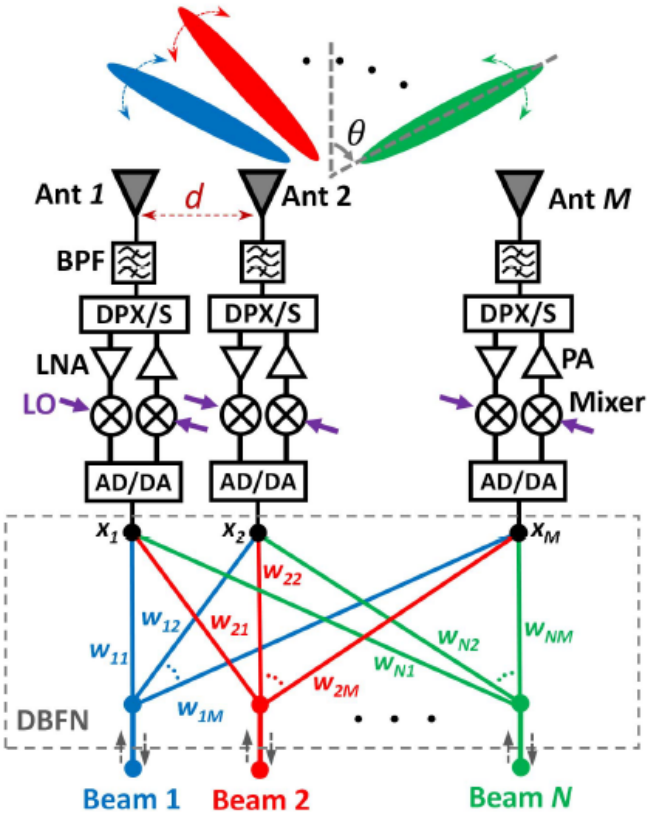


Figure 2.11: System Architecture for Digital Beamforming from [51]

The received RF signal from ULA is filtered, amplified and down converted and then transferred into digital domain via A/D. The signal can be represented as

$$X = [x_1 x_2, x_3, ..., x_M], \qquad m = 1, ..., M \tag{2.28}$$

Where $x_M$ is the complex BB signal from the $m^{th}$ antenna element. This signal contains both the in-phase (I) and quadrature (Q) components. A weighting matrix in the digital domain can be applied to the received BB samples defined as

$$W = \begin{bmatrix} W_1 \\ \cdot \\ \cdot \\ W_N \end{bmatrix} = \begin{bmatrix} W_{11} & W_{1M} \\ \cdot & \\ & \cdot \\ W_{N1} & W_{NM} \end{bmatrix} \tag{2.29}$$

Where $W_{nm} = a_{nm} e^{j\phi_{nm}}$ (m=1,..M and n=1,..N) is the complex weight for the nth beam coming from mth element. The coefficient $a_{nm}$ controls the amplitude tapering and $\phi_{nm}$ determines the phase delay for each antenna element. These values can be changed with respect to different frequencies. The output of the nth beam after applying weighting matrix would look like:

$$Y_n(\theta) = W_n^H X \tag{2.30}$$

Where H denotes the hermitian transpose of the weighting matrix. If the signal power is taken out of the equation, then the weighting vector for the nth beam towards $\theta_n = \arcsin(\frac{2n}{M-1})$ from broad side can be expressed as

$$W_N = \left[1, e^{j\frac{2\pi d}{\lambda}\sin\theta_n}, ..., e^{j(M-1)\frac{2\pi d}{\lambda}\sin\theta_n}\right]^T \tag{2.31}$$

For the transmission perspective, the weighting matirx can be multiplied to the digital BB signal of each beam to be transmitted. Then that signal would be converted into analog domain via D/A, upconverted and then radiated from ULA. By making an appropiate weighting matrix, independently controlled mulitple beams can be synthesized via digital domain.

In fully active digital beamforming each element has its own RF transciever chain, comprisinf from A/D, D/A to DSp processing chips. Since the number of processing chips and transciever chain is propotional to the number of beams. Therefore to digitally generate N parallel beams would require considereable amount of computational power. Alternative digital architectures have been proposed to reduce the number of RF chains, cost and complexity. The fixed sub-array based architecture for digital beam generation in shown in Figure 2.12. The M elements are divided into Q subarrays with each subarray having P=M/Q elements (i.e. provided M is divisibe by Q). This implies that the number of RF channels are now reduced from M to Q. This also relaxes the power and processing requirements.

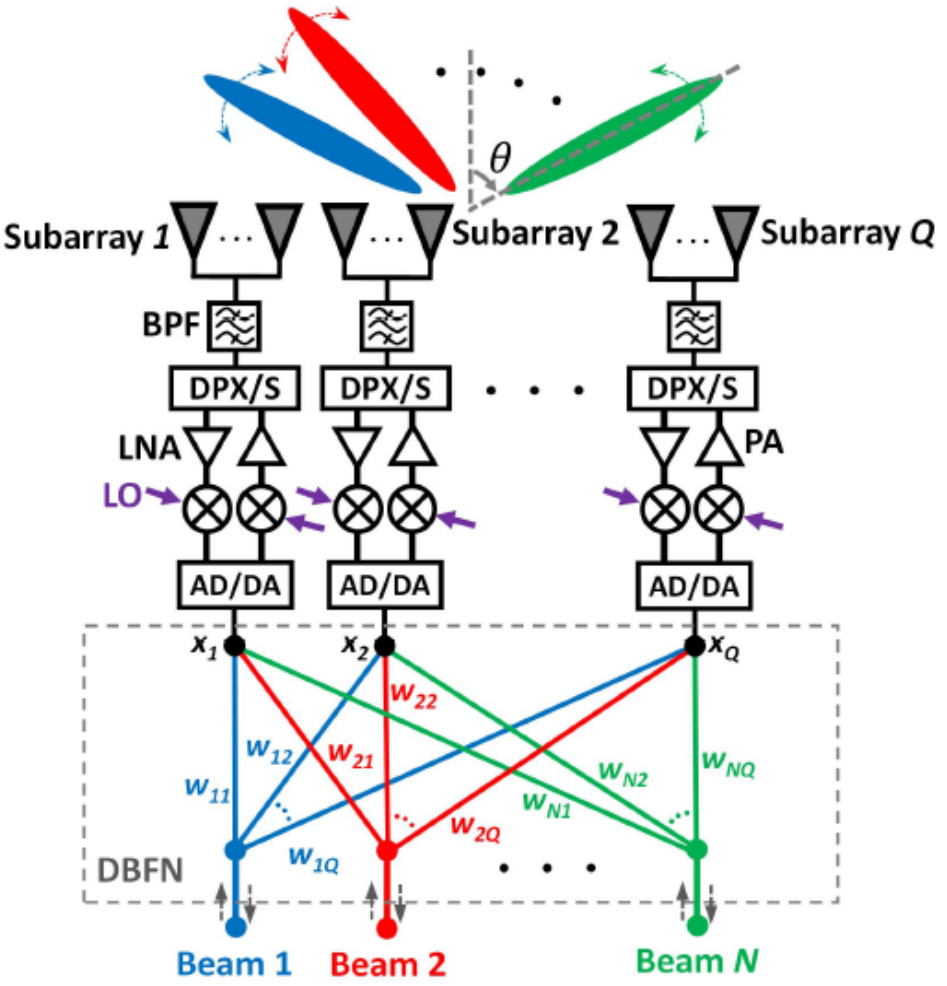


Figure 2.12: System Architecture for Digital Beamforming for M channels and N beams from [51]

### 2.4.3. Hybrid Beamforming

The previous section presented the analog and digital beamforming architectures and their operating principles. The analog architectures are easier to implement and operate. However phase shifters at higher frequencies especially at millimetre wave are difficult to accurately design. This effect beam precision, phase shift variation for different temperatures and insertion losses. The digital beamforming overcomes these issues by performing the phase shifting operation in digital domain. The digital beamforming offer more flexibility and control of independent multiple beams. It also enables to achieve very high beam resolutions. However, this requires to have RF transceiver behind each antenna element. This would cause high power consumption and dissipation along with increased cost issues for large array based massive MIMO 5G systems.

The hybrid beamforming aims to provide the solution to above mentioned problems. In addition to that, it can reach up to the performance of traditional digital beamforming techniques while using much less hardware complexity and power consumption [8]. The hybrid beamforming architecture uses the combination of RF phase shifters in analog domain together with digital beamforming in baseband domain. Instead of having RF chains equal to the number of elements as in the case of digital beamforming, the hybrid beamforming have number of RF chains atleast equal to or more than the number of beams to be generated. The concept behind hybrid beamforming is that number of transceiver chains are lower bounded by the number of data streams, the beamforming gain and spatial diversity is achieved by the number of antennas. The problem for hybrid beamforming was to decouple the RF and digital beamformer designs. However with advancement in signal processing techniques, the interest in hybrid beamforming particularly for massive MIMO has increased and various architectures have been proposed which are explained in the next section.

#### 2.4.3.1. Fully Connected Hybrid Beamforming

In fully connected hybrid beamforming architecture as shown in Figure 2.13, each RF chain is connected to all antenna elements via adders. Therefore the transmitted signal in $N_{RF}$ transceivers passes through $N_t$ RF paths (which contains mixer, power amplifier, phase shifter, etc.) and added together before being applied to each antenna element as depicted in Figure 2.13. The fully connected hybrid architecture offers full beamforming gain and higher flexibility in beam steering.

#### 2.4.3.2. Partially Connected Hybrid Beamforming

Although the fully connected beamforming architecture provide high beamforming gain per transceiver and more beam agility, but it all comes at the cost of high implementation complexity. The fully connected beamforming system would require adder for each antenna element. A typical fully connected system with $N_{RF}$ transceivers and $N_t$ RF paths, the signal will pass through in total $N_{RF} x N_t$ paths.

The partially connected hybrid beamforming reduces the complexity as shown in Figure 2.14. In partially connected architecture, the entire antenna array is divided into $\frac{N_t}{N_{RF}}$ number of subarrays. Then each of the $N_{RF}$ chain is connected to a certain subarray. This reduces the overall system complexity of $N_t$ RF paths but at the cost of $\frac{1}{N_{RF}}$ beamforming gain as compared to fully connected hybrid architecture. The combination of massive MIMO with partially connected hybrid beamforming can massively reduce number of transceivers and power consumption for 5G systems.

#### 2.4.3.3. Cosecant Subarray Beamforming

The hybrid beamforming provides a very effective alternative with less hardware complexity for multi-beam generation as compared to digital beamforming. One of the variants of hybrid beamforming is cosecant subarray beamforming which uses the cosecant elevation power equalization as presented in [69]. The concept behind the cosecant subarray beamforming is to provide similar power for all the users in the cell while reducing the hardware complexity of traditional hybrid beamforming.

As shown in Figure 2.15(a), a uniform linear array of subarrays is used for cosecant subarray beamforming. The azimuth beamforming across all the subarrays for N beams is performed in digital domain using standard beamforming algorithms as presented in the next chapter. The cosecant based power distribution as shown

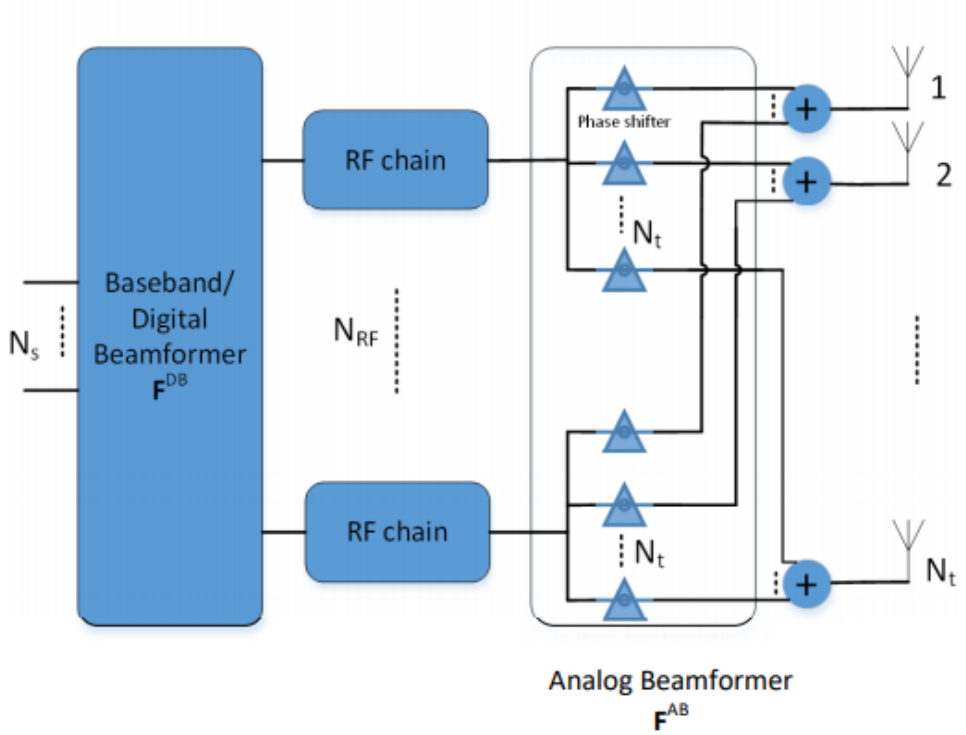


Figure 2.13: Fully Connected Hybrid beamforming from [8]

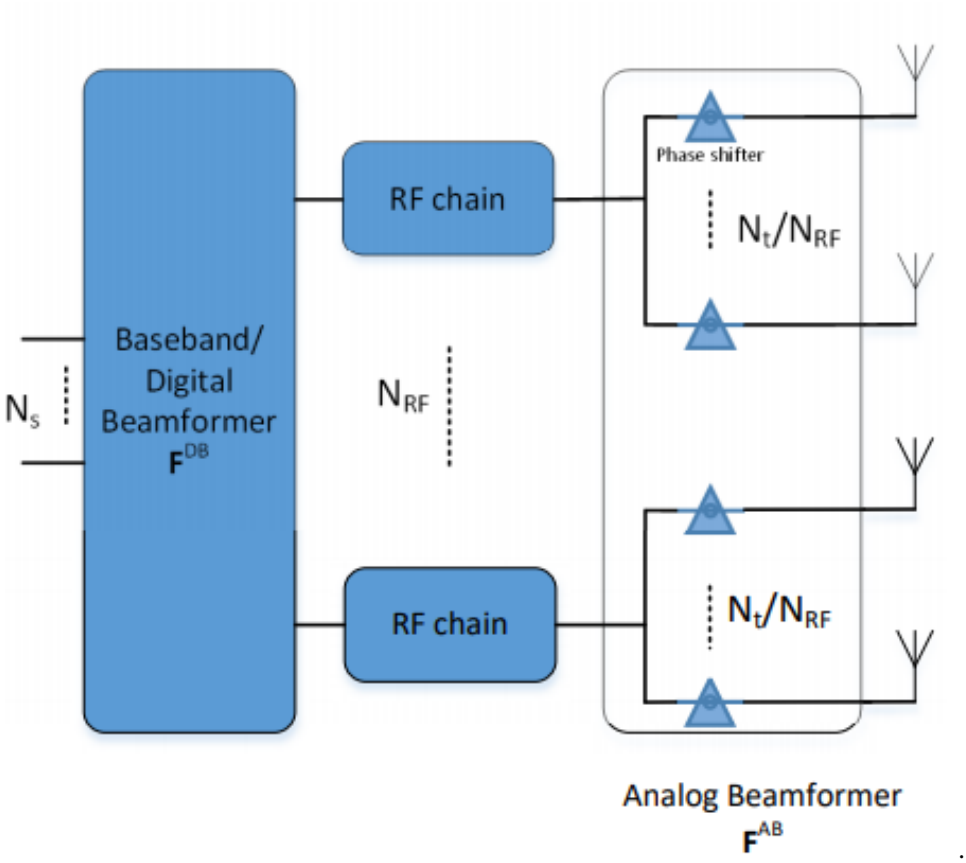


Figure 2.14: Partially Connected Hybrid beamforming from [8]

in Figure 2.15(b) is applied in elevation domain within each subarray. This would provide the farthest user which is has the lowest elevation angle from horizon with the highest gain. However, as the user approaches the base station its elevation angle with respect to horizon increases,; its gain will be reduced. Thus the cosecant subarray beamforming system attempts to provide similar signal to noise ratio (SNR) to all the users in cell.

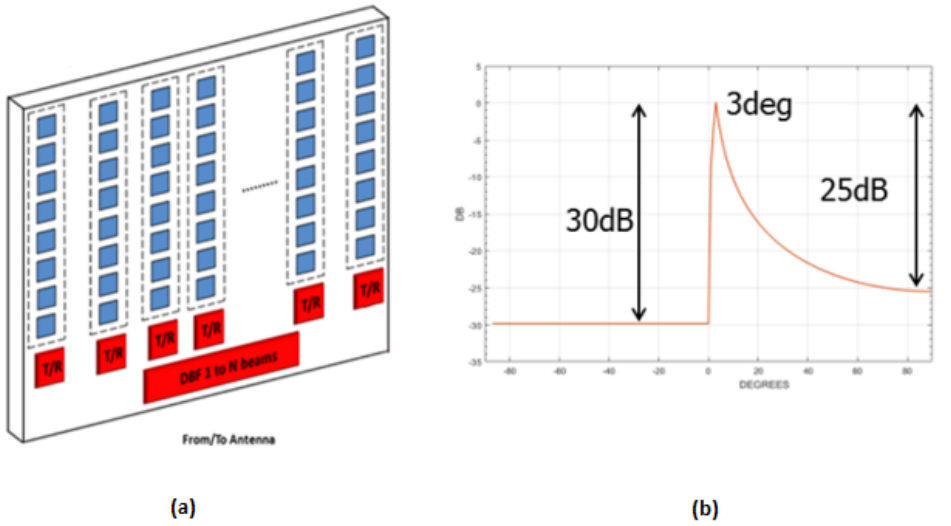


Figure 2.15: Cosecant Subarray Beamforming (a) Uniform linear array of subarrays (b) Cosecant-square power distribution in elevation

## 2.5. Conclusion

This chapter presented the overview of different potential beamforming architectures that can be used in the upcoming 5G system. The chapter started with a brief background of millimetre wave frequency band and challenges it offers to communication system. Then antenna basics were presented along with some formulas that would be useful in understanding the rest of the thesis. The various beamforming architecture with their implementation, advantages and dis-advantages are discussed. Finally, cosecant subarray beamforming concept is introduced which is a variant of hybrid beamforming and its operating principle is presented.

# 3

# Multiuser MIMO System

As discussed earlier, Massive MIMO is a multiuser MIMO (MU-MIMO) system where the number of antennas at the base station and number of users are very large. MU-MIMO is capable to have Spatial Division Multiple Access (SDMA) which enables to differentiate the users on the basis of their spatial footprint. The system then can form a beam directed towards each user using various beamforming algorithms to transmit the data as shown in Figure 3.1, thus increasing the overall system capacity and throughput. In this chapter, we begin with the description of system model for MU-MIMO system. Then we discuss the channel model formation and assumptions that were used in the thesis. This is followed by the introduction of digital beamforming algorithms from the uplink and downlink perspective. In the end, the orthogonal matching pursuit algorithm is presented that will be used for fully connected hybrid beamforming analysis in the next chapter.

## 3.1. System Model

The MU-MIMO system model consists of a single base station with K active users randomly distributed in a cell. The base station has an antenna array with M elements while each User Equipment (UE) has a single antenna. Generally, a user can also be equipped with multiple antenna elements but for the simplicity, our analysis considers only single antenna at user end. Figure 3.2 presents the multiuser MIMO system with K active users served by the base station (BS) having M antenna elements. It is assumed that all K active users share the same time-frequency resource. The cellular communication has two modes: in uplink UEs transmit the signal to the BS while in downlink the BS transmits the signal to the UEs. Moreover, it is assumed that the each BS serves a 90 degrees or ± 45 degrees sector, mutual coupling between antenna elements is ignored and modulation for carrier is 16-quadrature amplitude keying (QAM). In addition to that, we also assume that the BS has the perfect Channel State Information (CSI) which it already acquired during the training phase.

### 3.1.1. Channel Model Formation

The millimetre waves (mmWaves) domain is characterized by high free space path propagation loss (due to the decrease in effective aperture of the antenna as the wavelength decreases) which results in limited scattering and spatial selectivity. Likewise, large antenna arrays with closely spaced antenna elements for multiuser massive MIMO communication in mmWave domain leads to high antenna correlation. This combination of dense antenna arrays in a spatially selective scattering environment makes the traditional MIMO statistical fading analysis inaccurate for the mmWave channel realization and modelling. Therefore, a narrow band clustered geometric channel based on Saleh-Valenzuela model is adopted which enables to precisely capture the mathematical structure of mmWave channels [81], [87]. The channel matrix H is the sum of the rays coming from Ncl clusters with each cluster contributing Nray propagation paths to the channel. The discrete time narrow band channel H with M elements at BS and N elements at receiver can be presented as

$$H = \gamma \sum_{i,l} \alpha_{i,l} \Lambda_r(\phi^r_{i,l}, \theta^r_{i,l}) \Lambda_t(\phi^t_{i,l}, \theta^t_{i,l}) a_r(\phi^r_{i,l}, \theta^r_{i,l}) a_t(\phi^t_{i,l}, \theta^t_{i,l})^* \tag{3.1}$$

where $\gamma$ is the normalization factor given as $\sqrt{\frac{MN}{N_{cl}N_{ray}}}$, $\alpha_{i,l}$ is denoted as the complex gain for the $l^{th}$ ray

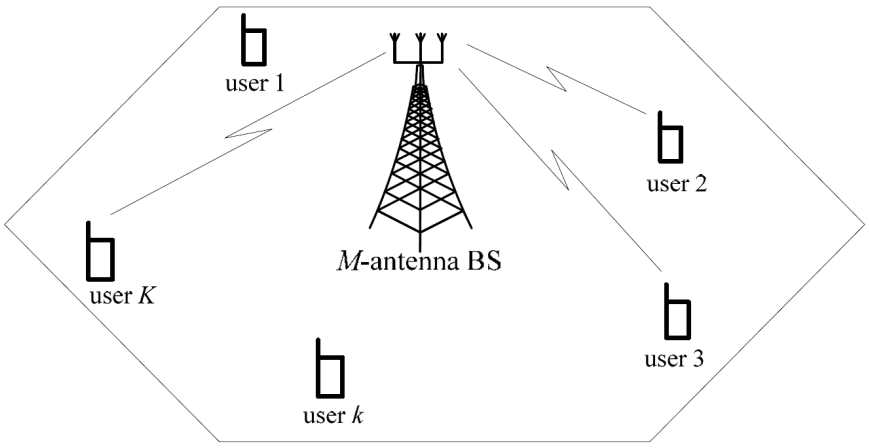


Figure 3.1: A Multiuser MIMO system with K number of active users served by the BS with M antenna elements, all sharing same frequency sub-band simultaneously from [63]

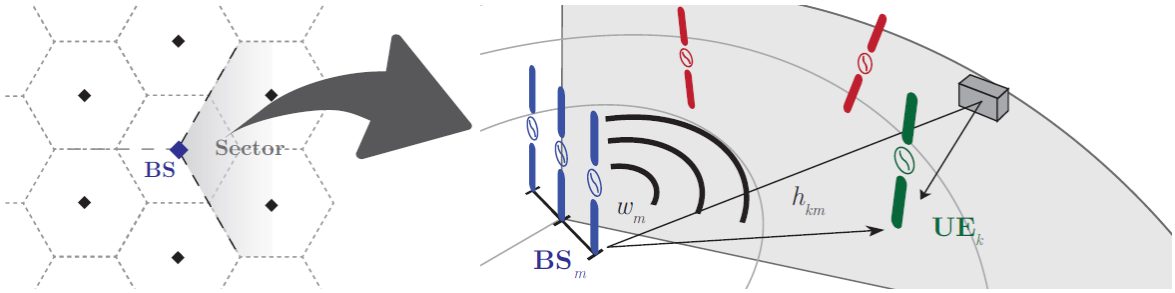


Figure 3.2: A M x K MU-MIMO cell with ±45 degree sector from [21]

in the $i^{th}$ scattering cluster, While $\phi^r_{i,l}$ ($\theta^r_{i,l}$) and $\phi^t_{i,l}$ ($\theta^t_{i,l}$) are the azimuth (elevation) angles of arrival and departure for $l^{th}$ ray, respectively. The functions $\Lambda_t(\phi^t_{i,l}$ and $\Lambda_r(\phi^r_{i,l},\theta^r_{i,l}$ represent the antenna element gain for transmitter and receiver at the corresponding angles of arrival and departure. The vectors $a_r(\phi^r_{i,l},\theta^r_{i,l})$ and $a_t(\phi^t_{i,l},\theta^t_{i,l})$ are the normalized receive and transmit steering vectors at an azimuth (elevation ) angle of $\phi^r_{i,l}$ ($\theta^r_{i,l}$) and $\phi^t_{i,l}$ ($\theta^t_{i,l}$) respectively. The complex gain $\alpha_{i,l}$ are assumed to be independent and identically distributed (i.i.d.) with zero mean and $\sigma^2_{\alpha,i}$ variance, where $\sigma^2_{\alpha,i}$ represents the average power of the $i_{th}$ cluster. The sum of all the average cluster power is such that

$$\sum_{i=1}^{N_{cl}} \sigma^2_{\alpha,i} = \gamma \tag{3.2}$$

The $\gamma$ is the normalization factor which satisfies $E\left\|H^2_F\right\| = N_t N_r$ [87]. The azimuth and elevation angles of departures,$\phi^t_{i,l}$ and $\theta^t_{i,l}$, in each cluster $I$ for $N_{ray}$ are assumed to be randomly distributed with mean cluster angle of $\phi^t_i$ and $\theta^t_i$ respectively and a constant angular spread (standard deviation) of $\sigma_{\phi^t}$ and $\sigma_{\theta^t}$ respectively. Similarly, the azimuth and elevation angles of arrival, $\phi^r_{i,l}$ and $\theta^r_{i,l}$, are randomly distributed with mean cluster angles of $(\theta^r_i,\phi^r_i)$ and angular spreads of $\sigma_{\phi^r}$ and $\sigma_{\theta^r}$ respectively. Various distributions have been proposed for angles of arrival and departures in the clustered channel models, laplacian distribution is found to be a good fit [37]. Likewise , different mathematical models are used for depicting the functions of $\Lambda_t(\phi^t_{il},\theta^t_{il})$ and $\Lambda_r(\phi^r_{il},\theta^r_{il})$. For instance, if transmitter contains ideal sectored antenna elements [80], $\Lambda_t(\phi^t_{il},\theta^t_{il})$ would be given as

$$\Lambda_t(\phi^t_{i,l},\theta^t_{il}) = \begin{cases} 1 & \forall\phi^t_{il} \in [\phi^t_{min},\phi^t_{max}], \forall\theta^t_{il} \in [\theta^t_{min},\theta^t_{max}], \\ 0 & otherwise \end{cases} \tag{3.3}$$

In equation 3.3, it is assumed to have a unity gain over the entire sector defined by $\phi^t_{il} \in [\phi^t_{min},\phi^t_{max}]$ and

$\theta^t_{il} \in [\theta^t_{min}, \theta^t_{max}]$ respectively. The receive antenna gain $\Lambda_r(\phi^r_{il}, \theta^r_{il})$ is also similarly defined over the azimuth and elevation sector angles defined by $\phi^r_{il} \in [\phi^r_{min}, \phi^r_{max}]$ and $\theta^r_{il} \in [\theta^r_{min}, \theta^r_{max}]$ respectively. However, instead of using the simplified antenna gain model presented in equation 3.3, $\Lambda_t(\phi^t_{il}, \theta^t_{il})$ and $\Lambda_r(\phi^r_{il}, \theta^r_{il})$ can be replaced with real far field patterns of antenna used in the system.

The array response vector for transmit and receive antennas are given by $a_t(\phi^t_{il}, \theta^t_{il})$ and $a_r(\phi^r_{il}, \theta_{il^r})$ respectively. These vectors depends on the structure of antenna arrays rather than the antenna element properties. The array response vector for two mostly used antenna arrays are presented. The array response vector for M element uniform linear array (ULA) oriented along y-axis can written as

$$a_{ULAy}(\phi) = \frac{1}{\sqrt{M}}[1, e^{jkd\sin\phi}, ..., e^{j(M-1)kd\sin\phi}]^T \tag{3.4}$$

Where $k = \frac{2\pi}{\lambda}$ and $d$ is the inter-element spacing in the antenna array. The equation 3.4 does not include $\theta$ the ULA response is invariant in the elevation domain. For uniform planar array (UPA) in the yz-plane with having W and H elements on the corresponding y and z axes respectively., the array vector is given as

$$a_{UPAy}(\phi, \theta) = \frac{1}{\sqrt{M}}[1, e^{jkd(m\sin\phi\sin\theta + n\cos\theta)}, ..., e^{jkd((W-1)\sin\phi\sin\theta + (H-1)\cos\theta)}]^T \tag{3.5}$$

Where $0 \leq m < W$ and $0 \leq n < H$ are the y and z indices of antenna elements respectively for antenna array of size $M = WH$.

### 3.1.2. Uplink Transmission

The uplink transmission is referred to the communication link where K active UE sends the data to the base station. Let $s_k$ , where $E|s_k|^2 = 1$ be the transmitted signal from the $k^{th}$ user to the base station. The K users are sharing the same time-frequency resources; therefore, the received signal vector of size $Mx1$ would be the combination signals sent by all $K$ users

$$y_{ul} = \sqrt{p_u}\sum_{k=1}^{K} h_k s_k + n \tag{3.6}$$

$$y_{ul} = \sqrt{p_u} HS + n \tag{3.7}$$

Where $p_u$ is the average signal to noise ratio (SNR) per user equipment, $n \in \mathbb{C}^{Mx1}$ is additive white Gaussian noise and $S = [s_1, ..., s_k]$ . The elements of $n$ are i.i.d. with zero random mean and unit variance, and also independent of channel matrix $H$.

Since the base station has the knowledge of CSI, the sum capacity of the multiple-access channel can be calculated from the received signal $y_{ul}$ as [41]

$$C_{ul,sum} = \log_2 det(I_k + p_u H^H H) \tag{3.8}$$

### 3.1.3. Downlink Transmission

The downlink transmission, also known as forward transmission, occurs when the base station (BS) send the data to the K active user equipment's in a cell. Let assume $x \in \mathbb{C}^{Mx1}$ where $E\|x\|^2 = 1$ as transmitted signal vector from base station (BS) antenna array to the $k^{th}$ user and is given as

$$y_{dl} = \sqrt{p_d}\sum_{k=1}^{K} h_k^T x + z_k \tag{3.9}$$

Where $p_d$ is the downlink signal to noise ratio and $z_k$ is the additive white Gaussian noise at the $k^{th}$ user. The $z_k$ is Gaussian distributed with zero mean and unit variance. The received signal in matrix form can be written as

$$y_{dl} = \sqrt{p_d} H^T S + z \tag{3.10}$$

Where $y_{dl} = [y_{(dl,1)} y_{(dl,2)}, ..., y_{(dl,K)}]^T$ , $z = [z_1 z_2, ... z_k]^T$ and H is the channel matrix. The downlink sum-capacity is given as

$$C_{sum} = max_{qk} \log_2 det(I_M + p_d H^* D_q H^T) \tag{3.11}$$

Where $D_q$ is the diagonal matrix with $k_{th}$ element is $q_k$.

## 3.2. Linear Processing Techniques

In order to obtain the optimal performance, the complex signal processing techniques are needed to be implemented. In the uplink mode, maximum likelihood (ML) multiuser detection is possible. For ML multiuser scenario, the BS has to perform the search for all the transmitted signal vectors s, and selects the best as follows

$$\hat{s} = argmin_{s \in S^K} \left\| y_{ul} - \sqrt{p_u} HS \right\|^2 \tag{3.12}$$

Where $k = 1, 2, ..., K$. The problem presented in equation 3.2 is a least square problem with finite alphabet constraint. The BS has to perform a search over $|S|^K$ vectors, where $|S|$ is the cardinality of set $S$. This implies maximum likelihood complexity is exponentially related to the number of users.

Therefore, the BS can use linear processing techniques to reduce the signal processing complexity. These linear processing schemes are not optimal. However, for large number of BS antenna elements, it is shown that [62],[79] linear processing becomes optimal. The explanation of linear processing techniques is presented in the following sections.

### 3.2.1. Linear processing Receivers (in the Uplink)

The received signal at the base station $y_{ul}$ is divided into K independent streams by multiplying it with an M x K linear detection matrix, A

$$\tilde{y_{ul}} = A^H y_{ul} = \sqrt{p_u} A^H HS + A^H n \tag{3.13}$$

As shown in Figure 3.3, each data stream is decoded independently. The complexity of this process is in the order of $K|S|$. From equation 3.13, the $k^{th}$ signal stream of $\tilde{y_{ul}}$ which is used to recover the data $s_k$ of $k^{th}$ user is given as

$$\tilde{y_{ul,k}} = \sqrt{p_u} a_k^H h_k s_k + \sqrt{p_u} \sum_{k' \neq k}^{K} a_k^H h_{k'} s_{k'} + a_k^H n \tag{3.14}$$

Where the first term in the equation 3.14 represents the desired signal from the intended user, while the second term represents the inter-user interference signal and the last term is the additive white Gaussian noise. The $a_k$ presents the $k_{th}$ column of A. The interference signal is treated combine as effective noise and the signal to interference plus noise ratio for the uplink is given as

$$SINR_k = \frac{p_u \left| a_k^H h_k \right|^2}{p_u \sum_{k' \neq k}^{K} \left| a_k^H h_{k'} \right|^2 + \left\| a_k^2 \right\|} \tag{3.15}$$

#### 3.2.1.1. Maximum-Ratio Combining receiver

The aim of the maximum ratio combining receiver (MRC) technique is to maximize the signal to noise ratio (SNR) while ignoring the effect of inter-user interference. From equation 3.14, the column of A (MRC receiver matrix) is given as

$$a_{mrc,k} = argmax_{a_k \in \mathbb{C}^{Mx1}} \frac{power\ (desired\ signal)}{power\ (noise)} \tag{3.16}$$

$$= argmax_{a_k \in \mathbb{C}^{Mx1}} \frac{p_u \left| a_k^H h_k \right|^2}{\|a_k\|^2} \tag{3.17}$$

Since

$$\frac{p_u \left| a_k^H h_k \right|^2}{\| a_k \|^2} \leq \frac{p_u \| a_k \|^2 \| h_k \|^2}{\| a_k \|^2} = p_u \| h_k \|^2 \tag{3.18}$$

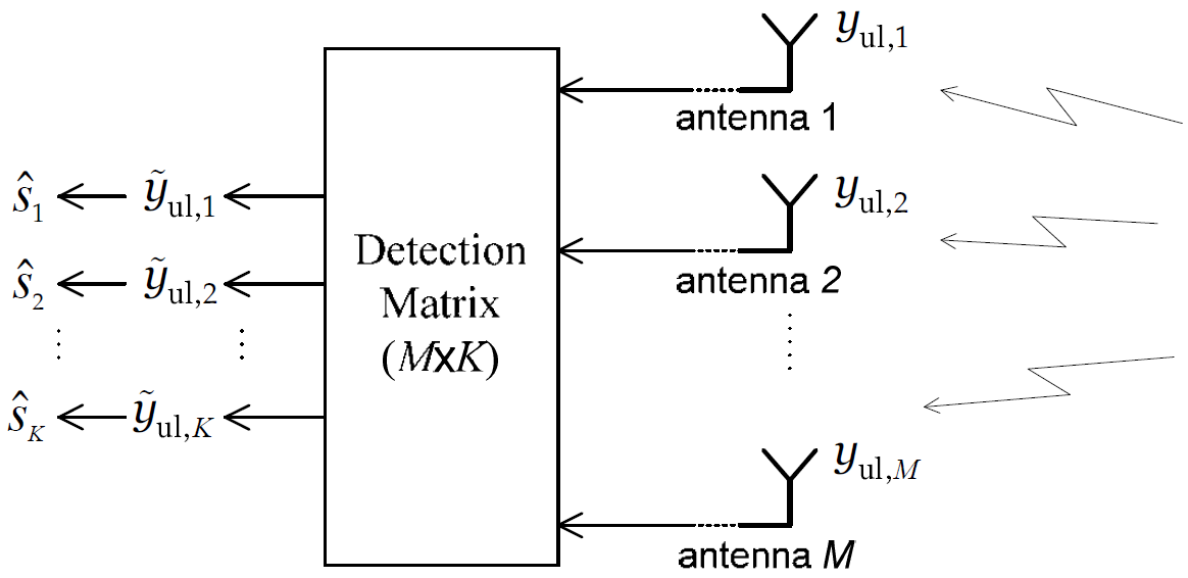


Figure 3.3: Linear detection at BS from [63]

And the equality will hold when $a_k = const.h_k$, the MRC receiver is then given as: $a_{mrc,k} = const.h_k$. plugging in the value of $a_{mrc,k}$ in equation 3.15, the received SINR for MRC is then given as

$$SINR_{mrc,k} = \frac{p_u \| h_k \|^4}{p_u \sum_{k' \neq k}^{K} \left\| h_k^H h_{k'} \right\|^2 + \| h_k \|^2} \tag{3.19}$$

$$SINR_{mrc,k} = \frac{\| h_k \|^4}{\sum_{k' \neq k}^{K} \left\| h_k^H h_{k'} \right\|^2} \quad as \quad p_u \to \infty \tag{3.20}$$

The obvious advantage of MRC is the simple signal processing which lowers the computation power requirements at the BS. The received signal is the multiplied with the conjugate-transpose of the channel matrix H. In addition to that, at low SNR $p_u$, $SINR_{mrc,k} \approx p_u \| h_k \|^2$. This means at low SNR, maximum-ratio combining provides the same array gain as it would in the case of single user system. However, MRC does not take into account the effect of inter-user interference signal. Therefore, its performance severely degrades in the case of interference-dominated scenario.

### 3.2.1.2. Zero-Forcing receiver

The zero-forcing (ZF) receiver takes into consideration the inter-user interference signal but ignores the effect of noise. In multiuser scenario, the ZF completely nullify the interference signal by projecting each stream orthogonal to each other. The $k_{th}$ column of the ZF matrix satisfies the following

$$\begin{cases} a_{zf,k}^H \neq 0 \\ a_{zf,k}^H = 0, \qquad \forall k' \neq k \end{cases} \tag{3.21}$$

The ZF matrix which would satisfy the condition mentioned in equation (3.21) can be obtained by the pseudo-inverse of the channel matrix H. For ZF we then have

$$\widetilde{y_{ul}} = \left( H^H H \right)^{-1} H^H y_{ul} = \sqrt{p_u} s + \left( H^H H \right)^{-1} H^H n \tag{3.22}$$

The ZF technique requires to have number of antenna elements at base station equal to or larger than the number of users ($M \geq K$) in a cell (to make $H^H H$ invertible). Each stream coming from the equation (3.22) would be interference free, therefore the kth stream from $\widetilde{y_{ul}}$ can be written as

$$\widetilde{y_{ul,k}} = \sqrt{p_u} s_k + \widetilde{n_k} \tag{3.23}$$

Where $\widetilde{n_k}$ represents the kth entry of $\left(H^H H\right)^{-1} H^H n$. The received SINR in the case of zero-forcing for kth stream can be given as

$$SINR_{zf,k} = \frac{p_u}{\left[\left(H^H H\right)^{-1}\right]_{kk}} \tag{3.24}$$

The zero forcing offers advantage over MRC in terms of superior inter-user interference suppression. The SINR can be increased as high as required by increasing the transmit power. However, ZF completely neglect the impact of noise, therefore works poor in high noise scenarios. In addition to that, if the channel matrix is not well conditioned; the pseudo-inverse can amplify the noise hence further degrading the overall performance. In comparison with MRC, ZF has higher computational complexity due to pseudo-inverse operation.

#### 3.2.1.3. Minimum Mean-Square Error Receiver

The goal of minimum mean square error (MMSE) receiver is to reduce the mean square error between estimate $A^H y_{ul}$and the transmitted signal $s$. It can be written as

$$A_{mmse} = argmin_{A \in \mathbb{C}^{MxK}} E\left\{\left\| A^H y_{ul} - s\right\|^2\right\} \tag{3.25}$$

$$A_{mmse} = argmin_{A \in \mathbb{C}^{MxK}} \sum_{k=1}^{K} E\left\{\left| a_k^H y_{ul} - s\right|^2\right\} \tag{3.26}$$

Where the kth column of A is denoted by $a_k$. Thus, the kth column of MMSE matrix is given as

$$a_{mmse,k} = argmin_{a_k \in \mathbb{C}^{MxK}} E\left\{\left| a_k^H y_{ul} - s\right|^2\right\} \tag{3.27}$$

$$a_{mmse,k} = cov\left(y_{ul}, y_{ul}\right)^{-1} cov\left(s_k, y_{ul}\right)^H \tag{3.28}$$

$$a_{mmse,k} = \sqrt{p_u}\left(p_u H H^H + I_M\right)^{-1} h_k \tag{3.29}$$

Here $cov(v_1, v_2) \triangleq E\{v_1, v_2^H\}$, where $v_1$ and $v_2$ are two column vectors with zero mean elements. The MMSE receiver tries to maximize the received SINR. Therefore in terms of SINR performance, MMSE receiver is the best among MRC and ZF receivers. As it can be seen in equation (3.29), at high SNR (i.e. at high $p_u$) the MMSE approaches ZF while at low SNR MMSE performance resembles that of MRC receiver. The received SINR of MMSE receiver can be given as

$$SINR_{mmse,k} = p_u h_k^H \left(p_u \sum_{i \neq k}^{K} h_i h_i^H + I_M\right)^{-1} h_k \tag{3.30}$$

### 3.2.2. Linear Precoder (in the Downlink)

In the downlink transmission, the data symbols are precoded with beamforming matrix and then transmitted from M elements of base station to the K active users in a cell. Let $x$ be the combination of symbols intended to transmit to the users. The symbol for the kth user is $q_k$ with $E\left\{\left|q_k\right|^2\right\} = 1$, then the signal vector $x$ with precoding is given as

$$x = \sqrt{\alpha} W q \tag{3.31}$$

Where $q \triangleq \left[q_1\ q_2 \ldots\ q_K\right]^T$, $W \in \mathbb{C}^{MxK}$ is the precoding matrix containing the beamforming vectors and $\alpha$ is the normalization factor selected to satisfy the power constraint $E\left\{\left\|x\right\|^2\right\} = 1$. The normalization constant can be calculated as

$$\alpha = \frac{1}{E\{tr(WW^H)\}} \tag{3.32}$$

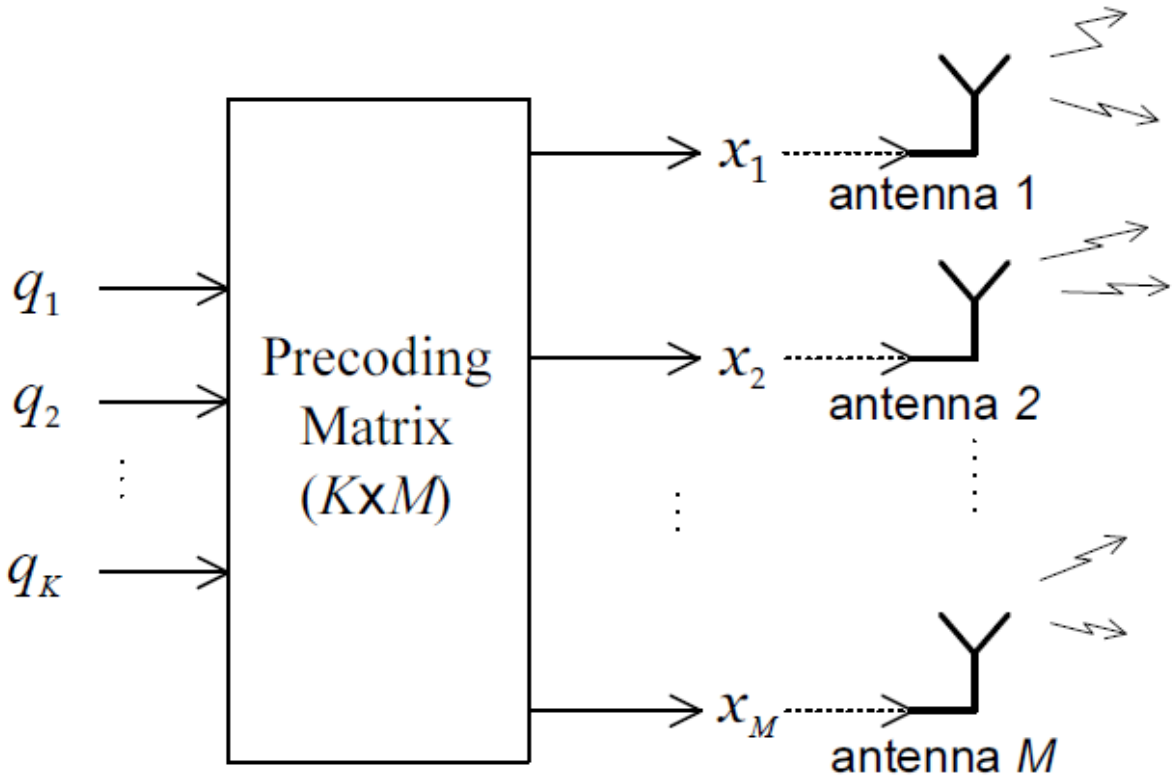


Figure 3.4: LLinear Precoding at BS from [63]

The block diagram showing the precoding operation on individual data stream at the base station end is shown in Figure 3.4. By using the Equation (3.31), the received signal at the kth user in a cell is given as

$$y_{dl} = \sqrt{\alpha p_d} h_k^T W q + + z_k \tag{3.33}$$

$$y_{dl} = \sqrt{\alpha p_d} h_k^T w_k q_k + \sqrt{\alpha p_d} \sum_{k' \neq k}^{K} h_k^T w_{k'} q_{k'} + z_k \tag{3.34}$$

The SINR for the downlink transmission at the $k_{th}$ user end can be given as

$$SINR_k = \frac{\alpha p_d |h_k^T w_k|^2}{\alpha p_d \sum_{k' \neq k}^{K} |h_k^T w_k|^2 + 1} \tag{3.35}$$

The traditional digital precoding techniques that are used for downlink transmission are Maximum Ration Transmission (MRT) also known as conjugate beamforming, ZF and MMSE. These precoders have similar operational theory and properties as MRC, ZF and MMSE receivers respectively. Therefore the formulas for the above mentioned three precoding techniques are presented as follows

$$W = \begin{cases} H^* & for\ MRT \\ H^*(H^T H^*)^{-1} & for\ ZF \\ H^*\left(H^T H^* + \frac{K}{p_d} I_K\right)^{-1} & for\ MMSE \end{cases} \tag{3.36}$$

Where $H$ is the channel matrix and $K$ denotes the total number of users in a cell. The sum rate for the kth user having $SINR_k$ is given as

$$SR = \sum_{k=1}^{K} E\{\log_2(1 + SINR_k)\} \tag{3.37}$$

As in the case of uplink, the MMSE precoding techniques outperforms ZF and MRT in terms of SINR. In low SNR regime, MRC is better than ZF and ZF performs better than MRC for higher SNR scenerio's.

## 3.3. Hybrid mmWave Precoders

The previous section discussed the linear precoding technique for downlink transmission. However, these techniques are well suited for digital beamforming systems where entire signal processing for beam formation and steering is performed in digital domain. On the other hand, hybrid beamforming technique is being proposed for upcoming 5G systems due to their advantage in terms their cost and power consumption. Figure 3.5 presents architecture of a fully connected hybrid beamforming architecture employing hybrid precoding technique in the transmitter. The transmitter precoding matrix is divided and applied in digital ($F_{BB}$) and RF ($F_{RF}$) domains.

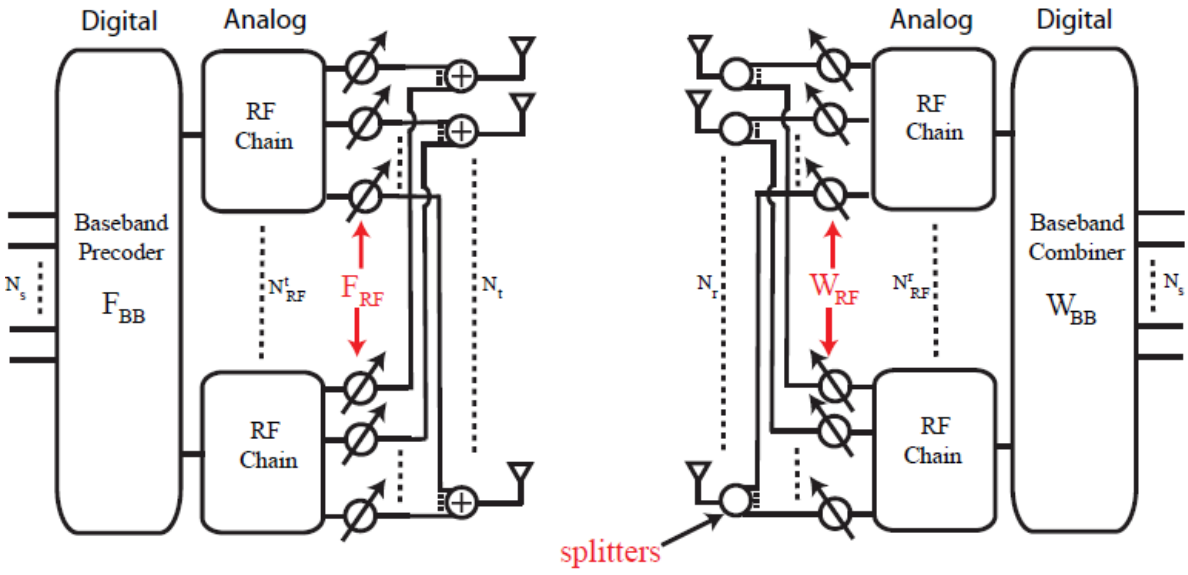


Figure 3.5: Block diagram for fully connected hybrid beamforming architecture having hybrid precoding from [19]

In order to perform multi-stream transmission for multi-user communication, the transmitter has $N_t^{RF}$ transmit chains such that $N_s \leq N_t^{RF} \leq N_t$. The architecture shown in Figure 3.5 allows to apply $N_t^{RF}$x $N_s$ baseband precoder $F_{BB}$ via its $N_t^{RF}$ transmit chains and $N_t$ x $N_t^{RF}$ RF precoder via phase shifters in analog domain. Let's take $s$ be the $N_s$x 1 transmit symbol vector with $E\ [ss^*] = \frac{1}{N_s} I_{N_s}$, so the precoded transmit signal is given as

$$x = F_{RF} F_{BB} s \tag{3.38}$$

Since $F_{RF}$ is applied via RF phase shifter, the constraints on its elements is $\left(F_{RF}^{(i)} F_{RF}^{(i)*}\right)_{l,l} = {N_t}^{-1}$, where $(.)_{l,l}$ is the $l^{th}$ diagonal element of a matrix i.e. all $F_{RF}$ elements have equal norm. The power constraint on the total transmit power is enforced by normalizing $F_{BB}$ such that $\|F_{RF} F_{BB}\|_F^2 = N_s$. The received signal at the input of UE for the hybrid precoded transmitted symbols is given as

$$y = \sqrt{\rho} H F_{RF} F_{BB} s + n \tag{3.39}$$

Where $y$ is the $N_r$ x 1 received signal vector, H is the $N_r$ x $N_t$ channel matrix such that $E\left[\|H\|_F^2\right] = N_t N_r$, $\rho$ is the average received power at the user end and $n$ is the zero mean additive white Gaussian noise with $\sigma_n^2$ variance. Moreover like linear precoding, the perfect channel state information is assumed to be known at the base station and at the receiver. From receiver perspective, the receiver has $N_s \leq N_r^{RF} \leq N_r$ RF chains

and the corresponding analog phase shifters to achieve beamforming. The processed received signal at the UE can be given as

$$\tilde{y} = \sqrt{\rho} W_{BB}^{*} W_{RF}^{*} H F_{RF} F_{BB} s + W_{BB}^{*} W_{RF}^{*} n \tag{3.40}$$

Where $W_{RF}$ is the $N_r$ x $N_r^{RF}$ combining matrix applied in RF domain and $W_{BB}$ is the $N_r^{RF}$ x $N_s$ combining matrix in baseband domain. Similarly as in the case of RF precoder, $W_{RF}$ is applied via RF phase shifters therefore $\left(W_{RF}^{(i)} W_{RF}^{(i)*}\right)_{l,l} = {N_r}^{-1}$. The spectral efficiency of the system is given as [41]

$$R = \log_2\left(\left| I_{N_s} + \frac{\rho}{N_s} R_n^{-1} W_{BB}^{*} W_{RF}^{*} H F_{RF} F_{BB} \times \; F_{BB}^{*} F_{RF}^{*} H^{*} W_{RF} W_{BB} \right|\right) \tag{3.41}$$

Where $R_n = \sigma_n^2 W_{BB}^{*} W_{RF}^{*} W_{RF} W_{BB}$ is the noise covariance matrix after combining. The goal of hybrid precoders $(F_{RF}, F_{BB})$ is to maximize the spectral efficiency presented in equation (3.41). However, this would be a joint maximization over four variables $(F_{RF}, F_{BB}, W_{RF}, W_{BB})$. However, to find a global optimum for such joint optimization problem is difficult [85]. In addition to that, the non-convex constraints on $F_{RF}$ and $W_{RF}$ makes the solution unlikely [19]. Therefore in order to simplify the transceiver design, the joint transmitter-receiver optimization problem is decoupled and focus on the design of hybrid precoders $(F_{RF}, F_{BB})$. Since the thesis is focused to evaluate the performance of beamforming techniques in downlink, the emphasis would be on the design of precoders. So we design $F_{RF}\ F_{BB}$ to maximize the mutual information over the mmWave channel

$$I(F_{RF}, F_{BB}) = \log_2\left(\left| I + \frac{\rho}{N_s \sigma_n^2} H F_{RF} F_{BB} F_{BB}^{*} F_{RF}^{*} H^{*} \right|\right) \tag{3.42}$$

The precoder optimization problem can be stated as

$$\left(F_{RF}^{opt}, F_{BB}^{opt}\right) = argmax_{F_{RF}, F_{BB}} I(F_{RF}, F_{BB}) \tag{3.43}$$

$$s.t. \qquad F_{RF} \in \mathscr{F}_{RF}$$
$$\|F_{RF} F_{BB}\|_F^2 = N_s$$

Where $\mathscr{F}_{RF}$ is the set of all possible RF precoders. There is no general solution exist due to the existence of non-convex constaints $F_{RF} \in \mathscr{F}_{RF}$ [19]. The step towards the solution of the problem presented in Equation (3.43) can be taken by re-writing the equation (3.42) in terms of "distance" between $F_{RF} F_{BB}$ and the optimal precoding vector for the channel $F_{opt}$. The singular value decomposition is performed for the channel $H = U \sum V^{*}$ where $U$ is an $N_r$ x rank(H) unitary matrix, $\sum$ is a rank(H) x rank(H) diagonal matrix of singular values and $V$ is $N_t$ x rank(H) unitary matrix. By using the singular value decomposition and standard mathematical operations, equation (3.42) can be re-written as

$$I(F_{RF}, F_{BB}) = \log_2\left(\left| I + \frac{\rho}{N_s \sigma_n^2} \sum\nolimits^2 V^{*} F_{RF} F_{BB} F_{BB}^{*} F_{RF}^{*} V \right|\right) \tag{3.44}$$

The partitions of matrices $\sum$ and $V$ is given as

$$\sum = \begin{bmatrix} \sum_1 & 0 \\ 0 & \sum_2 \end{bmatrix}, \qquad V = \begin{bmatrix} V_1 & V_2 \end{bmatrix} \tag{3.45}$$

Where $\sum_1$ has dimension $N_s \times N_s$ and $V_1$ has dimension $N_t \times N_s$, therefore the optimal unconstraint unitary precoder for channel matrix H is given by $F_{opt} = V_1$. However $V_1$ cannot be decomposed into $F_{RF}\ F_{BB}$ with $F_{RF} \in \mathscr{F}_{RF}$ [19]. Therefore if the hybrid precoders $(F_{RF}\ F_{BB})$ are made sufficiently close to $F_{opt}$, then the mutual information from $F_{RF}\ F_{BB}$ can be compared with the one obtained with $F_{opt}$. Following assumptions are made for further analysing the optimization problem [19]:

1. The eigenvalues for the matrix $I_{N_s} - {V_1}^{*} F_{RF} F_{BB} F_{BB}^{*} F_{RF}^{*} V_1$ are quite small. For mmWave precoding, it can be written as ${V_1}^{*} F_{RF} F_{BB} \approx I_{N_s}$.

2. The singular value for the matrix ${V_2}^{*} F_{RF} F_{BB}$ are very small, infact ${V_2}^{*} F_{RF} F_{BB} \approx 0$.

These approximations enables to further simplify the analysis of mutual information $I(F_{RF}, F_{BB})$. By using the partitions as presented in equation (3.45) and using schur complement for matrix determinants, a detailed mathematical derivation is presented in [19] which transforms the optimization problem of equation (3.43) into

$$\left(F_{RF}^{opt}, F_{BB}^{opt}\right) = argmin_{F_{RF},F_{BB}} \left\| F_{opt} - F_{RF}F_{BB} \right\|_F \tag{3.46}$$

$$s.t. \qquad F_{RF} \in \mathscr{F}_{RF}$$
$$\|F_{RF}F_{BB}\|_F^2 = N_s$$

This can be summarized as finding the projection of $F_{opt}$ on the set of hybrid precoders $F_{RF}F_{BB}$ with constraint $F_{RF} \in \mathscr{F}_{RF}$. The projection is described in Frobenius norm $\|.\|_F^2$. However due to the non-convex nature of $\mathscr{F}_{RF}$, the problem remains still un-resolveable. In order to solve the optimization problem presented in equation (3.46), the structure of the mmWave MIMO channel can be exploited [19]. The following observation can be made

1. Since the optimal precoder is $F_{opt} = V_1$, the columns of unitary matrix $V$ forms the orthonormal basis for channel row space.
2. By the analysing the structure of channel matrix H presented in section 3.1.1,it can be observed that the array response vector $\mathrm{a}_t\left(\phi_{il}^t, \theta_{il}^t\right),\ \forall i,l,\theta_{il}^t$ also forms the finite spanning set for the channel row space.
3. It can be deduced from observation 1 that the columns of optimal precoder $F_{opt} = V_1$ are related to the array response vector $\mathrm{a}_t\left(\phi_{il}^t, \theta_{il}^t\right)$ via linear transformation. This implies that columns of $F_{opt}$ can be written in form of linear combinations of $\mathrm{a}_t\left(\phi_{il}^t, \theta_{il}^t\right),\ \forall i,l,\theta_{il}^t$.
4. The array response vector $\mathrm{a}_t\left(\phi_{il}^t, \theta_{il}^t\right)$ is only a constant magnitude phase that can be applied via RF phase shifters. Therefore for RF precoder $F_{RF}$, the transmitter can apply $N_t^{RF}$ of the vectors $\mathrm{a}_t\left(\phi_{il}^t, \theta_{il}^t\right)$ and can make arbitrary combinations with digital precoder $F_{BB}$. This means, a linear combination can be created that minimizes $\left\| F_{opt} - F_{RF}F_{BB} \right\|_F$.

The above mentioned observations indicate that the hybrid precoders can be found by restricting $\mathscr{F}_{RF}$ to a set of vectors of the form $\mathrm{a}_t\left(\phi_{il}^t, \theta_{il}^t\right)$ and by solving

$$\left(F_{RF}^{opt}, F_{BB}^{opt}\right) = argmin_{F_{RF},F_{BB}} \left\| F_{opt} - F_{RF}F_{BB} \right\|_F \tag{3.47}$$

$$s.t. \qquad F_{RF}^{(i)} \in \left\{\mathrm{a}_t\left(\phi_{il}^t, \theta_{il}^t\right),\ \forall i,l,\theta_{il}^t\right\}$$
$$\|F_{RF}F_{BB}\|_F^2 = N_s$$

This implies that using the basis vectors $\mathrm{a}_t\left(\phi_{il}^t, \theta_{il}^t\right)$ can be used to find the low dimension representation of $F_{opt}$. So this precoding problem can be defined as by finding the "best" $N_t^{RF}$ array response vector and then reaching to their optimal baseband combination. The constraint of $F_{RF}^{(i)}$ can be included in the optimization problem which results in following form

$$\widetilde{F_{BB}^{opt}} = argmin_{\widetilde{F_{BB}}} \left\| F_{opt} - A_t\widetilde{F_{BB}} \right\|_F \tag{3.48}$$

$$s.t. \qquad \left\| diag(\widetilde{F_{BB}}\widetilde{F_{BB}^*}) \right\|_0 = N_t^{RF}$$
$$\left\| A_t\widetilde{F_{BB}} \right\|_F^2 = N_s$$

Where $A_t = \left[\mathrm{a}_t\left(\phi_{1,1}^t, \theta_{1,1}^t\right), \ldots, \mathrm{a}_t\left(\phi_{N_{cl},N_{ray}}^t, \theta_{N_{cl},N_{ray}}^t\right)\right]$ is a matrix of array response vector with dimension $N_t \times N_{cl}N_{ray}$ and $\widetilde{F_{BB}}$ is a $N_{cl}N_{ray} \times N_s$ matrix. The optimal hybrid precoders $F_{RF}^{opt}$ and $F_{BB}^{opt}$ are pbtained from auxiliary variables $A_t$ and $\widetilde{F_{BB}}$ respectively. The $\left\| diag(\widetilde{F_{BB}}\widetilde{F_{BB}^*}) \right\|_0 = N_t^{RF}$ sparsity constraint states that $\widetilde{F_{BB}}$ cannot have more than $N_t^{RF}$ non-zero rows. Therefore $F_{BB}^{opt}$ will be equal to the $N_t^{RF}$ non-zero rows of $\widetilde{F_{BB}^{opt}}$ and the RF precoder $F_{RF}^{opt}$ will be given as the corresponding $N_t^{RF}$ columns of $A_t$.

The algorithm for obtaining the hybrid precoder is summarized in Figure 3.6. First, find a vector $a_t\left(\phi_{il}^t, \theta_{il}^t\right)$ for which the optimal precoder has the maximum projection. Then appends the selected column vectors of $a_t\left(\phi_{il}^t, \theta_{il}^t\right)$ to $F_{RF}$. Once the dominant vector is obtained, the $F_{BB}$ is obtained via least square solution (step 7 of Figure 3.6). Thereafter, the input of selected vector of previous step is removed and the algorithm goes on to find the column for which the "residual precoding matrix" $F_{res}$ has the largest projection. The algorithm continue till all the $N_t^{RF}$ beamforming vectors are obtained. In the end, this process would yield $N_t \times N_t^{RF}$ RF precoder $F_{RF}$ and $N_t^{RF} \times N_s$ baseband precoder $F_{BB}$ which minimizes $\left\|F_{opt} - F_{RF}F_{BB}\right\|_F^2$. The step 10 in Figure 3.6 ensures that the transmitter power constraint is fulfilled.

**Require:** $\mathbf{F}_{\text{opt}}$

1: $\mathbf{F}_{\text{RF}} = \text{Empty Matrix}$

2: $\mathbf{F}_{\text{res}} = \mathbf{F}_{\text{opt}}$

3: **for** $i \leq N_{\text{t}}^{\text{RF}}$ **do**

4: $\quad \mathbf{\Psi} = \mathbf{A}_t^* \mathbf{F}_{\text{res}}$

5: $\quad k = \arg\max_{\ell=1,\ \ldots,\ N_{\text{cl}}N_{\text{ray}}} \left(\mathbf{\Psi}\mathbf{\Psi}^*\right)_{\ell,\ell}$

6: $\quad \mathbf{F}_{\text{RF}} = \left[\mathbf{F}_{\text{RF}} \middle| \mathbf{A}_t^{(k)}\right]$

7: $\quad \mathbf{F}_{\text{BB}} = \left(\mathbf{F}_{\text{RF}}^* \mathbf{F}_{\text{RF}}\right)^{-1} \mathbf{F}_{\text{RF}}^* \mathbf{F}_{\text{opt}}$

8: $\quad \mathbf{F}_{\text{res}} = \frac{\mathbf{F}_{\text{opt}} - \mathbf{F}_{\text{RF}}\mathbf{F}_{\text{BB}}}{\|\mathbf{F}_{\text{opt}} - \mathbf{F}_{\text{RF}}\mathbf{F}_{\text{BB}}\|_F}$

9: **end for**

10: $\mathbf{F}_{\text{BB}} = \sqrt{N_{\text{s}}} \frac{\mathbf{F}_{\text{BB}}}{\|\mathbf{F}_{\text{RF}}\mathbf{F}_{\text{BB}}\|_F}$

11: **return** $\mathbf{F}_{\text{RF}},\ \mathbf{F}_{\text{BB}}$

Figure 3.6: Spatially Sparse Precoding using Orthogonal Matching Pursuit (OMP) from [19]

## 3.4. Conclusion

This chapter presented the Multi user MIMO system model from both uplink and downlink transmission. The millimetre wave channel modelling using Saleh-Vanezula model is discussed in detail along with its under lying assumptions. This is followed by the description of modelling MIMO signal equation from uplink and downlink perspective. The linear processing techniques which are used in digital beamforming are presented along with their principle of operation and their respective performance metric formulas. The last half of the chapter is focused on the hybrid mmWave precoding problem formulation and algorithm description to obtain optimal hybrid precoding vectors.

# 4

# Analysis

This chapter describes the development of simulation environment in MATLAB to evaluate the performance of aforementioned antenna and RF front end topologies for multi-beam generation intended for 5G systems. In millimetre wave frequency band, it was experimentally determined in [33] that most of the signal power resides in line of sight or one dominant path. Therefore in-order to simplify the analysis, only one dominant path or Line of sight path is considered for propagation. It is worthy of note that the proposed model can easily be extended to NLoS scenario if there is a single dominant multi-path component. Monte-Carlo simulations were performed to conduct statistical analysis for multiple possible scenarios of user locations that are served simultaneously in the same frequency sub-band with respect to base station. The first part of the chapter deals with describing the model parameters and model verification analysis. The second part contains all the simulation results of uniformly-fed sub-array, cosecant sub-array and hybrid beamforming using orthogonal matching pursuit algorithm for multibeam generation. In uniformly-fed subarray, there is no optimized beamforming in the elevation domain while in cosecant sub-array; a cosecant power distribution is performed in elevation plane to achieve optimized beamforming. Although, azimuth beamforming in digital domain is performed in both uniformly-fed sub-array and cosecant sub-array. The orthogonal matching pursuit algorithm multibeam generation topology uses phase shifters and adder behind in each antenna element in sub-array to perform beamforming. The OMP performs beamforming in both elevation and azimuth domain.

## 4.1. Model Parameters

The objective was to develop a 5G system behavioural model to assess the performance of beamforming algorithms and find out requirements on the integrated antennas. This model would then be used to evaluate the performance of different antenna topologies, beamforming networks and techniques. The model consists of an array of sub-arrays, each subarray having one input port. There are total 16 subarrays with each subarray containing 12 patch elements referred as uniform linear array (ULA) of arrays from now on in the remainder of report. The number of users are taken to be K=4 which are randomly distributed in a cell of radius 200 meters. The patch element is simulated in MATLAB using FR4 substrate with copper thickness 34 microns and a loss tangent of 0.002 is shown in Figure 4.1(a). The 3D directivity of patch element with maximum value of 7.44 dBi along x-axis is shown in Figure 4.1(b). The geometry of ULA of arrays is presented in Figure 4.1(c) showing different colours for each sub-array. The random user distribution of 4 users for azimuth separation of at-least $1.2 * (\lambda/d)$ radians or more is shown in Figure 4.2(a). One of the random distributions for all users indicating their respective azimuth and elevation angles is shown in Figure 4.2(b). The user equipment is assumed to have a single isotropic antenna element. The focus of this simulation and analyses is on downlink beamforming i.e. from base station to user equipment. The Orthogonal frequency division multiplexing (OFDM) is being proposed and expected to be used for the millimetre wave wideband communication system. In OFDM, a wideband carrier is divided into multiple narrow band carriers. This makes the signal bandwidth less than the channel coherence bandwidth and hence a flat frequency channel can be assumed. Therefore in the designed system, a single narrow band carrier is assumed having 16-quadrature amplitude modulation (16-QAM) with 1,000,000 bits transmission. The geometric modelling used for channel propagation is also assumed to be narrow band with flat frequency response. The rest of

Table 4.1: Model Parameters

| | |
|---|---|
| Array | Uniform Linear Array(ULA) of subarray |
| Antenna Element | Patch |
| Number sub-arrays | 16 |
| Array Axis | yz plane |
| Substrate | FR4 |
| Substrate Thickness | 0.508 mm |
| Copper thickness | 34 microns |
| Relative permittivity | 2.20 |
| Frequency | 28 GHz |
| Array Element Spacing (row and column wise) | 0.5*wavelength |
| Max. radial distance of a user from base station | 200 meters |
| Min. radial distance of a user from base station | 20 meters |
| Azimuth Scan range | $\pm$ 45 degrees |
| Base Station height | 10 meters |
| Number of Users | 4 |
| User Distribution | Random distribution within sector |
| User azimuth separation | $M*(\lambda/D)$ with $M = 0.6, 0.8, 1, 1.2 and 1.4$, D= antenna aperture |
| Directivity of a Cosecant sub-array ($D_{max}$) | 15.70 dB (at the cell edge, i.e. $3^o$ below horizon) |
| Directivity of a normal sub-array ($D_{max}$) | 16.39 dB |
| Power Amplifier Output | +20 dBm |
| Gain of Cosecant sub-array | $G(\theta_n, \phi_n) = 10^{(\frac{D_{max}}{20})} \frac{csc\,\theta_n}{\text{csc}3^o} \sqrt{\cos\phi_n}$ |
| Gain of uniformly fed sub-array | $G(\phi_n) = 10^{(\frac{D_{max}}{20})} \sqrt{\cos\phi_n}$ |
| Directivity of Receiver | 0 dB |
| Noise floor of receiver | -80 dBm |
| Modulation | 16-QAM |
| Number of bits | 1e6 |
| Number of realizations | 1,000 |
| Propagation Scenario | Single dominant path or Line of Sight (LoS) |
| Beamforming Techniques | Adaptive Beam Steering (ABS)<br>Adaptive Beam Steering + Taylor window<br>Zero Forcing beamforming (ZF)<br>Minimum Mean Sqaure Error (MMSE)<br>Grid of Beams (GoBs)<br>Orthognal Matching Pursuit (OMP) |

the simulation parameters are summarized in Table 4.1. The performance at the user end is evaluated and compared for different beamforming techniques using received signal to interference noise ratio (SINR) and bit error rate (BER). The model is used to analyse the impact of minimum inter-user azimuth spacing on system performance metrics (such as SINR & BER) and for determining its optimum value for the simulated scenarios under different beamforming techniques.

In uniform-fed subarray, there is no optimized beamforming in elevation domain. The weights for azimuth beamforming are applied at the inputs of sub-arrays in baseband. The term uniformly-fed sub-array in Table 4.1 refers to a planar phased sub-array without any optimized beamforming in elevation domain. For the case of Cosecant subarray beamforming, the elevation beamforming in each sub-array is achieved by having fixed phase shifting network realized via feed lines. In hybrid beamforming using orthogonal matching pursuit algorithm, the beamforming is divided in analog and digital domains. The digital weights are applied at sub-array level in basedband while the analog weights are applied at each element using phase shifters in RF domain. The path loss to evaluate signal to noise ratio is modelled using free space model.

## 4.2. Model Verification

The simulation model performance was verified before proceeding with further analysis. E. Bjornson et al. in [24] presents results for impact of number of antennas on system capacity for four randomly distributed

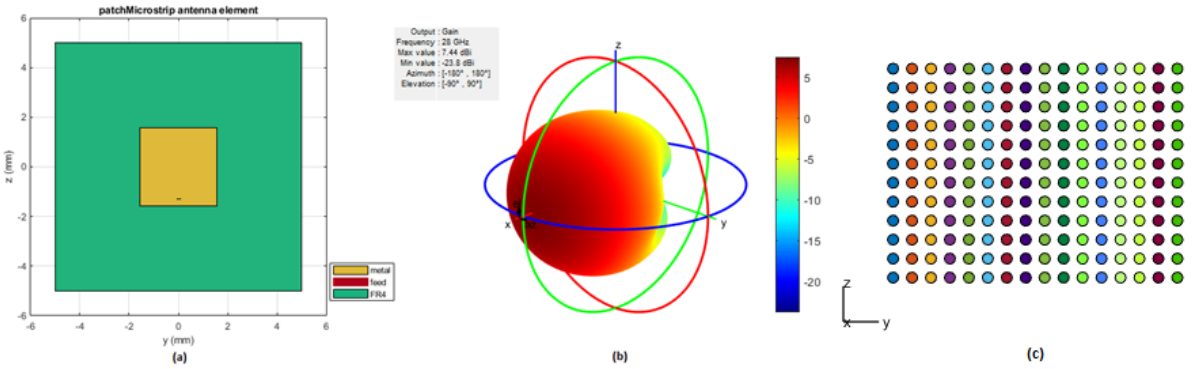


Figure 4.1: (a) Patch Antenna Element (b) 3D-Pattern of Isolated Patch Antenna Element (c) 12 X 16 ULA of subarrays

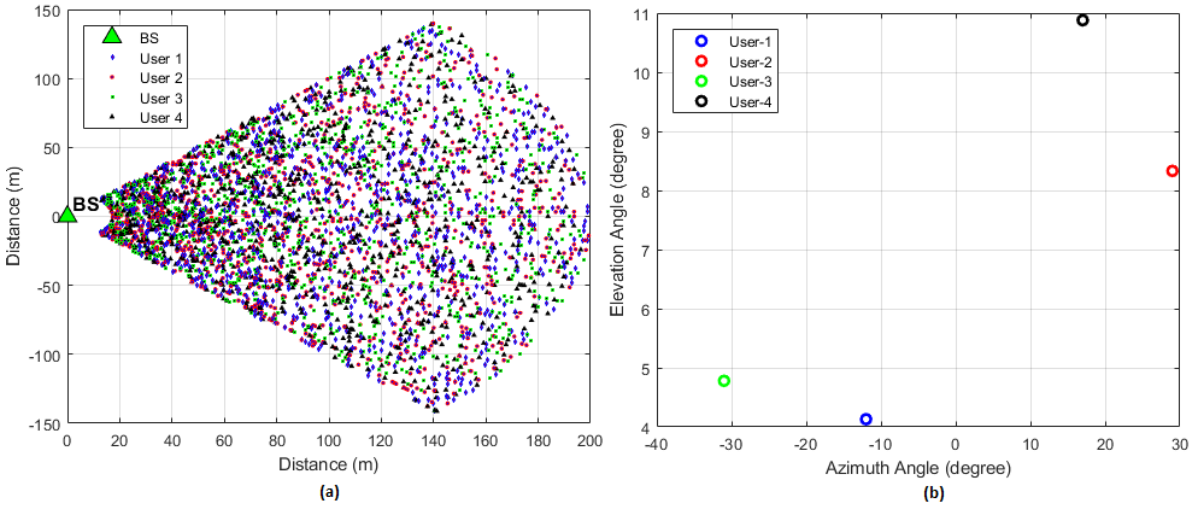


Figure 4.2: (a) Random User distribution of 4 users in a cell with azimuth separation at-least 1.2($\frac{\lambda}{d}$) or more (b) A Sample User distribution randomly selected from a cell

users while using various digital beamforming techniques. The graph in Figure 4.3 (a) and Figure 4.3 (b) shows average sum rate of four randomly distributed users as a function of signal to noise ratio for number of antennas 4 and 12 respectively as presented in [24]. The beamforming techniques used includes Maximum Ratio transmission (MRT), Zero forcing beamforming (ZFBF), and Minimum mean square error (MMSE). The similar scenario of [24] was emulated using the developed system model with the exception of user spacing as it was not mentioned in [24]. The average sum rate of four user having azimuth separation of 15 degrees considering line of sight path for number of antennas 4 and 12 are shown in Figure 4.4(a) and (b) respectively. It can be seen that the plots from the developed model follows the similar pattern as shown by Figure 4.3 for MRT, ZFBF and MMSE. This validates the approach used in this thesis project for the development of simulation model.

## 4.3. Simulation Results

### 4.3.1. Partially Connected Hybrid Beamforming

#### 4.3.1.1. Amplitude tapering window

The sidelobe levels in antenna pattern are a big concern in high density multi user systems. Any energy residing in other than mainlobe (i.e. in sidelobes) can cause interference to adjacent user(s). Therefore a mask is defined in antenna synthesis to reduce the power levels of sidelobes. The amplitude tapering provides a way to decrease the energy in sidelobes at the cost of increase in beamwidth of the mainlobe. So, there is always a

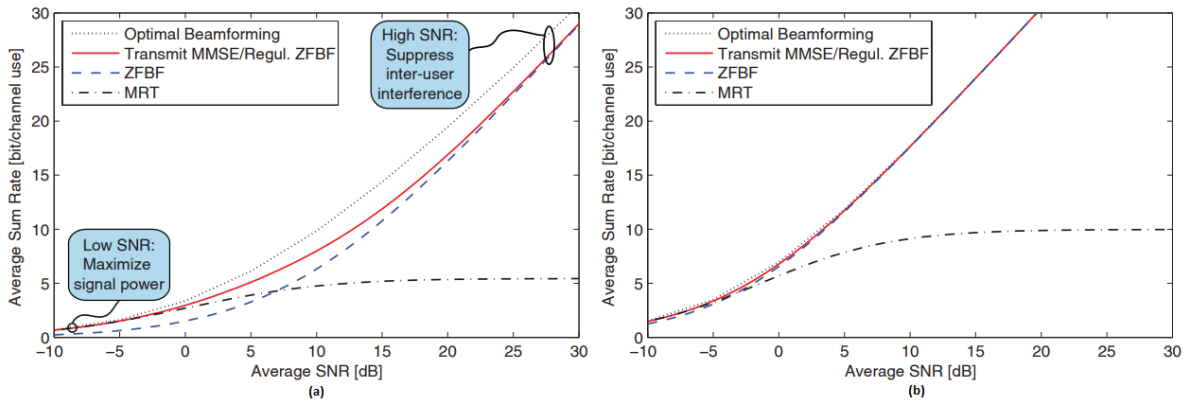


Figure 4.3: Average sum rate for K=4 users in [24] for (a) Number of antennas =4 (b) Number of antennas=12

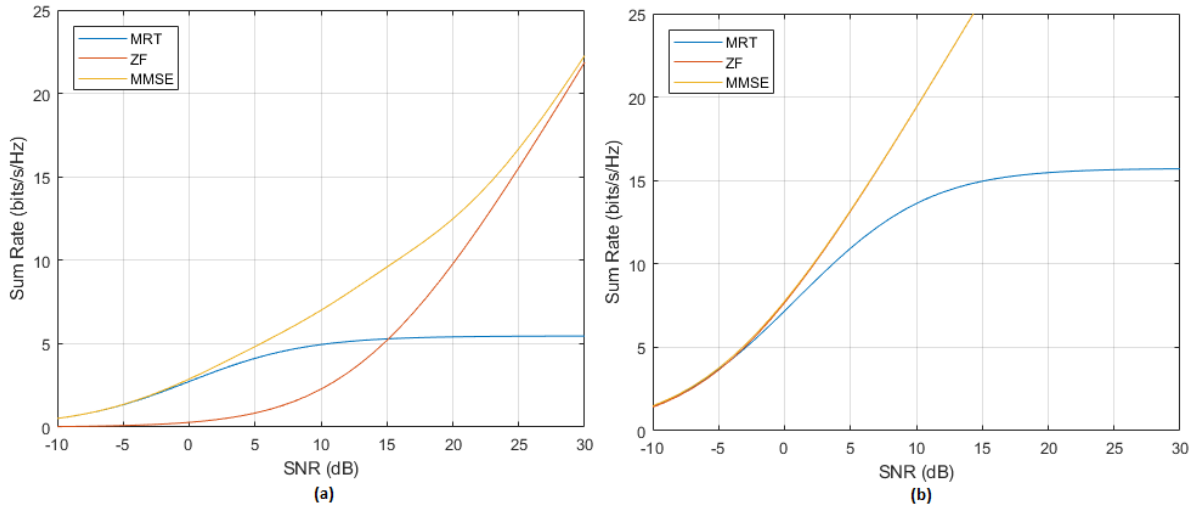


Figure 4.4: Average sum rate for K=4 users of developed model for (a) Number of antennas =4 (b) Number of antennas=12

tradeoff between the level of sidelobe and beamwidth of the system. Generally, sidelobe level is an application and environment specific design parameter. Once the antenna system is designed and fabricated, it cannot be changed. The developed simulation model allows to evaluate the system performance against different sidelobe power levels such as $-20$ dB, $-25$ dB,$-30$ dB etc. Therefore, the impact of different sidelobe power level on the SINR of the overall system is analysed and a comparative study was carried out. The most commonly used windows for amplitude tapering for antenna arrays Chebyshev and Taylor window are selected for the analyses. The Figure 4.5(a) and Figure 4.5(b) presents the cumulative distribution function of SINR for different sidelobe levels for Chebyshev and Taylor window respectively. As it can be seen in Figure 4.5(a) and Figure 4.5(b), initially as the sidelobe power level decreases the SINR performance improved. However after a certain level as it happens to be $-25$ dB in this case, the SINR performance starts to degrade as the sidelobe levels are further reduced. This occurs because of the fact that as the sidelobe levels are further reduced, the beamwidth of the mainlobe increases upto a point where it starts to interfere in adjacent user signal.

The selection criteria was set to be power spread of weighting vector. In MIMO systems with large phased arrays, the efficiency of power amplifier for each RF chain is of high importance. Therefore it is desired that all power amplifiers in the system operates at uniform fixed power level, though the nature of MIMO systems dictates the other way. For a weighting matrix "$W$" and number of users "$k$", the mean power "$\mu$" and the variance "$\sigma^2$" for each antenna is given as:

$$\mu = E\left[\left|\sum_{k=1}^{K} W_{:,k}\right|^2\right]; \qquad \sigma^2 = Var\left[\left|\sum_{k=1}^{K} W_{:,k}\right|^2\right]$$

Where the mean power should be uniform and the variance should be minimum. The overall array power spread "$PS$" can be calculated as:

$$PS = \max(\mu + \sigma^2)/\min(\mu - \sigma^2)$$

Where 0 dB presents the desired ideal constant uniform power feeding. The power spread analysis for sidelobe level of -25dB was performed for Taylor window (n=10) and Chebyshev window. The Taylor window slightly outperformed Chebyshev with a power spread value of 9.72 dB in comparison to 10.28 dB for Chebyshev. Although the difference is not that significant to create a huge impact on systems performance, but Taylor window with n=10 and sidelobe level of -25 dB is selected for the rest of the simulations in this project.

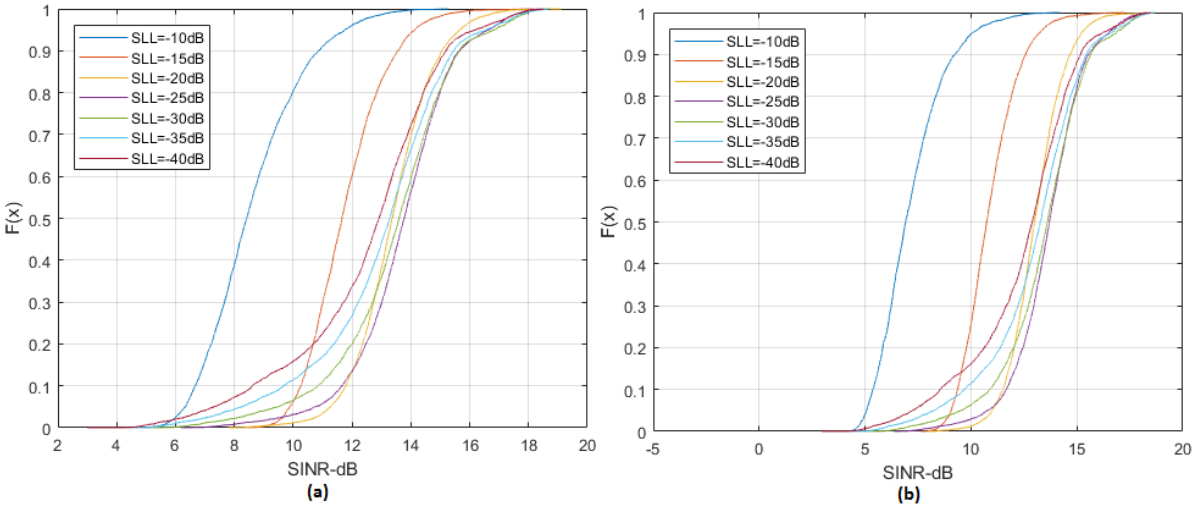


Figure 4.5: CDF-SINR for different sidelobe levels of (a) Chebyshev window (b) Taylor window

### 4.3.1.2. Uniformly-Fed Sub-Array

As stated earlier, the 12 by 16 phased array is divided in to 16 sub-arrays with each sub-array containing 12 elements. For uniformly-fed sub-array approach, all the elements in sub-array are fed in the same phase therefore, no optimized beamforming is achieved in elevation. The beamforming for azimuth scanning is performed only at the input of16-sub-arrays in digital domain as shown in Figure 4.6. The azimuth and elevation cuts for directivity of each subarray is shown in Figure 4.7. The azimuth cut at 0 degree elevation has a very wide beam width due to small aperture size of single sub-array along y-axis with maximum directivity value reaching above 16 dBi (not taking into account mutual coupling effect). The elevation cut as shown in Figure 4.7(b) has a narrow beam width due to longer aperture of sub-array along z axis. However, the directivity has variations and even nulls at some angles along the elevation. Since there is no optimized elevation beamforming, these changes in directivity with respect to elevation can cause degradation in overall system performance. The antenna patterns using different beamforming techniques for a randomly selected user distribution in a cell of Figure 4.2(b) is shown in Figure 4.8. As it can be seen in Figure 4.8, some users have higher gain than the other; this is because of the difference in elevation angle among the users. Therefore the large variation in elevation directivity pattern for phased planar sub-array results in large difference in antenna gain for the users at different elevation angles. This variation in turn effects the systems SINR and BER as will be discussed in the upcoming paragraph.

The cumulative distribution function (CDF) for the received signal to interference noise ratio (SINR) at the users end is evaluated and plotted for precoding techniques such as ABS, ABS with Taylor window having sidelobe level -25 dB, ZF and MMSE. The inter-user azimuth spacing is varied from $0.6(\lambda/D)$ radians to $1.2(\lambda/D)$ radians with the steps of $0.2(\lambda/D)$ for all beamforming techniques and is shown in Figure 4.9. The notion for inter-user spacing is used in radians in the form of $\lambda/D$ instead of a more conventional separation in degrees. Since the antenna design parameters such as beamwidth (can be approximated as $0.89(\lambda/D)$ are specified in terms of lambda $\lambda$ and aperture of antenna (D), therefore the user spacing interms of $\lambda/D$ builds an intuitive bridge between system performance metrics (SINR and BER) and antenna design parameters via

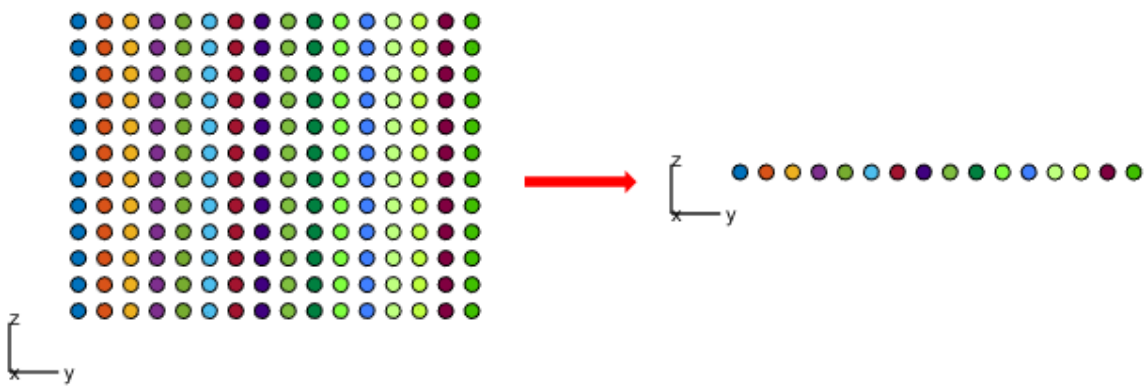


Figure 4.6: Beamforming performed at 16 subarrays for Uniformly-fed Phased Sub-array system

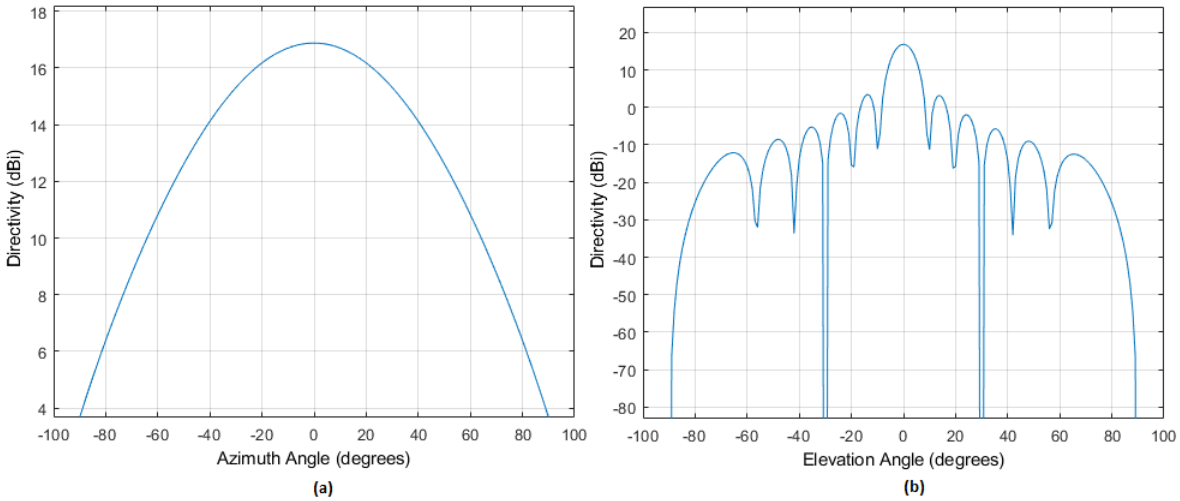


Figure 4.7: Uniformly-fed Phased Sub-array (a) Azimuth cut (elevation= $0^o$) (b) Elevation cut (azimuth=$0^o$)

user spacing.

The Figure 4.9(a) presents the CDF of SINR for adaptive beam steering precoding. The user separation $0.6(\lambda/D)$ yields the lowest CDF of SINR among all simulated user separations. Since the $0.6(\lambda/D)$ radians user spacing is less than the beamwidth of the antenna, therefore this results indicates high interference from the sidelobes of adjacent users. As the user separation is increases, the SINR value improves and converges to a final value of 15.79 dB for higher percentile of users; however the increase margins become very small for any user spacing $\lambda/D$ or beyond. The amplitude distribution or windowing operation on beamforming weights can be used to decrease the sidelobe level (SLL) at the cost of increase in beamwidth of antenna. The beamwidth determines the minimum user separation hence the number of concurrent users being served in a cell. The Figure 4.9(b) graph shows SINR for beamsteering with Taylor window amplitude distribution with sidelobe level of -25 dB. Due to the increase in beamwidth, the SINR for low angular user separation decrease. The decrease for $0.6(\lambda/D)$ is quite high as compared to $0.8(\lambda/D)$. The SINR improved slightly for user separation $\lambda/D$ however the SINR value dramatically improved as the users are well separated with $1.2(\lambda/D)$ and $1.4(\lambda/D)$ radians respectively. The graph in Figure 4.9(c) presents the SINR for zero forcing beamforming. As in zero forcing techniques null are created at the location of simultaneous co-frequency users, therefore all the user separations from $0.6(\lambda/D)$ to $1.2(\lambda/D)$ has almost similar SINR values. In addition to that the CDF converges to a slightly higher value of 16.27 dB then ABS. The MMSE beamforming produce quite similar results to zero forcing as presented in Figure 4.7(d) with the a small degradation of less than a percentile for $0.6(\lambda/D)$. The similar performances of zero forcing and MMSE also indicates that the system

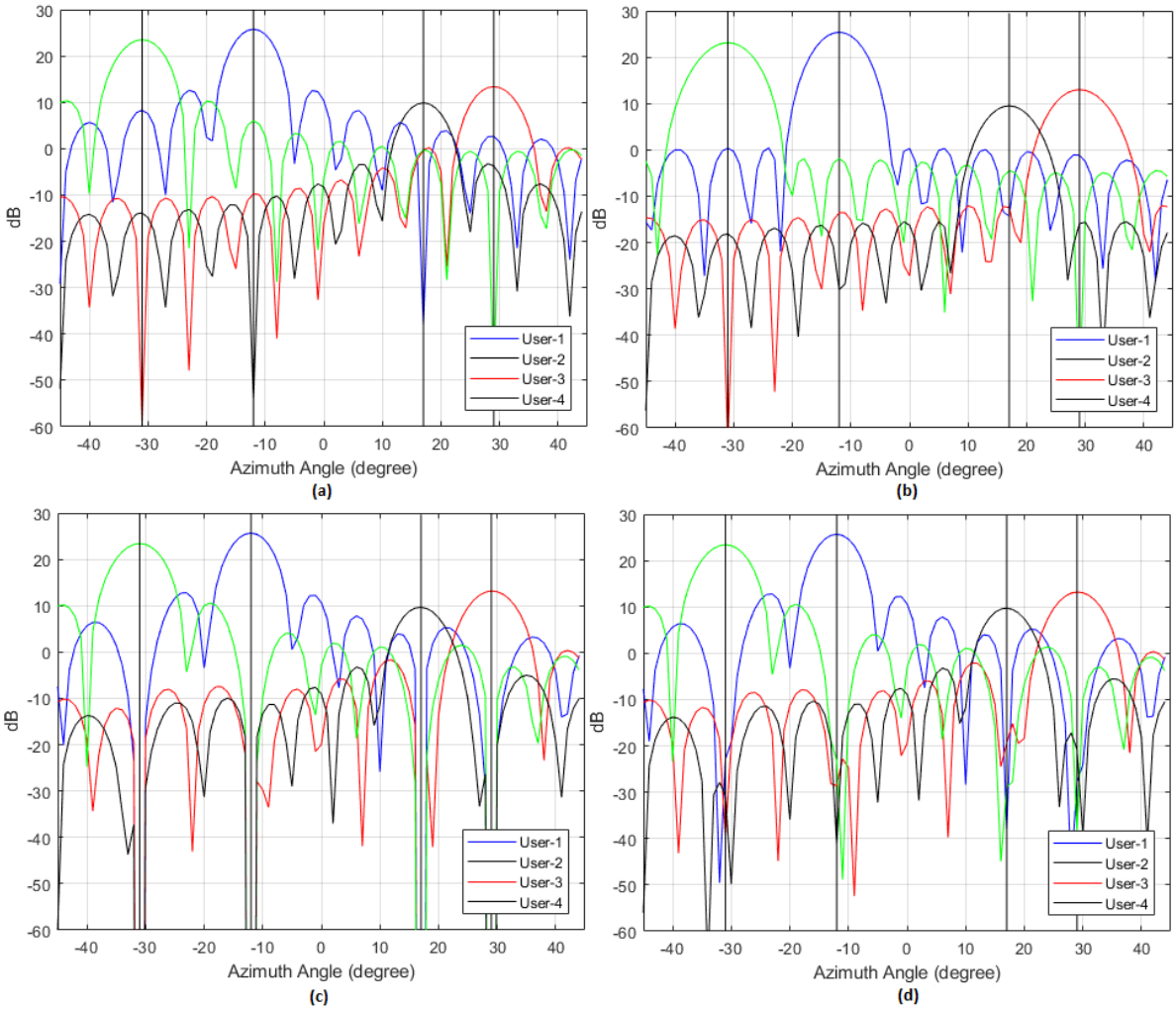


Figure 4.8: Antenna Patterns of Uniformly-fed phased sub-array for sample user distribution using (a) ABS (b) ABS with Taylor window (c) Zero Forcing beamforming (d) MMSE beamforming

under simulation is more interference dominated then noise.

The impact of user separation on bit error rate is same as of on signal to interference noise ratio. Figure 4.10 shows the Cumulative distributive function of bit error rate for ABS, ABS with Taylor window, ZF and MMSE beamforming. All the beamforming techniques converges to a very high final value of bit error rate (i.e. 0.5). This indicates majority of the users in the cell are not able to receive the correct data for the simulated link budget. Those users who got the correct data follows a similar trend as for SINR. The BER for $0.6(\lambda/D)$ is the worst among all inter-user azimuth separations. The Taylor window amplitude distribution reduces the BER performance for inter-user separations less than $\lambda/D$ and improves BER for above than that. The user separation from $0.6(\lambda/D)$ to $1.2(\lambda/D)$ has no impact on BER performance for zero forcing and MMSE. The final converged BER value for ZF and MMSE is smaller as compared to ABS and ABS with Taylor distribution.

In mobile communication system performance is usually evaluated for worst case scenario i.e. at cell edge or $5^{th}$ percentile of cumulative distribution function (CDF) [39]. Therefore for SINR, $5^{th}$ percentile CDF (i.e. 95% of the users would have SINR equal to or greater than this value) and $95^{th}$ percentile CDF for BER (i.e. 95% of the users would have BER equal to or less than this value). The Table 4.2 presents the values of $5^{th}$ percentile SINR for different user separations using various beamforming techniques and Figure 4.11(a) presents its graph. As it is evident from the Table 4.2 and Figure 4.11(a), that $5^{th}$ percentile SINR for phased array is in negative and it gets worse with the application of beamforming. Similar effect of worsening BER is observed for $95^{th}$ percentile as shown in Table 4.3 and Figure 4.11(b). This shows that for the system under simulation, the $5^{th}$ percentile SINR and $95^{th}$ percentile BER performance at user end are quite worse using uniformly-fed sub-array multi beam generation. Therefore if the system performance needs to be improved,

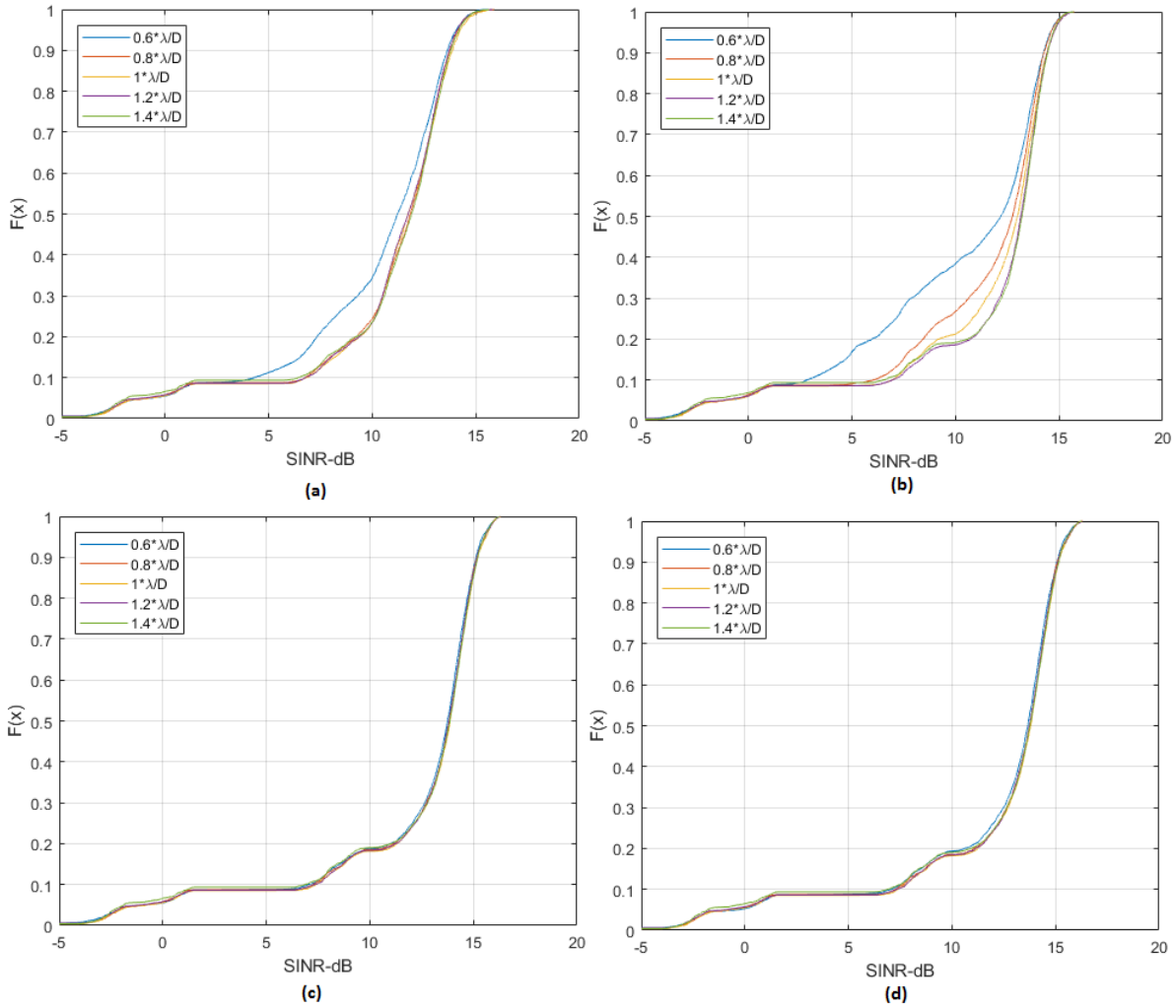


Figure 4.9: Uniformly-fed Phased sub-array CDF-SINR for (a) ABS (b) ABS with Taylor window (SLL=-25dB) (c) Zero-Forcing (d) MMSE

the link budget parameters would require to be modified which in most cases are constraints and costly or beamforming methodology needs to be changed.

Table 4.2: $5^{th}$ Percentile SINR in dB for Uniformly-fed Phased Sub-array

| **Beamforming Technique** | **$5^{th}$ Percentile SINR in dB for 4 Users with azimuth separation in radians** | | | | |
|---|---|---|---|---|---|
| | $0.6(\lambda/D)$ | $0.8(\lambda/D)$ | $1.0(\lambda/D)$ | $1.2(\lambda/D)$ | $1.4(\lambda/D)$ |
| **ABS** | -0.70 | -0.80 | -0.79 | -1.09 | -1.86 |
| **ABS with Taylor Window (SLL=-25 dB)** | -1.27 | -1.14 | -1.15 | -1.32 | -2.18 |
| **ZF** | -0.83 | -0.84 | -0.81 | -1.14 | -1.89 |
| **MMSE** | -0.45 | -0.73 | -0.73 | -0.93 | -1.79 |

### 4.3.1.3. Cosecant Sub-Array

In the previous section, the SINR and BER analyses for multi-beam generation without optimized beamforming in elevation using uniformly-fed sub-array was presented. It worked well for users which lies in the elevation angle range where the gain is maximum. However, for users who lie at elevation pattern null or other elevation angles with low elevation gain, the SINR and BER performance severely degraded. This effect was also reflected in $95^{th}$ percentile results with negative SINR values and BER approaching 0.5. This shows that

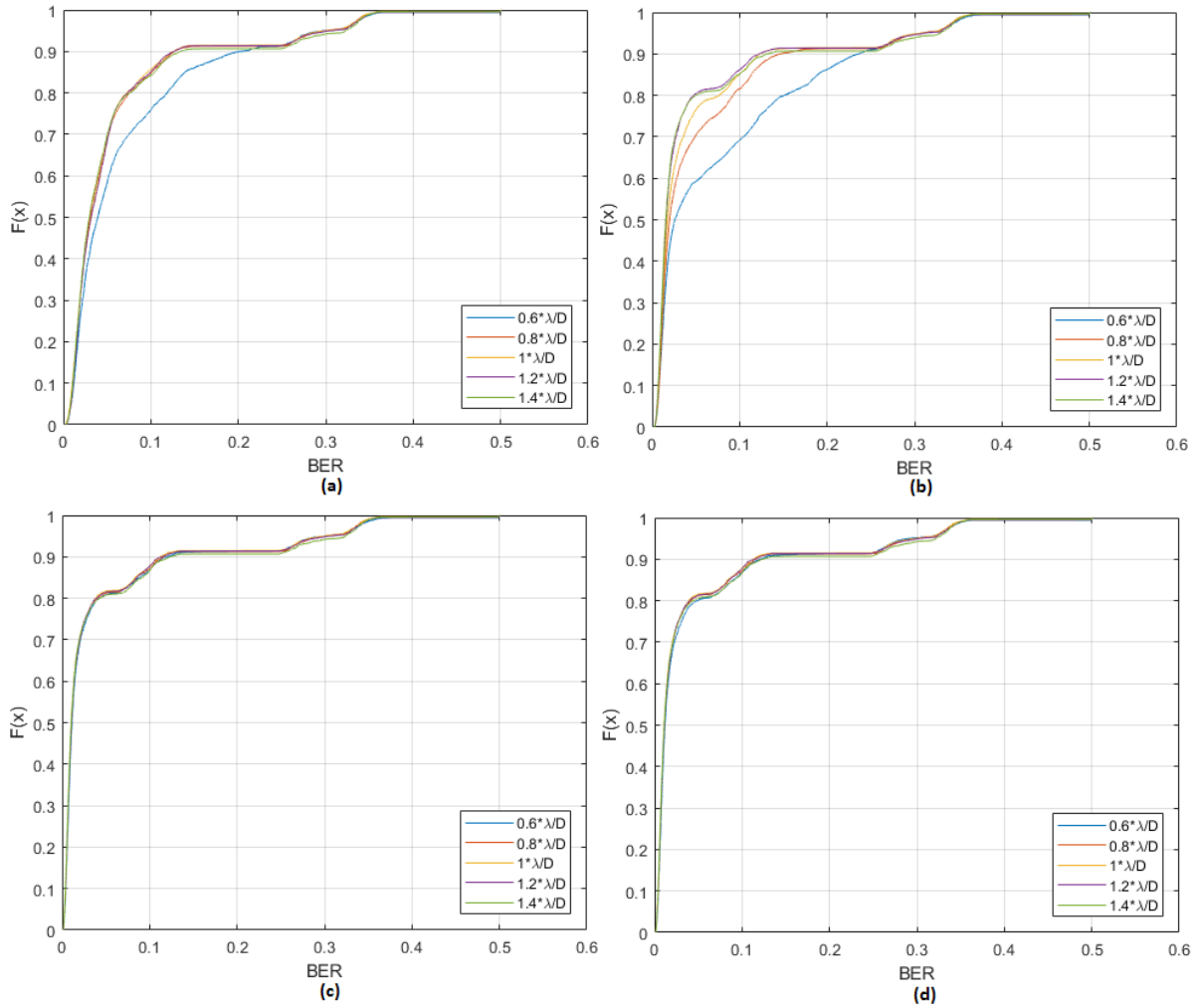


Figure 4.10: Uniformly-fed Phased Sub-array CDF-BER for (a) ABS (b) ABS with Taylor window (SLL=-25dB) (c) Zero-Forcing (d) MMSE

Table 4.3: $95^{th}$ Percentile BER for Uniformly-fed Phased Sub-array

| **Beamforming Technique** | $95^{th}$ **Percentile BER for 4 Users with azimuth separation in radians** | | | | |
|---|---|---|---|---|---|
| | $0.6(\lambda/D)$ | $0.8(\lambda/D)$ | $1.0(\lambda/D)$ | $1.2(\lambda/D)$ | $1.4(\lambda/D)$ |
| **ABS** | 0.297 | 0.301 | 0.300 | 0.304 | 0.323 |
| **ABS with Taylor Window (SLL=-25 dB)** | 0.311 | 0.308 | 0.308 | 0.310 | 0.330 |
| **ZF** | 0.300 | 0.301 | 0.301 | 0.305 | 0.324 |
| **MMSE** | 0.291 | 0.299 | 0.299 | 0.302 | 0.322 |

phased planar sub-array with no elevation scanning cannot be used with the applied link budget. In order to overcome this problem, instead of modifying any other link budget parameter; the optimized beamforming is introduced in each sub-array.

The ambition of this optimized beamforming is to produce an elevation pattern that provide highest gain to the farthest user and the lowest to the nearest one. At the same time in-order to keep the system less complex and power hungry, cosecant power distribution in elevation domain was implemented as shown in Figure 4.12(b). This elevation pattern has the highest gain at the angle 3 degrees below horizon and it decreases as the user elevation angle increases (i.e. as user approaches base station) [37]. Despite the decrease in elevation gain as user comes closer to Base station, the mean gain value across all elevation angles is higher

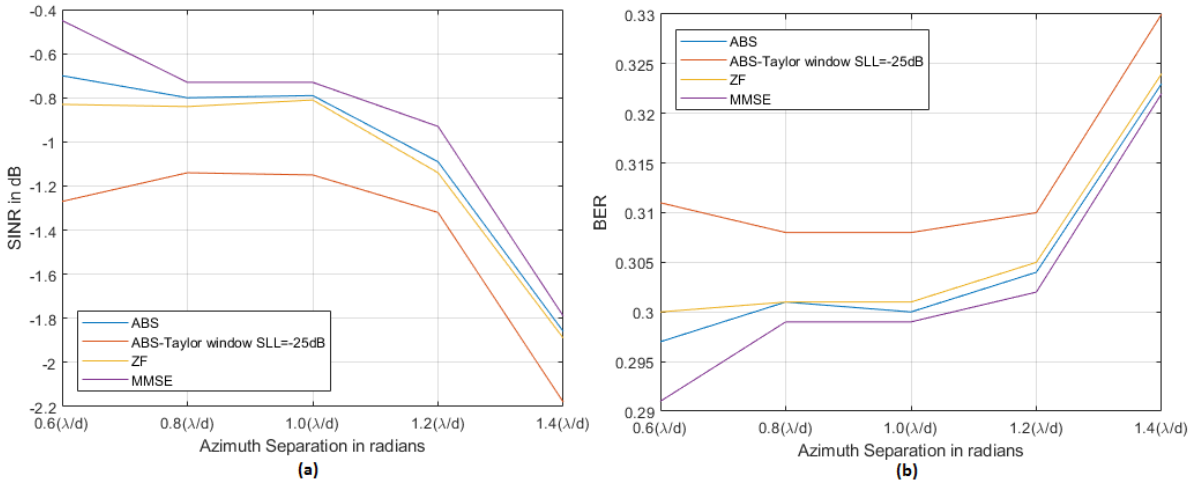


Figure 4.11: Performance of various Beamforming techniques under different user separation at cell edge using Uniformly-fed Phased Sub-array (a) $5^{th}$ percentile CDF for SINR (b) $95^{th}$ percentile for BER

than uniformly fed sub-array with no optimized elevation beamforming. The azimuth cut with elevation angle zero degrees for a sub-array remains the same as shown in Figure 4.12(a). The antenna patterns generated of a sample user distribution for different beam forming techniques using cosecant sub-array are shown in Figure 4.13. In comparison to antenna patterns of uniformly-fed sub-array shown in Figure 4.8, the cosecant power distribution in elevation provides higher gain to user 2 and user 4 of about 4 dB to 6 dB. Thus the variation in elevation gain for user at different elevation angles is drastically reduced as compared to uniformly-fed sub-array. This improvement of gain for users is also reflected in SINR and BER analysis.

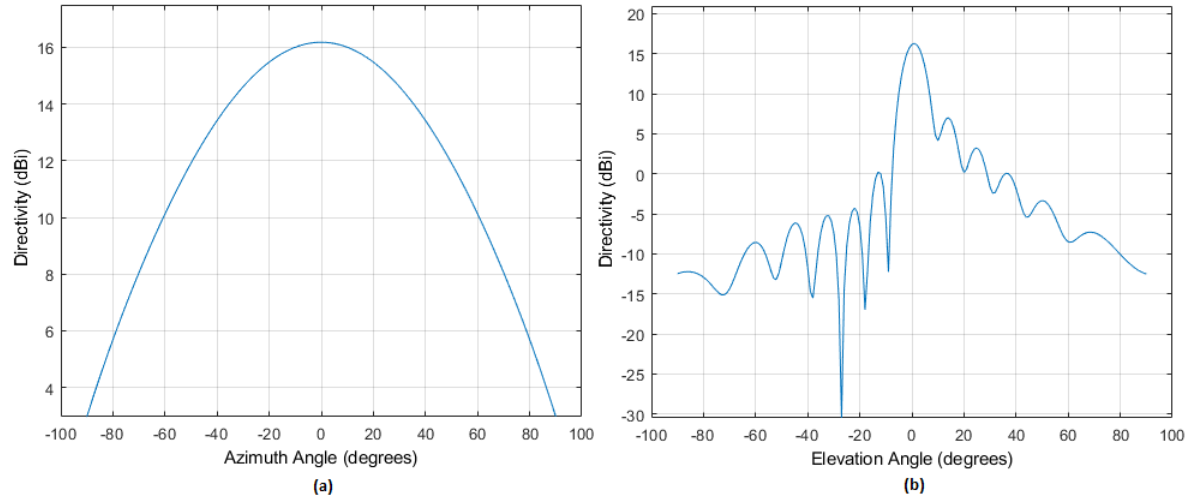


Figure 4.12: Cosecant Sub-array (a) Azimuth cut (elevation=$0^o$) (b) Cosecant Elevation cut (azimuth=$0^o$)

The cumulative distribution function of SINR using all beamforming technique is shown in Figure 4.14. A similar pattern as of in the case of planar phased sub-array is observed on SINR performance with respect to inter-user azimuth spacing. For adaptive beam steering, the 0.6*($\lambda/D$) has the lowest SINR among all user separation. The improvement in SINR starts to saturate for any user separation above 0.8*($\lambda/D$) and converges to a final value of 18.07 dB, about 2.3 dB higher than uniformly sub-array system. The SINR for adaptive beam steering with Taylor window amplitude distribution is shown in Figure 4.14(b). The SINR performance for 0.6*($\lambda/D$) and 0.8*($\lambda/D$) has degraded as compared to only adaptive beam steering due to increase in beam width, thus increase in adjacent user interference while SINR for $\lambda/D$ remains same. However, the SINR value for user separation beyond $\lambda/D$ improved by more than 1 dB and converges to a final value of 18.76 dB. The final converged value of SINR for zero-forcing and MMSE is about 0.5 dB better than

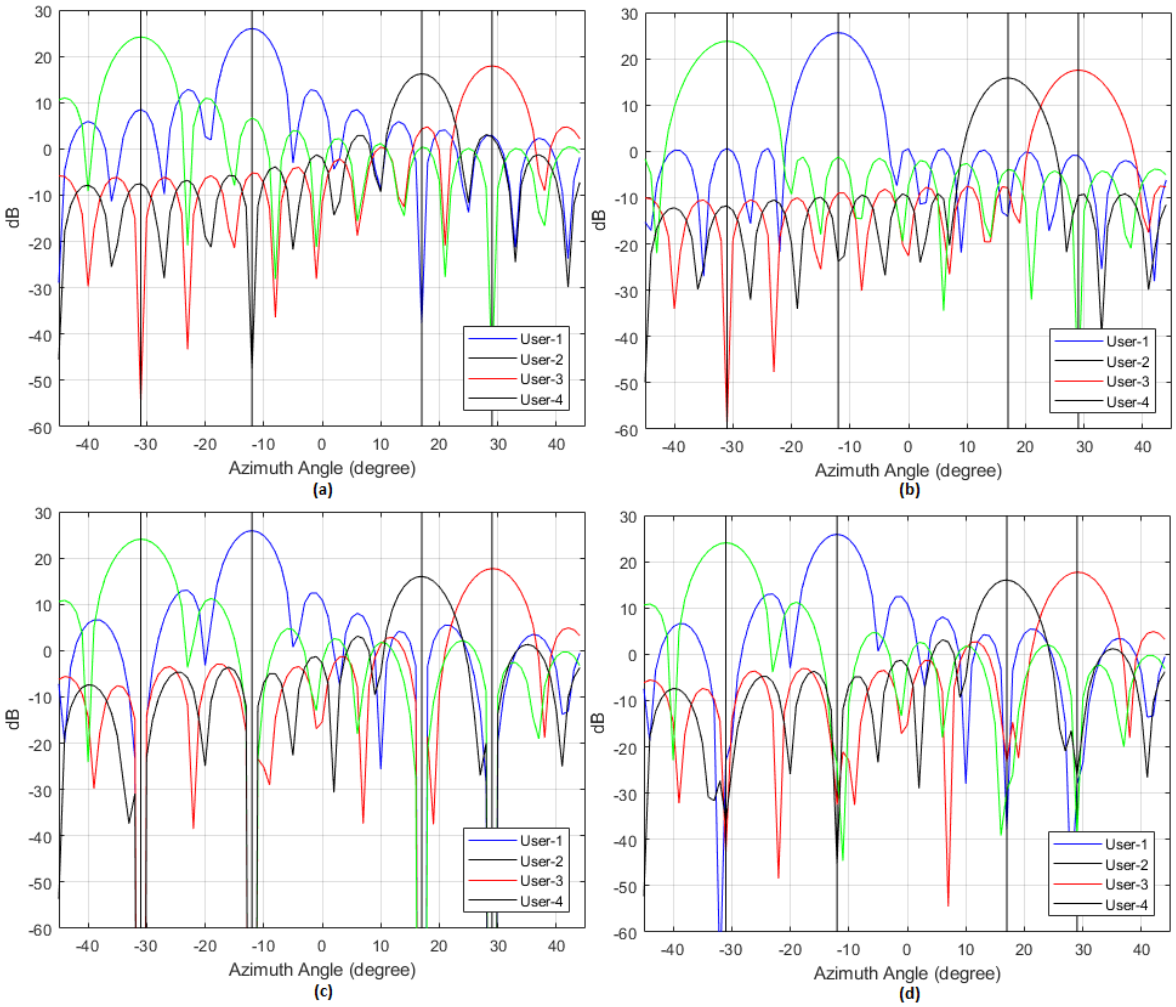


Figure 4.13: Antenna Patterns of Cosecant phased planar sub-array for sample user distribution using (a) ABS (b) ABS with Taylor window (c) Zero Forcing beamforming (d) MMSE beamforming

ABS with Taylor window with 19.62 dB. In addition to that, bit error rate analysis was also carried out for the cosecant phased planar sub-array using different user separations. Similar conclusions were drawn about the impact of inter-user separation on BER as for the case of SINR. The zero-forcing and MMSE beamforming outperformed adaptive beam steering and adaptive beam steering with Taylor window distribution.

In-order to evaluate the performance of different beamforming techniques for cosecant phased planar sub-array, a numerical analysis for 95 percent of the users is considered. The 5th percentile SINR is presented in Table 4.4 and shown as graph in Figure 4.16(a). For user separation less than $\lambda/D$, the adaptive beam steering performs better than adaptive beam steering with Taylor window amplitude distribution by a margin of 1.5 dB or more. However for user separation $\lambda/D$ and above, Taylor window amplitude distribution performs better from 0.5 dB to 1.5 dB for separations $\lambda/D$, 1.2*($\lambda/D$) and 1.4*($\lambda/D$) respectively. The zero forcing and MMSE maintains almost similar SINR for all user spacing outperforming other beamforming techniques. However the performance gap reduces as the user spacing increases with the margin reduces to 0.5 dB for user spacing 1.2*($\lambda/D$) and 1.4*($\lambda/D$) respectively. Correspondingly, the $95^{th}$ percentile bit error rate value are shown in Table 4.5 and plotted in Figure 4.16(b). The BER results follow the same analogy as of SINR. The BER value for beamsteering decreases as the user spacing increases and reduces to half of the value it had at 0.6*($\lambda/D$), at 1.4*($\lambda/D$). The beamsteering with Taylor window amplitude distribution outperforms normal beamsteering for user spacing above $\lambda/D$ and approaches zero-forcing and MMSE as shown in Figure 4.16(b). The zero-forcing and MMSE maintained same BER values for all user spacing's along with having the lowest BER among all the beamforming techniques.

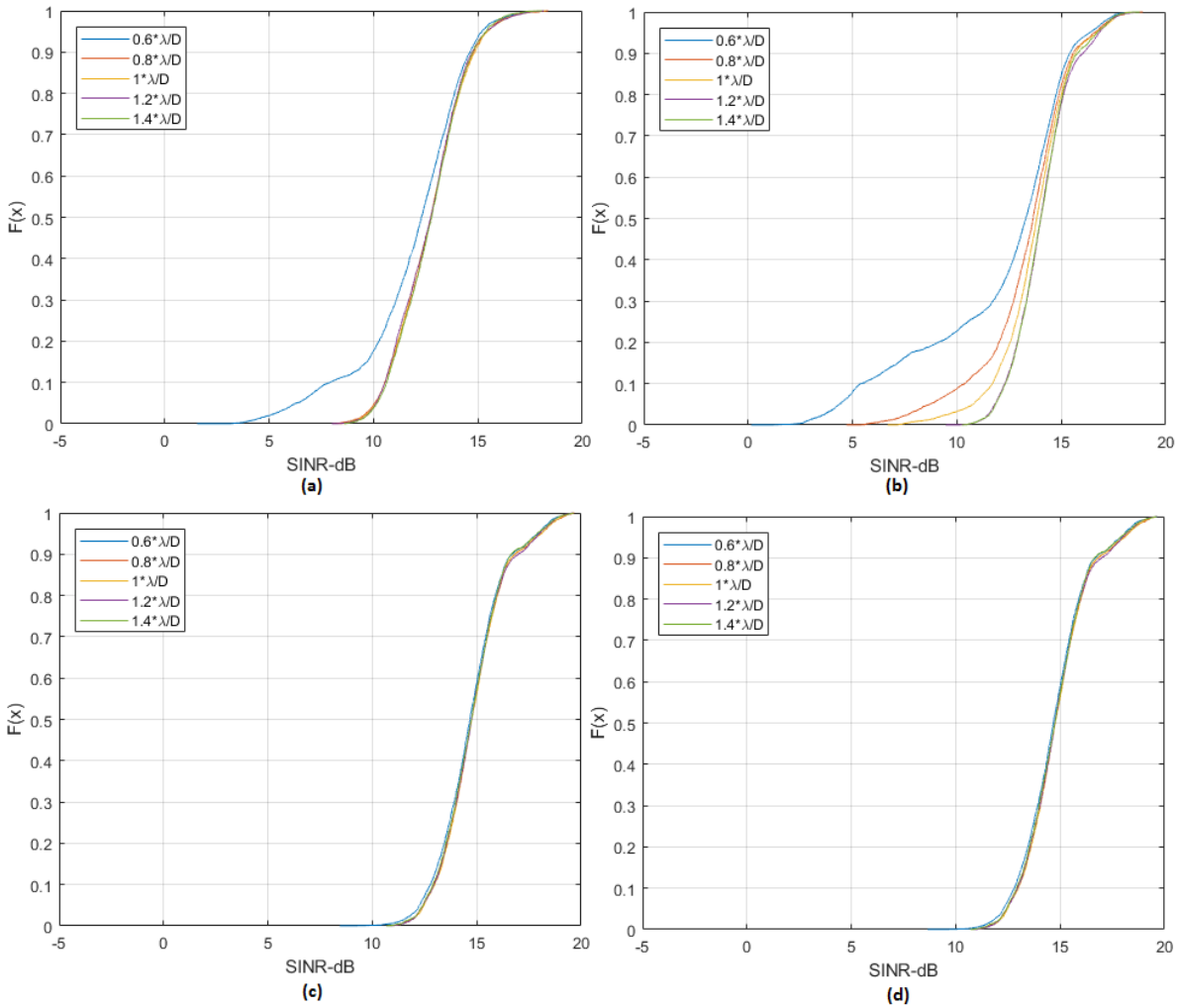


Figure 4.14: Cosecant Phased sub-array CDF-SINR for (a) ABS (b) ABS with Taylor window (SLL=-25dB) (c) Zero-Forcing (d) MMSE

Table 4.4: $5^{th}$ Percentile SINR in dB for Cosecant Phased Sub-array

| **Beamforming Technique** | **$5^{th}$ Percentile SINR in dB for 4 Users with azimuth separation in radians** | | | | |
|---|---|---|---|---|---|
| | $0.6(\lambda/D)$ | $0.8(\lambda/D)$ | $1.0(\lambda/D)$ | $1.2(\lambda/D)$ | $1.4(\lambda/D)$ |
| **ABS** | 6.30 | 10.04 | 10.11 | 10.11 | 10.17 |
| **ABS with Taylor Window (SLL=-25 dB)** | 4.38 | 8.72 | 10.76 | 11.82 | 11.85 |
| **ZF** | 12.26 | 12.45 | 12.47 | 12.43 | 12.43 |
| **MMSE** | 12.29 | 12.46 | 12.48 | 12.44 | 12.44 |

### 4.3.1.4. Grid of Beams Cosecant Sub-Array

The grid of beam (GoB) method creates multiple beams using pre-computed weights for different spatial directions. The grid of beam offers a very effective and yet relatively less complex way for generating multiple beams. The aim of this investigation is to combine GoB with cosecant power distribution for sub-array to come up with a computationally less extensive system and evaluates its performance against adaptive beamforming techniques. The grid of beams was created by using different cross over points of between adjacent beams (i.e. dB down from respective mainlobe) for the azimuth scanning range of ± 45 degrees. For various cross over points, azimuth angles were identified and then their respective weighting vectors are created. The Table 4.6 presents the azimuth angles at adjacent beam cross over points (in dB) of 1dB, 2dB and 3.9dB

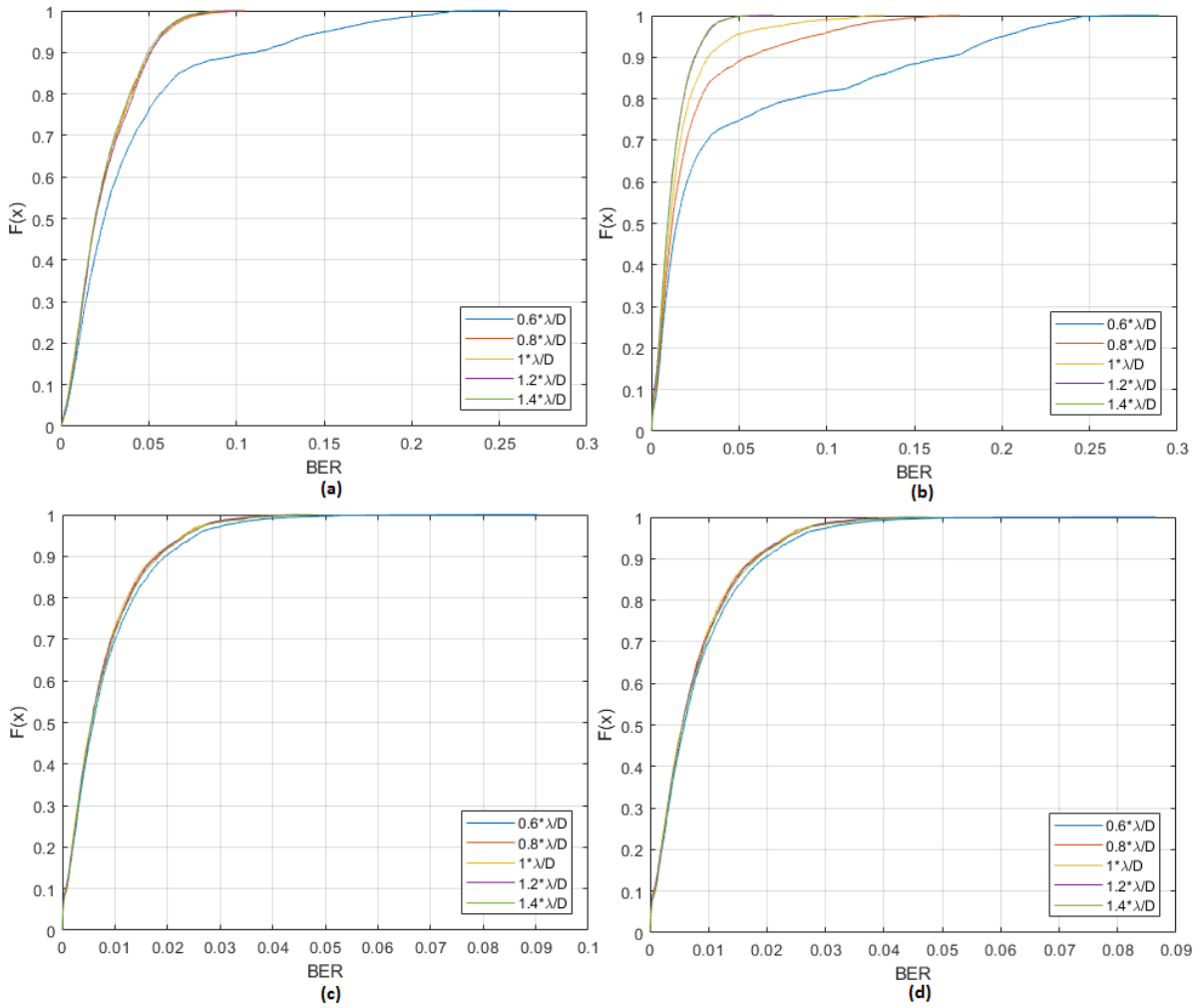


Figure 4.15: Cosecant Phased Array CDF-BER for (a) ABS (b) ABS with Taylor window (SLL=-25dB) (c) Zero-Forcing (d) MMSE

Table 4.5: $95^{th}$ Percentile BER for Cosecant Phased Sub-array

| **Beamforming Technique** | $95^{th}$ **Percentile BER for 4 Users with azimuth separation in radians** | | | | |
|---|---|---|---|---|---|
| | $0.6(\lambda/D)$ | $0.8(\lambda/D)$ | $1.0(\lambda/D)$ | $1.2(\lambda/D)$ | $1.4(\lambda/D)$ |
| **ABS** | 0.151 | 0.061 | 0.059 | 0.059 | 0.058 |
| **ABS with Taylor Window (SLL=-25 dB)** | 0.201 | 0.090 | 0.047 | 0.031 | 0.031 |
| **ZF** | 0.025 | 0.023 | 0.023 | 0.023 | 0.023 |
| **MMSE** | 0.025 | 0.023 | 0.023 | 0.023 | 0.023 |

with and without Taylor window respectively (since windowing increases the beamwidth, hence this results in different cross over point angles for windowing). The antenna patterns for identified cross over angles mentioned in Table 4.6 with and without Taylor window amplitude distribution are plotted in Figure 4.17 and Figure 4.18 respectively. For the case of without Taylor windowing, in 2 dB GoB; the mainlobe of each beam lies at the second sidelobe of the neighbouring beam of its adjacent beam as shown in Figure 4.17(b). The GoB for 3.9 dB without Taylor windowing produces orthogonal beams i.e. at the maximum of mainbeam, other beams have nulls as shown in Figure 4.17(c). The application of Taylor windowing reduces the sidelobes at the cost of increase beamwidth and thus loss of orthogonality in the case of 3.9dB GoB.

The statistical analysis for the performance evaluation of grid of beams approach is performed on the already developed simulation model. The number of users are considered to be 4, randomly distributed in the

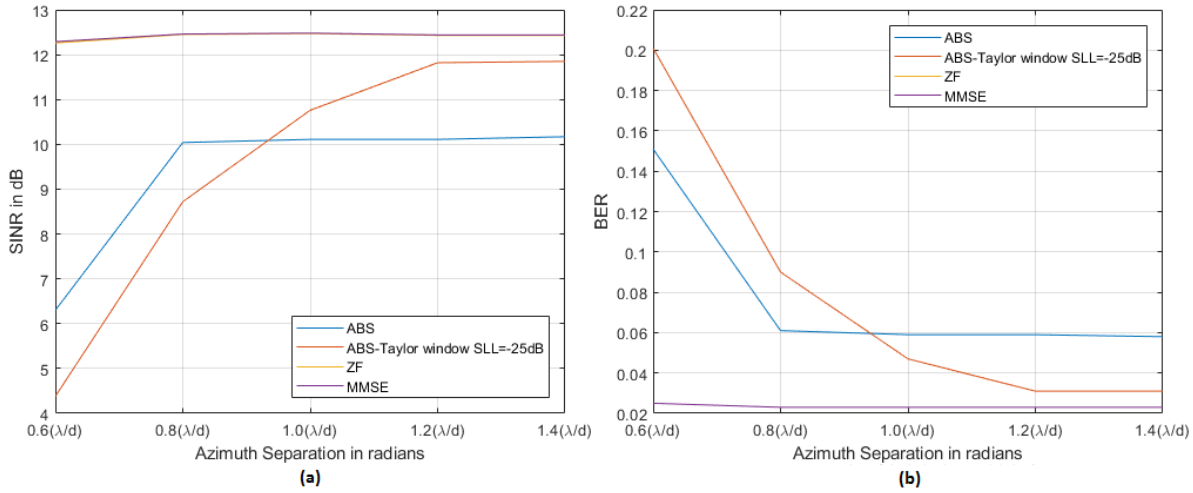


Figure 4.16: Performance of various Beamforming techniques under different user separation at cell edge using Cosecant Phased Sub-array (a) 5th percentile CDF for SINR (b) 95th percentile for BER

Table 4.6: Azimuth Angles for different Beam Cross over points

| **Main lobe Azimuth angles in degrees at Consecutive Beams cross-over points (i.e dB down from the mainlobe) for a scan range of ±45 degrees** | | | | | |
|---|---|---|---|---|---|
| **With-out Taylor window** | | | **With Taylor window** | | |
| **3.9 dB** | **2 dB** | **1 dB** | **3.9 dB** | **2 dB** | **1 dB** |
| -38.75 | -39.75 | -40.75 | -36.25 | -37.5 | -43.5 |
| -30 | -33.25 | -36 | -26.25 | -32 | -37.75 |
| -22 | -27.25 | -31.5 | -17.25 | -25 | -32.5 |
| -14.75 | -21.5 | -27.25 | -8.5 | -18.5 | -27.5 |
| -7.25 | -16 | -23 | 0 | -12.5 | -22.75 |
| 0 | -10.5 | -19 | 8.5 | -6.25 | -18 |
| 7.25 | -5.25 | -15 | 17.25 | 0 | -13.5 |
| 14.75 | 0 | -11.25 | 26.25 | 6.25 | -9 |
| 22 | 5.25 | -7.5 | 36.25 | 12.5 | -4.5 |
| 30 | 10.5 | -.3.75 | | 18.5 | 0 |
| 38.75 | 16 | 0 | | 25 | 4.5 |
| | 21.5 | 3.75 | | 32 | 9 |
| | 27.25 | 7.5 | | 37.5 | 13.5 |
| | 33.25 | 11.25 | | | 18 |
| | 39.75 | 15 | | | 22.75 |
| | | 19 | | | 27.5 |
| | | 23 | | | 32.5 |
| | | 27.25 | | | 37.75 |
| | | 31.5 | | | 43.5 |
| | | 36 | | | |
| | | 40.75 | | | |

cell. Like the previous analysis for the cases of cosecant sub-array it was observed that for inter user azimuth separation 1.2*($\lambda/D$) radians or beyond, the increase in SINR performance gets saturated as also depicted in Figure 4.16(a). Therefore, the comparative analysis for different GoB's was performed for user distribution with separation at least 1.2*($\lambda/D$) radians or more. The SINR performance of all the GoB's was compared with the SINR performance of ZF and MMSE precoding techniques. The rest of the simulation parameters

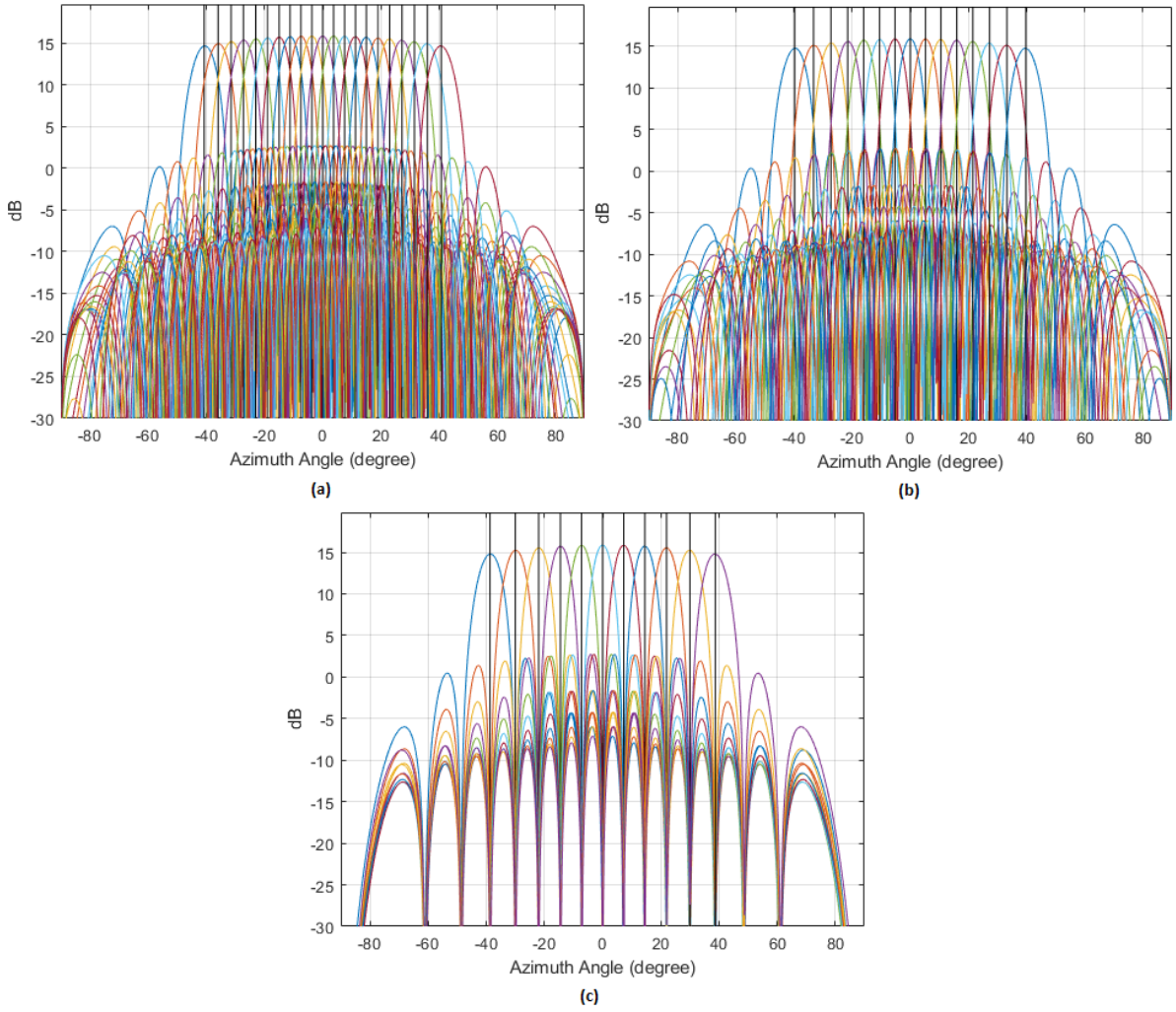


Figure 4.17: Antenna Grid of beam without-Taylor window for cross-over of (a) 1dB (b) 2dB (c) 3.9 dB

are same as used in the previous section. Figure 4.19 presents the cumulative distribution function of SINR for different GoB, ZF and MMSE. The linear precoding technique such as ZF and MMSE yields the best SINR performance with converging to final value of 19.66 dB as shown in Figure 4.19. Among all the GoB's without Taylor windowing, the 1 dB GoB performs better as compared to other. This high performance can be attributed to the fine angular resolution and more number of beams in the grid. It is closely followed by the 2dB GoB curve of SINR. The 3.9dB GoB performs worst among all the without amplitude tapered techniques for less than $50^{th}$ percentile. However for $55^{th}$ percentile or above, the 3.9dB GoB performs better than 2dB GoB and beyond $70^{th}$ percentile it outperforms 1dB GoB also. Thereafter it converges to final value of 19.66 dB. The underperformance for lower percentile is due to its lower spatial resolution less number of beams in the grid. Therefore, in most cases user lies out of its mainlobe and thus receives low power. The sudden rise in SINR performance and even surpassing 1dB and 2 dB GoB's for higher percentile stems from the orthogonal nature of grid of beams. If the intended user lies in the mainlobe, it would receive zero interference signal. These instances would result in a very high SINR values thus outperforming 1 dB and 2 dB GoB's for those cases.

The Taylor window amplitude distribution GoB's overall performs better than uniform amplitude distribution GoB's. Here also, the 1dB GoB performs better among all other tapered GoB followed by 2dB and 3.9 dB GoB's respectively. However unlike its un-tapered counterpart, the 3.9 dB Taylor windowed GoB does not performs better than 2dB or 1 dB for any percentile. This due to the fact that the it lost its orthogonal nature because of windowing. In-order to analyse all the GoB's and linear precoding techniques quantitatively, the 5th percentile SINR is compared and summarized in Table 4.7. The linear precoding techniques such as zero

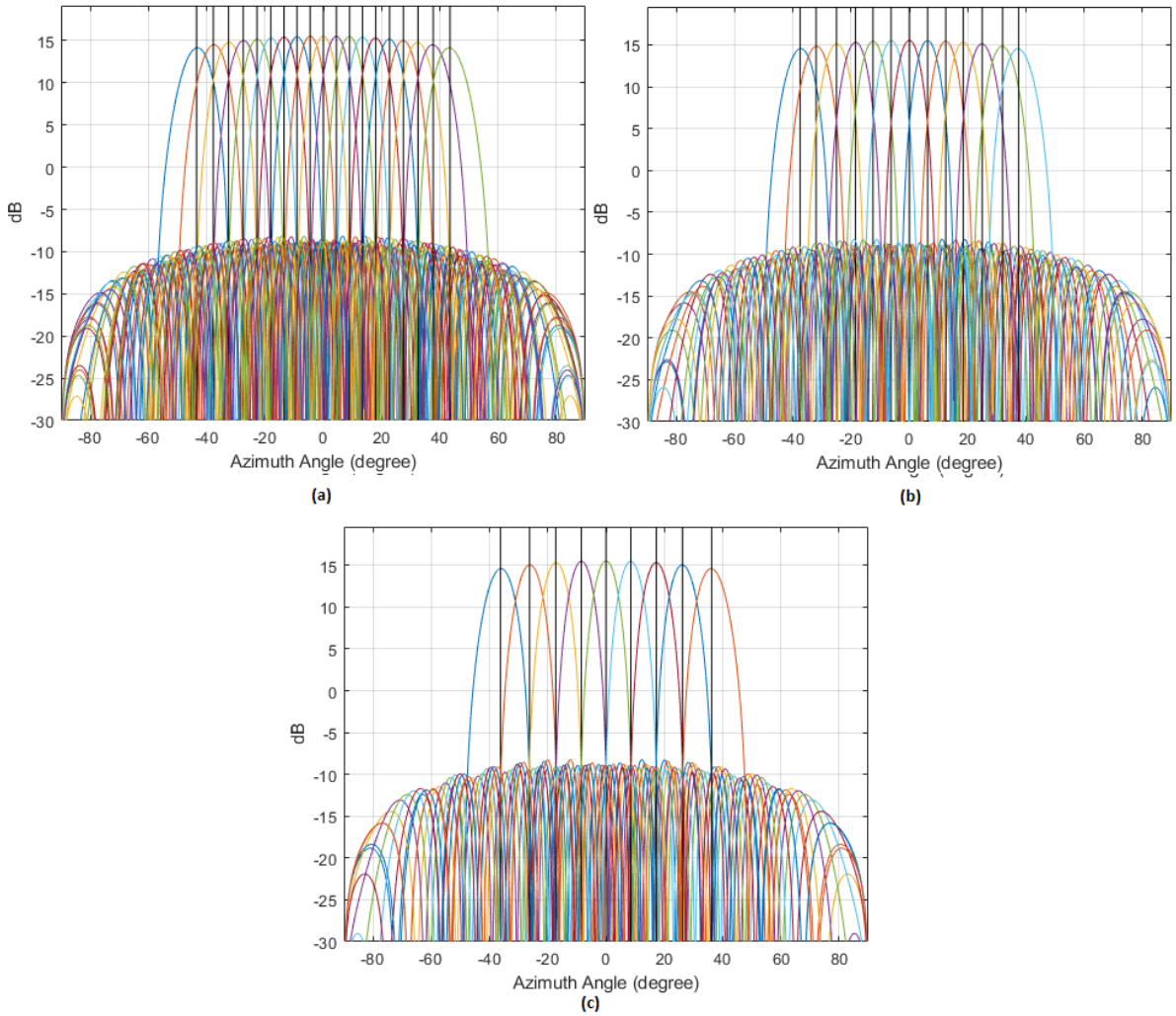


Figure 4.18: Antenna Grid of beam with-Taylor window for cross-over of (a) 1dB (b) 2dB (c) 3.9 dB

forcing (ZF) and Minimum mean square error (MMSE) yields the highest SINR at 5th percentile with 12.45 dB and 12.46 dB respectively. The 3.9 dB un-tapered GoB outperformed its amplitude tapered counterpart by 4.45 dB. The 2dB GoB both versions (i.e. with and without Taylor windowing) produce higher SINR then 3.9 dB GoB's and less than 1 dB GoB's all versions. The 1dB GoB with Taylor window amplitude distribution outperforms its un-tapered counterpart by a margin of 1.31 dB. Moreover among all the GoB techniques with and without Taylor amplitude distribution, the 1 dB GoB with tapering performance closest to linear precoding techniques of ZF and MMSE. The performance gap for 5th percentile SINR of 1 dB GoB's with amplitude tapering and linear precoding techniques of ZF and MMSE is about 1.82 dB.

### 4.3.2. Fully Connected Hybrid Beamforming

The previous sections discuss the subarray based hybrid beamforming techniques. This section deals with the implementation of fully connected hybrid beamforming technique using orthogonal matching pursuit algorithm (OMP) as described in previous chapter. The OMP algorithm would later be use as a performance bench mark for partially connected hybrid beamforming techniques in order to evaluate their performance.

#### 4.3.2.1. Orthogonal Matching Pursuit Algorithm (OMP)

As discussed in earlier chapter, the fully connected hybrid beamforming divides the spatial focussing of beam in analog and digital domain. The analog weights are applied the element level by using phase shifters and the digital weights are applied at sub-array level in baseband domain. The OMP algorithm is used for the

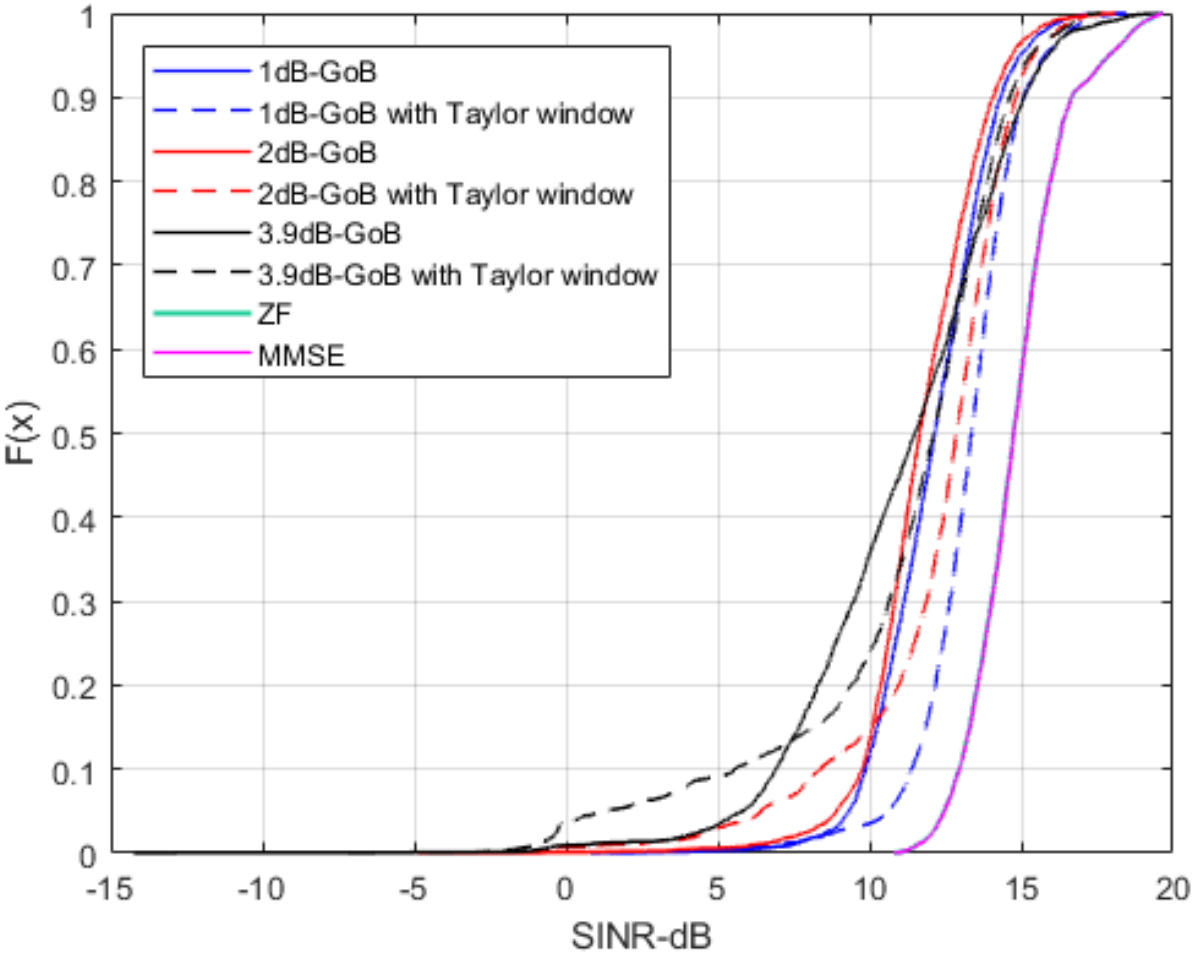


Figure 4.19: Cumulative distribution function of SINR using Grid of Beams, ZF and MMSE for 4 users with azimuth separation of at-least $1.2(\lambda/D)$

Table 4.7: 5th Percentile SINR in dB of various Grid of Beams, ZF and MMSE for 4 users with azimuth separation of at-least $1.2(\lambda/D)$

| **Beamforming Techniques** | $5^{th}$ **Percentile CDF-SINR in dB** |
|---|---|
| ZF | 12.45 |
| MMSE | 12.46 |
| 1dB GoB | 9.32 |
| 1dB GoB with Taylor window | 10.63 |
| 2dB GoB | 8.91 |
| 2dB GoB with Taylor window | 6.41 |
| 3.9dB GoB | 5.79 |
| 3.9dB GoB with Taylor window | 1.34 |

calculation of weighting vectors which are closest to the optimum weights. The model developed in the beginning of this chapter is used for the implementation of OMP. The number of users are considered to be 4 and are randomly distributed in the cell. Their inter-user separation is varied to analyse the impact of user spacing on signal to interference noise ratio (SINR). The Figure 4.20 presents the antenna directivity patterns

for a randomly selected Monte-Carlo user distribution from cell to depict the antenna beam patterns.

The cumulative distribution function of SINR against different user separations is plotted in Figure 4.21. It follows a very similar trend as we observed in the previous sections. The user separation $0.6(\lambda/D)$ performs worst among all with lowest SINR. It started off with smaller SINR value even less than 5 dB but converges to a SINR values of same as of higher user separation cases. As the user spacing increases further, the SINR also increases. However, this increase in SINR performances gets saturated or converges as the user spacing's are increases for any value $\lambda/D$ radians or beyond as can be seen in Figure 4.21. The SINR for all the user separations converges to similar value of about 26.2 dB.

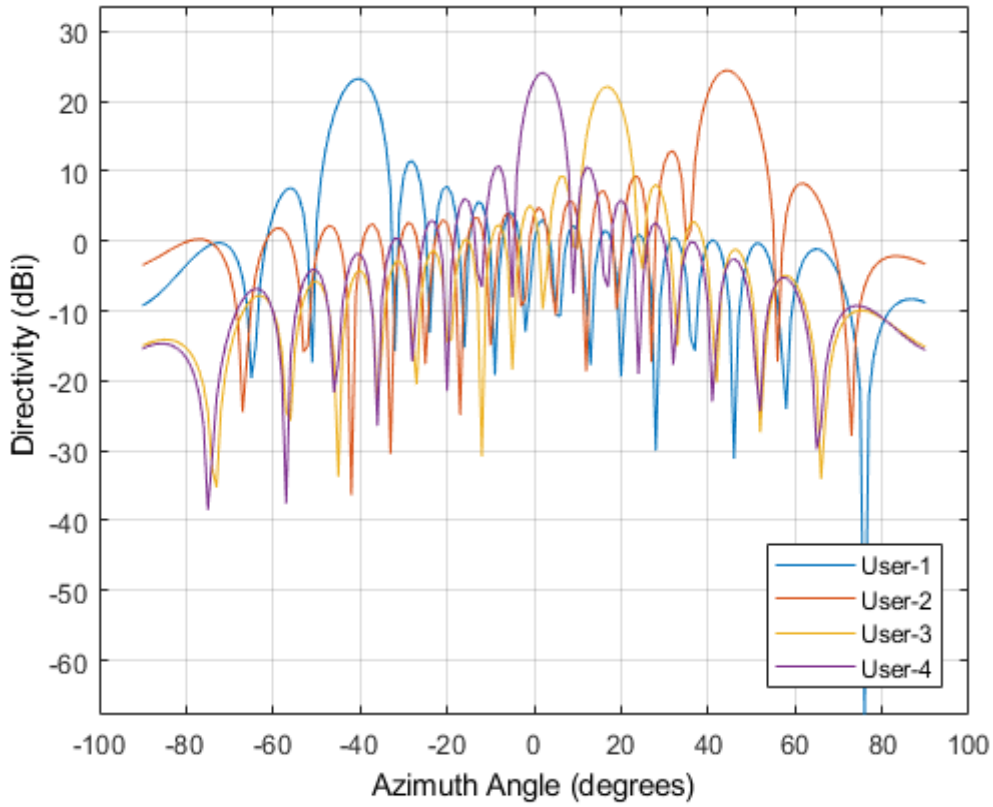


Figure 4.20: Azimuth cut with elevation 0 degrees for a sample 4-user distribution using Orthogonal Matching pursuit algorithm

## 4.4. Conclusion

In this chapter, a simulation model was developed to analyse the different well established beamforming techniques and their impact on service to the user of a communication system. First the impact of various antenna sidelobe levels on system performance was investigated using SINR values. Initially the SINR value improves as the sidelobe levels decreases upto -25 dB from mainlobe. However for any value below -25 dB from mainlobe, the SINR value reduces. So it was found out that the sidelobe level of 25dB down from mainlobe gives the optimum SINR performance among all other sidelobe levels for the system under taken. The newly proposed power equalization technique in the elevation plane using cosecant antenna pattern for 5G base stations was also implemented and studied using the developed model. Initially, the subarray based hybrid beamforming techniques were implemented and a thorough analysis via different simulation scenarios was performed to evaluate the impact of inter-user azimuth separation on system performance metrics such as SINR and BER. Thereafter, the fully connected hybrid beamforming technique using OMP algorithm is also implemented using the same model to serve as a performance benchmark for all the partially connected hybrid beamforming methods. The comparative analysis is performed among all the implemented beamforming techniques. Since during the previous simulations, it was observed that there is a very little increase in SINR performance of system for inter-user spacing's $1.2(\lambda/D)$ or beyond, therefore the comparison among

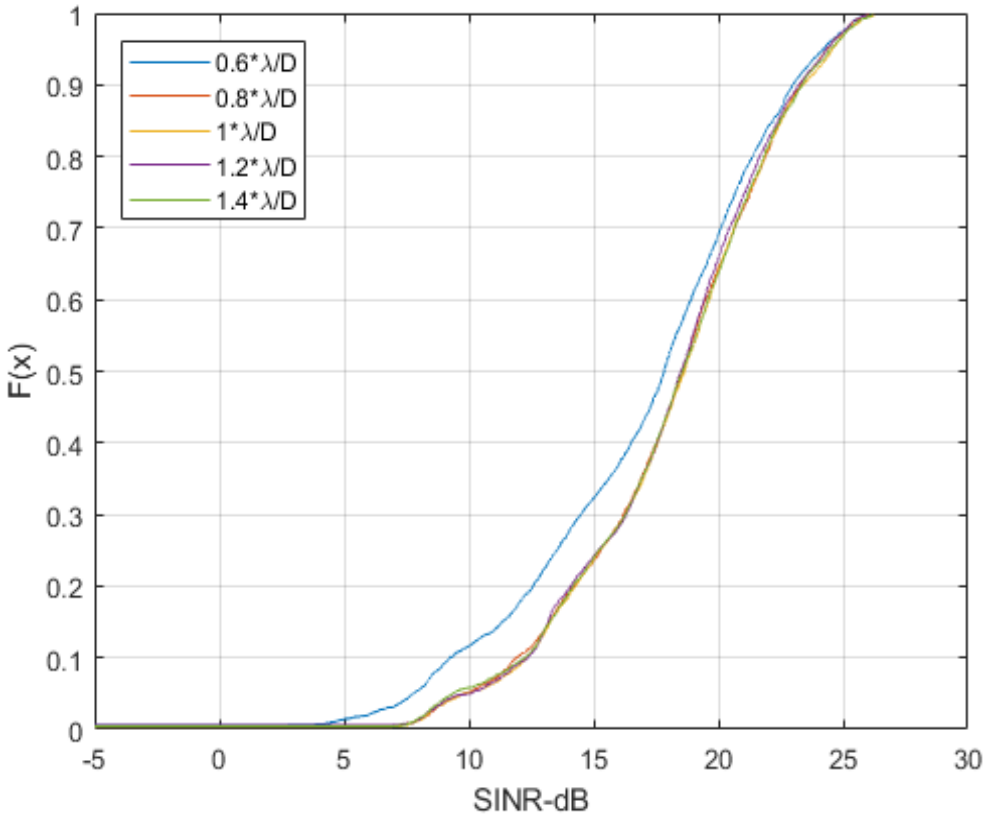


Figure 4.21: Azimuth cut with elevation 0 degrees for a sample 4-user distribution using Orthogonal Matching pursuit algorithm

subarray and fully connected beamforming was carried out for simulation using $1.2(\lambda/D)$ radians inter-user azimuth separation.

The cumulative distribution function of SINR for all the beamforming techniques is plotted in Figure 4.22. The fully connected hybrid beamforming using OMP algorithms outperform all other techniques in terms of overall SINR performance and converge to a very high value of 26.27 dB. The OMP is followed by the cosecant elevation scanning with ZF/MMSE, adaptive beam steering with amplitude tapering and 1 dB Grid of beam with Taylor window amplitude distribution. The uniform planar array without elevation scanning performs the worst among all and yielding the lowest SINR's. However, quite interesting results are seen when the $95^{th}$ percentile analyses was carried out to compare all the techniques quantitatively for a satisfactory cellular performance. The Table 4.8 presents the $5^{th}$ percentile CDF-SINR values for all the beamforming methods. It was observed that for $5^{th}$ percentile (i.e. 95% user coverage), all the cosecant beamforming methods performs better than OMP algorithm. The cosecant power distribution beamforming with zeroforcing (ZF) or minimum mean square error (MMSE) performs better among other cosecant scanning techniques, outperforming OMP by 2.45 dB in SINR matrix. The cosecant power distribution with amplitude tapered adaptive beamsteering has a SINR value 1.84 dB higher than OMP. The cosecant power distribution 1dB gird of beam with Taylor window amplitude tapering also performs better than OMP by a margin of 0.65 dB. This can be concluded that for the simulation scenario under taken, the cosecant power distribution in the elevation domain performs better than the conventional hybrid beamforming generation method using OMP for $5^{th}$ percentile SINR analysis.

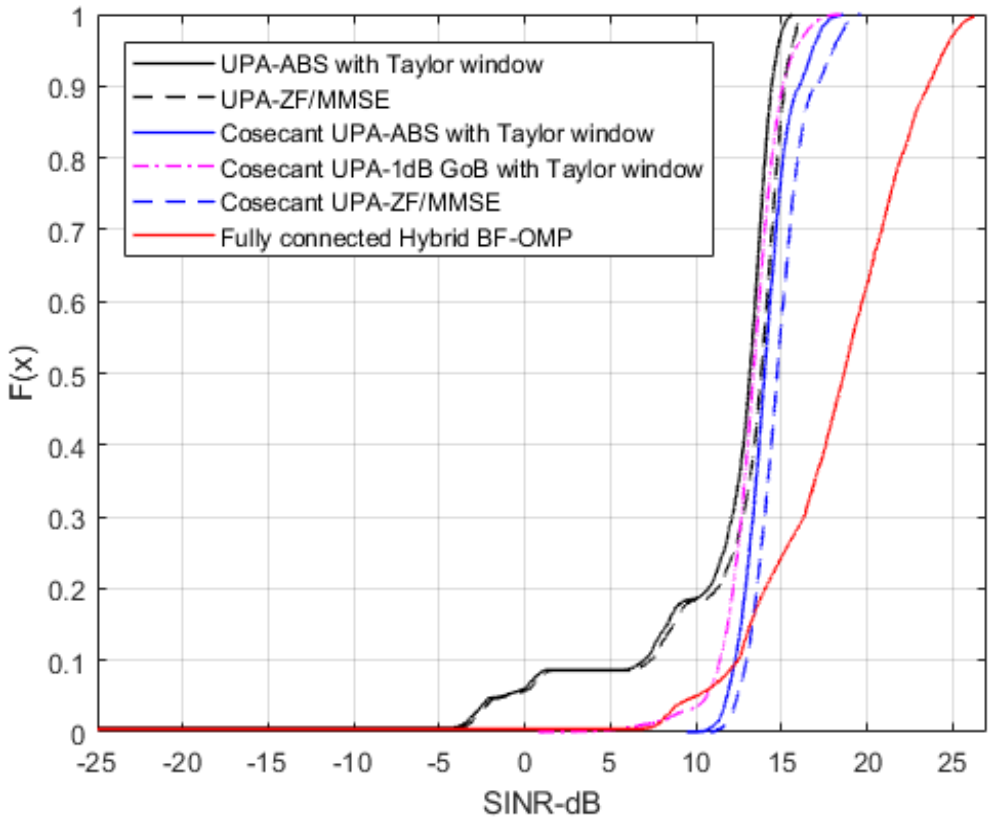


Figure 4.22: Cumulative distribution function of SINR using various beamforming techniques for randomly distributed users K=4 with azimuth separation of at-least 1.2($\lambda/D$) and a 16x12 uniform planar array at base station

Table 4.8: $5^{th}$ Percentile SINR in dB of various beamforming techniques for randomly distributed users K=4 with azimuth separation of at-least 1.2($\lambda/D$) and a 16x12 uniform planar array at base station

| **Beamforming Techniques** | $5^{th}$ **Percentile CDF-SINR in dB** |
|---|---|
| UPA-ABS with Taylor window | -1.32 |
| UPA-ZF/MMSE | -1.14 |
| Cosecant UPA-ABS with Taylor window | 11.82 |
| Cosecant UPA-1dB GoB with Taylor window | 10.63 |
| Cosecant UPA-ZF/MMSE | 12.43 |
| Fully connected Hybrid BF-OMP | 9.98 |

# 5

# Conclusions and Recommendations

## 5.1. Conclusions

The main goal of this thesis was to develop an adaptive system model for 5G mobile communication applications that is compatible with multiple beamforming topologies with different complexity levels and allows to understand the effect of the investigated beamforming approaches on the statistical system performance. Traditionally, antenna design which falls into the analog domain and system performance metrics such as BER and their analysis lying in the digital domain are dealt by hardware engineers and system designers as unconnected distinct disciplines. Therefore, the direct implication of antenna parameters (sidelobe level, beamwidth, directivity etc.) on system performance or viceversa is not intuitively visible. The developed model provides a novel approach that connects the user end performance metrics and RF frond-end technical requirements. The proposed system model enables derivation of antenna system and beamforming network design parameters from the performance requirement at the user end. To the author's knowledge for the first time, the impact of antenna sidelobe levels on overall system performance has been investigated and a detailed statistical analysis carried out to recommend a maximum allowable sidelobe power level for best possible performance for the system under study. The project was divided in to three parts: development of a detailed model for the up-coming 5G system with a large antenna array at the base station and multiple simultaneous single antenna users, verification of the system model and parametric analyses to provide conclusions/recommendations.

One of the major challenges faced in this research work was formulating a channel model and link budget that complies with the recently proposed hybrid cosecant beamforming concept. In addition to that, building a simulator that is adaptive to different application scenarios (in terms of number of users, user separation, number of antennas, position of antennas, beamforming algorithm to be used, base station height, cell range, PA output etc.) was also key issue that was addressed. The other challenge was in bridging the gap between different point of views and approaches of signal processing experts and antenna experts by combining the work of these different disciplines. In the end, the important step is to derive application-specific conclusions on base station antennas from the outcome of the channel modelling beamforming simulations.

The model was built on the philosophy of simultaneous multiple users in a cell using same frequency band of operation. The initial link budget parameters were taken from a project titled as "Advanced 5G Solutions - Antenna Topologies and Front-end Configurations for Multiple Beam Generation" supported by NXP semiconductors and NWO at Delft University of Technology (TU Delft). The system takes into account only a single dominant path between the base station and user equipment which is assumed to be Line of Sight (LoS), but can be modified to Non-LoS with a single strong multipath component with modified propagation loss. The geometric channel model was adopted for modelling millimetre wave 5G channel with a single communication path between base station and user equipment. Thereafter multiple beamforming techniques were implemented such as adaptive beam steering (ABS), zero forcing (ZF), minimum mean square error (MMSE), grid of beams and orthogonal matching pursuit (OMP). Before proceeding further with analyses, the credibility of the developed simulation model was determined by performing a verification analyses

using [24]. It was found out that the model is developed correctly and the results under the same input parameters as [24] produces similar output results.

Once the simulation model was developed, tested and verified; the system analysis was performed via Monte Carlo simulations. Since in 5G systems, requirements and implications of large antenna arrays (power consumption, heat dissipation, processing complexity, cost etc.) would play a crucial role in determining the overall systems performance, this thesis aims to bridge the gap between antenna technical design requirement and user performance metrics. Then newly proposed cosecant power distribution radiation pattern in the elevation domain [69] was also implemented and its impact was also studied on system using statistical analysis. A uniform linear array of 16-subarrays with 12 patch elements in each subarray was considered at the base station as it is being used in an on-going NXP semiconductors and NWO 5G project at TU Delft.

The impact of inter-user azimuth separation on overall system performance metrics such as SINR and BER was analysed in detail. This analyses enables derivation of the antenna system design parameters (number of elements, beamwidth, sidelobe level etc.). In addition to that, it would also allow the system management to get the idea for separating users in frequency domain when the severe SINR degradation occurs. The inter-user separation for user distribution in a cell is considered in terms of $\lambda/D$ radians where $\lambda$ is the wavelength and D is the aperture size of antenna array. Since the antenna design parameters such as beamwidth are described and derived in the form of wavelength ($\lambda$) and aperture size (D), therefore this analysis would directly relate minimum user separation for acceptable system performance and antenna system requirements for different beamforming techniques. The simulations were performed for various user inter-user separations such as $0.6(\lambda/D)$, $0.8(\lambda/D)$, $1(\lambda/D)$, $1.2(\lambda/D)$ and $1.4(\lambda/D)$ respectively. In addition to that, impact of other antenna related metrics such as sidelobe level, element excitation amplitudes and array directivity on system performance is also evaluated.

The antenna sidelobe level analysis was performed to determine the optimum sidelobe level which then can be implemented using a suitable amplitude distribution while synthesizing antenna arrays. It was observed that the performance of the particular system of interest improves as the sidelobe level reduces down to -25 dB as shown in Figure 4.5. Below that level, the system performance starts to degrade and gets worse as the sidelobe levels further go down. It was found out that as the sidelobe levels are further reduces, the beamwidth of the mainlobe increases and reaches up to a level where it starts interfering with the adjacent user signal. Thus, reducing the overall SINR performance of the system. Therefore, the sidelobe level of -25 dB was used for the rest of the analyses in the project when constant max. SLL approach was compared with the other beamforming techniques. In MIMO phased arrays, it is desirable to have all power amplifiers close to nominal power levels. The analysis shows that the Taylor window has a slightly lower power spread as compared to a Chebyshev window. Although the difference is not large and either of the windows can be used for analyses, it was decided to use Taylor window with $n = 10$ and sidelobe level of -25 dB for the rest of the thesis.

Initially the beamforming techniques were evaluated using uniformly-fed sub-array with patch elements and no optimized elevation beamforming. The analysis showed that the SINR and BER performance of the systems improves as the user separation increases. However, with inter-user spacing above $1.2(\lambda/D)$ radians, the SINR values starts to converge and remains almost the same. The SINR values for all user spacing's were found to be below 0 dB and the BER was approaching 0.5 for beamforming using uniformly-fed subarray. In addition, it was observed that amplitude tapering degrades the overall SINR and BER performance of the system. Thereafter, the analyses on cosecant subarray was performed. The cosecant elevation radiation pattern provides an equal distribution of power flux among users with respect to their distance from the base station which tends to equalize the data throughput. Similar system parameters were used to evaluate SINR and BER. The cosecant sub-array performs dramatically better than the uniformly fed sub-array by a margin of more than 12 dB for $5^{th}$ percentile SINR. The ZF and MMSE performs best among all the beamforming methods yielding highest SINR values for all user separations from $0.6(\lambda/D)$ radians to $1.4(\lambda/D)$ radians. The adaptive beamsteering performs better interms of SINR and BER for user separations $\lambda/D$ or beyond as shown in Figure 4.16(a) and 4.16(b). The adaptive beamsteering coupled with amplitude tapering performs even better and improves the overall SINR performance for user separations $1.2(\lambda/D)$ or beyond by more than 1.5 dB as compared to only adaptive beamsteering for $5^{th}$ percentile.

The grid of beams (GoB) analyses was also carried out using the cosecant- square elevation power distri-

bution. Various grids of beams were created using different cross over points between adjacent beams such as 1 dB, 2dB and 3.9 dB down from peak. The grid of beams with amplitude distribution was also created to evaluate its impact on SINR. The ZF and MMSE SINR are used as a reference comparison for all GoB performance evaluation. The 1 dB GoB with taylor window amplitude distribution perfoms best among all other GoB's with or without amplitude tapering. The $5^{th}$ percentile CDF SINR values as presented in Table4.7 shows that the 1 dB GoB with Taylor window amplitude distribution came close to ZF/MMSE precoding but its SINR remains 1.82 dB less.

In the end, fully connected hybrid beamforming is implemented using orthogonal matching pursuit (OMP) algorithm which uses a phase shifter and adder behind each element in an array. The OMP technique is used to used as the bench mark for systems SINR performance with which all other beamforming techniques are compared. The CDF of SINR for all the best performing beamforming combinations among all analyses is plotted in Figure 4.22 with OMP algorithm SINR. It was observed that in terms of overall SINR value, the OMP algorithm converges to a higher value of SINR i.e. 26.2 dB. However for $5^{th}$ percentile SINR (i.e. SINR for 95% of users in cell), the cosecant elevation power distribution using ZF/MMSE, ABS with amplitude tapering and 1 dB GoB also with amplitude tapering outperforms OMP by a margin of 2.45 dB, 1.84 dB and 0.65 dB respectively.

The analyses performed in this thesis project resulted in some insightful conclusions. Since the user density in a cell has a profound impact on the overall system performance, it has to be taken account while designing the antenna system and beamforming networks so that the system performance goals can be achieved. Every beamforming technique's performance varies with the number of users and their azimuth separation. For instance, the linear precoding techniques such as ZF and MMSE perform equally well for all analysed user separations from $0.6(\lambda/D)$ radians to $1.4(\lambda/D)$ radians in terms of SINR. However, for the cosecant power distribution with constant sidelobe levels SINR performance approaches that of linear precoding techniques for minimum inter user azimuth separations above $1.2(\lambda/D)$ radians. This allows smart system management i.e. to select appropriate linear precoding technique with respect to inter-user separation to achieve desired system performance. Moreover, ZF and MMSE require prior channel matrix knowledge and computationally extensive operations such as channel matrix inversion for beamforming weights evaluation. In addition to that, the fully connected hybrid beamforming using OMP algorithm employs an adder and phase shifter behind each antenna element. For larger arrays, as that would be the case for 5G systems; this can be very complex to implement in terms of cost and power consumption of the system. Therefore cosecant power distribution in elevation plane offers an attractive alternative for achieving high SINR performance at low complexity. So a system with minimum user separation of $1.2(\lambda/D)$ radians by using cosecant power distribution in elevation with taylor window tapering can be created, which would give SINR values approaching ZF/MMSE based systems (of about 1.5 dB less after statistical analysis in the system that was considered for this thesis). In addition to that, this simulation model also proves to be a tool to check, analyse and verify the impact of different antenna systems and beamforming topologies on system performance. Therefore, the guidelines for beamforming topology selection and antenna system design for mulitbeam generation system such as 5G (for single dominant path) can be derived by using this simulation model.

## 5.2. Recommendations

In this thesis work, the simulation model for multibeam generation using different beamforming techniques particularly for 5G was developed. The model was takes into account only single dominant path or line of sight (Los) path per user in the propagation channel modelling. In addition to that, the signal was considered to be narrow band as the individual carriers in orthogonal frequency division multiplexing (OFDM) are narrow band. The quantization effect is also not considered in this research work. Therefore, the following areas can be explored for future work:

- The Channel model can be constructed and use to take into account non-line of sight paths and effect of multipath propagation system performance.
- The performance of beamforming algorithms for wideband signals.
- The impact of signal quantization and quantization errors on overall system performance.
- The effect of adjacent cell base station interference on the intended user performance.

# Bibliography


[1] "5G: A Technology Vision". Report, Huawei Technologies, 2013. URL https://www.huawei.com/ilink/en/download/HW_314849.

[2] "Cisco visual networking index: Forecast and methodology, 20131–2018". White paper, Cisco, 2014. URL http://www.anatel.org.mx/docs/interes/Cisco_VNI_Forecast_and_Methodology.pdf.

[3] "IMT-2020(5G)PG". Report, Promotion Group, 2016. URL http://www.wwrf.ch/files/wwrf/content/files/5GHuddles/2ndhuddle/Ming%20Lei%20Presentation.pdf.

[4] W. B. Abbas and M. Zorzi. "Towards an Appropriate Receiver Beamforming Scheme for Millimeter Wave Communication: A Power Consumption Based Comparison". In *European Wireless 2016; 22th European Wireless Conference*, pages 1–6, May 2016.

[5] A. Acampora. "Digital error rate performance of active phased array satellite systems". *IEEE Transactions on Antennas and Propagation*, 26(6):833–842, Nov 1978. ISSN 0018-926X. doi: 10.1109/TAP.1978.1141951.

[6] W. Aerts, P. Delmotte, and G. A. E. Vandenbosch. "Conceptual Study of Analog Baseband Beam Forming: Design and Measurement of an Eight-by-Eight Phased Array". *IEEE Transactions on Antennas and Propagation*, 57(6):1667–1672, June 2009. ISSN 0018-926X. doi: 10.1109/TAP.2009.2016716.

[7] M. Agiwal, A. Roy, and N. Saxena. "Next Generation 5G Wireless Networks: A Comprehensive Survey". *IEEE Communications Surveys Tutorials*, 18(3):1617–1655, thirdquarter 2016. ISSN 1553-877X. doi: 10.1109/COMST.2016.2532458.

[8] I. Ahmed, H. Khammari, A. Shahid, A. Musa, K. S. Kim, E. De Poorter, and I. Moerman. "A Survey on Hybrid Beamforming Techniques in 5G: Architecture and System Model Perspectives". *IEEE Communications Surveys Tutorials*, pages 1–1, 2018. doi: 10.1109/COMST.2018.2843719.

[9] A. Alkhateeb, O. El Ayach, G. Leus, and R. W. Heath. "Hybrid precoding for millimeter wave cellular systems with partial channel knowledge". In *2013 Information Theory and Applications Workshop (ITA)*, pages 1–5, Feb 2013. doi: 10.1109/ITA.2013.6522603.

[10] A. Alkhateeb, G. Leus, and R. W. Heath. "Limited Feedback Hybrid Precoding for Multi-User Millimeter Wave Systems". *IEEE Transactions on Wireless Communications*, 14(11):6481–6494, Nov 2015. ISSN 1536-1276. doi: 10.1109/TWC.2015.2455980.

[11] P. V. Amadori and C. Masouros. "Low RF-Complexity Millimeter-Wave Beamspace-MIMO Systems by Beam Selection". *IEEE Transactions on Communications*, 63(6):2212–2223, June 2015. ISSN 0090-6778. doi: 10.1109/TCOMM.2015.2431266.

[12] N. Amani, C. Bencivenni, A. A. Glazunov, M. V. Ivashina, and R. Maaskant. "MIMO channel capacity gains in mm-wave LOS systems with irregular sparse array antennas". In *2017 IEEE-APS Topical Conference on Antennas and Propagation in Wireless Communications (APWC)*, pages 264–265, Sept 2017. doi: 10.1109/APWC.2017.8062297.

[13] N. Amani, R. Maaskant, A. A. Glazunov, and M. Ivashina. "Network model of a 5G MIMO base station antenna in a downlink multi-user scenario". *to be published in Proc. 12th EuCAP*, April 2018.

[14] J. G. Andrews, S. Buzzi, W. Choi, S. V. Hanly, A. Lozano, A. C. K. Soong, and J. C. Zhang. "What Will 5G Be?". *IEEE Journal on Selected Areas in Communications*, 32(6):1065–1082, June 2014. ISSN 0733-8716. doi: 10.1109/JSAC.2014.2328098.

[15] Y. Aslan, J. Puskely, A. Roederer, and A. Yarovoy. "Synthesis of multiple beam linear arrays with uniform amplitudes". *to be published in Proc. 12th EuCAP*, April 2018.

[16] Y. Aslan, J. Puskely, A. Roederer, and A. Yarovoy. "Heat transfer enhancement in passively cooled 5G base station antennas using thick ground planes". *submitted for publication in Proc. 13th EuCAP*, April 2019.

[17] Y. Aslan, J. Puskely, J. H. J. Janssen, M. Geurts, A. Roederer, and A. Yarovoy. "Thermal-aware synthesis of 5G base station antenna arrays via layout sparsity". *IEEE Access*, submitted for publication.

[18] Y. Aslan, J. Puskely, A. Roederer, and A. Yarovoy. "Thermal-aware multiple beam synthesis of 5G planar arrays using convex optimization". *IEEE Transactions on Antennas and Propagation*, submitted for publication.

[19] O. E. Ayach, S. Rajagopal, S. Abu-Surra, Z. Pi, and R. W. Heath. "Spatially Sparse Precoding in Millimeter Wave MIMO Systems". *IEEE Transactions on Wireless Communications*, 13(3):1499–1513, March 2014. ISSN 1536-1276. doi: 10.1109/TWC.2014.011714.130846.

[20] B. Bangerter, S. Talwar, R. Arefi, and K. Stewart. "Networks and devices for the 5G era". *IEEE Communications Magazine*, 52(2):90–96, February 2014. ISSN 0163-6804. doi: 10.1109/MCOM.2014.6736748.

[21] C. Bencivenni. *"Aperiodic array synthesis for telecommunications"*. PhD thesis, Chalmers University of Engineering and Technology, Gothenburg, Sweden, 2017.

[22] C. Bencivenni, A. A. Glazunov, R. Maaskant, and M. V. Ivashina. "Effects of regular and aperiodic array layout in multi-user MIMO applications". In *2017 IEEE International Symposium on Antennas and Propagation USNC/URSI National Radio Science Meeting*, pages 1877–1878, July 2017. doi: 10.1109/APUSNCURSINRSM.2017.8072981.

[23] E. Bjornson, E. G. Larsson, and T. L. Marzetta. Massive mimo: ten myths and one critical question. *IEEE Communications Magazine*, 54(2):114–123, February 2016. ISSN 0163-6804. doi: 10.1109/MCOM.2016.7402270.

[24] E. Bjrnson, M. Bengtsson, and B. Ottersten. "Optimal Multiuser Transmit Beamforming: A Difficult Problem with a Simple Solution Structure [Lecture Notes]". *IEEE Signal Processing Magazine*, 31(4):142–148, July 2014. ISSN 1053-5888. doi: 10.1109/MSP.2014.2312183.

[25] F. Boccardi, R. W. Heath, A. Lozano, T. L. Marzetta, and P. Popovski. "Five disruptive technology directions for 5G". *IEEE Communications Magazine*, 52(2):74–80, February 2014. ISSN 0163-6804. doi: 10.1109/MCOM.2014.6736746.

[26] J. Brady, N. Behdad, and A. M. Sayeed. "Beamspace MIMO for Millimeter-Wave Communications: System Architecture, Modeling, Analysis, and Measurements". *IEEE Transactions on Antennas and Propagation*, 61(7):3814–3827, July 2013. ISSN 0018-926X. doi: 10.1109/TAP.2013.2254442.

[27] K. Chandra. *"Towards realizing 5G: Efficient medium access and beamwidth adaptation in 60 GHz communications"*. PhD thesis, Delft University of Engineering and Technology, Delft, The Netherlands, 2017.

[28] K. Chandra, R. V. Prasad, I. G. M. M. Niemegeers, and A. R. Biswas. "Adaptive beamwidth selection for contention based access periods in millimeter wave WLANs". In *2014 IEEE 11th Consumer Communications and Networking Conference (CCNC)*, pages 458–464, Jan 2014. doi: 10.1109/CCNC.2014.6866610.

[29] K. Chandra, A. Doff, Z. Cao, R. V. Prasad, and I. Niemegeers. "60 GHz MAC standardization: Progress and way forward". In *2015 12th Annual IEEE Consumer Communications and Networking Conference (CCNC)*, pages 182–187, Jan 2015. doi: 10.1109/CCNC.2015.7157974.

[30] P. Chen, W. Hong, H. Zhang, J. Chen, H. Tang, and Z. Chen. "Virtual Phase Shifter Array and Its Application on Ku Band Mobile Satellite Reception". *IEEE Transactions on Antennas and Propagation*, 63(4):1408–1416, April 2015. ISSN 0018-926X. doi: 10.1109/TAP.2015.2393887.

[31] S. Chen and J. Zhao. "The requirements, challenges, and technologies for 5G of terrestrial mobile telecommunication". *IEEE Communications Magazine*, 52(5):36–43, May 2014. ISSN 0163-6804. doi: 10.1109/MCOM.2014.6815891.

[32] E. Dahlman, G. Mildh, S. Parkvall, J. Peisa, J. Sachs, Y. Sel and J. Skld. "5G wireless access: requirements and realization". *IEEE Communications Magazine*, 52(12):42–47, December 2014. ISSN 0163-6804. doi: 10.1109/MCOM.2014.6979985.

[33] V. Degli-Esposti, F. Fuschini, E. M. Vitucci, M. Barbiroli, M. Zoli, L. Tian, X. Yin, D. A. Dupleich, R. Mller, C. Schneider, and R. S. Thom"Ray-Tracing-Based mm-Wave Beamforming Assessment". *IEEE Access*, 2: 1314–1325, 2014. doi: 10.1109/ACCESS.2014.2365991.

[34] S. Dutta, C. N. Barati, A. Dhananjay, and S. Rangan. "5G millimeter wave cellular system capacity with fully digital beamforming". In *2017 51st Asilomar Conference on Signals, Systems, and Computers*, pages 1224–1228, Oct 2017. doi: 10.1109/ACSSC.2017.8335546.

[35] Ali Ehab, Ismail Mahamod, Nordin Rosdiadee, and Abdulah Nor Fadzilah. "Beamforming techniques for massive MIMO systems in 5G: overview, classification, and trends for future research". *Frontiers of Information Technology & Electronic Engineering*, 18(6):753–772, June 2017. ISSN 2095-9230. doi: 10.1631/FITEE.1601817.

[36] E. P. Ekelman, E. C. Kohls, A. I. Zaghfoul, and F. T. Assal. "Measured performance of a Ku-band multi-beam high-power phased-array". In *Proceedings of IEEE Antennas and Propagation Society International Symposium and URSI National Radio Science Meeting*, volume 2, pages 852–855 vol.2, June 1994. doi: 10.1109/APS.1994.407931.

[37] A. Forenza, D. J. Love, and R. W. Heath. "Simplified Spatial Correlation Models for Clustered MIMO Channels With Different Array Configurations". *IEEE Transactions on Vehicular Technology*, 56(4):1924–1934, July 2007. ISSN 0018-9545. doi: 10.1109/TVT.2007.897212.

[38] X. Ge, R. Zi, H. Wang, J. Zhang, and M. Jo. "Multi-User Massive MIMO Communication Systems Based on Irregular Antenna Arrays". *IEEE Transactions on Wireless Communications*, 15(8):5287–5301, Aug 2016. ISSN 1536-1276. doi: 10.1109/TWC.2016.2555911.

[39] Marco Giordani, Marco Mezzavilla, Aditya Dhananjay, Sundeep Rangan, and Michele Zorzi. "Channel Dynamics and SNR Tracking in Millimeter Wave Cellular Systems". *CoRR*, abs/1604.05623, 2016. URL `http://arxiv.org/abs/1604.05623`.

[40] Godara. "Applications Of Antenna Arrays To Mobile Communications, Part I: Performance Improvement, Feasibility, And System Considerations". *Proceedings of the IEEE*, 85(7):1029–1030, July 1997. ISSN 0018-9219. doi: 10.1109/JPROC.1997.611114.

[41] A. Goldsmith, S. A. Jafar, N. Jindal, and S. Vishwanath. "Capacity limits of MIMO channels". *IEEE Journal on Selected Areas in Communications*, 21(5):684–702, June 2003. ISSN 0733-8716. doi: 10.1109/JSAC.2003.810294.

[42] Andrea Goldsmith. *Wireless Communications*. Cambridge University Press, UK, 2005.

[43] G. Gottardi, G. Oliveri, and A. Massa. "New antenna design concept for future generation wireless communication systems". *to be published in Proc. 12th EuCAP*, April 2018.

[44] Xiang Guan, H. Hashemi, and A. Hajimiri. "A fully integrated 24-GHz eight-element phased-array receiver in silicon". *IEEE Journal of Solid-State Circuits*, 39(12):2311–2320, Dec 2004. ISSN 0018-9200. doi: 10.1109/JSSC.2004.836339.

[45] A. Gupta and R. K. Jha. "A Survey of 5G Network: Architecture and Emerging Technologies". *IEEE Access*, 3:1206–1232, 2015. doi: 10.1109/ACCESS.2015.2461602.

[46] P. S. Hall and S. J. Vetterlein. "Review of radio frequency beamforming techniques for scanned and multiple beam antennas". *IEE Proceedings H - Microwaves, Antennas and Propagation*, 137(5):293–303, Oct 1990. ISSN 0950-107X. doi: 10.1049/ip-h-2.1990.0055.

[47] S. Han, C. l. I, Z. Xu, and C. Rowell. "Large-scale antenna systems with hybrid analog and digital beamforming for millimeter wave 5G". *IEEE Communications Magazine*, 53(1):186–194, January 2015. ISSN 0163-6804. doi: 10.1109/MCOM.2015.7010533.

[48] R. C. Hansen. *Phased Array Antennas*. Wiley, USA, 1998.

[49] H. Hashemi, Xiang Guan, A. Komijani, and A. Hajimiri. "A 24-GHz SiGe phased-array receiver-LO phase-shifting approach". *IEEE Transactions on Microwave Theory and Techniques*, 53(2):614–626, Feb 2005. ISSN 0018-9480. doi: 10.1109/TMTT.2004.841218.

[50] F. Hillebrand. "The creation of standards for global mobile communication: GSM and UMTS standardization from 1982 to 2000". *IEEE Wireless Communications*, 20(5):24–33, October 2013. ISSN 1536-1284. doi: 10.1109/MWC.2013.6664470.

[51] W. Hong, Z. H. Jiang, C. Yu, J. Zhou, P. Chen, Z. Yu, H. Zhang, B. Yang, X. Pang, M. Jiang, Y. Cheng, M. K. T. Al-Nuaimi, Y. Zhang, J. Chen, and S. He. "Multibeam Antenna Technologies for 5G Wireless Communications". *IEEE Transactions on Antennas and Propagation*, 65(12):6231–6249, Dec 2017. ISSN 0018-926X. doi: 10.1109/TAP.2017.2712819.

[52] A. Jain. "Multibeam synthetic aperture radar for global oceanography". *IEEE Transactions on Antennas and Propagation*, 27(4):535–538, Jul 1979. ISSN 0018-926X. doi: 10.1109/TAP.1979.1142135.

[53] S. Jeon, Y. J. Wang, H. Wang, F. Bohn, A. Natarajan, A. Babakhani, and A. Hajimiri. "A Scalable 6-to-18 GHz Concurrent Dual-Band Quad-Beam Phased-Array Receiver in CMOS". *IEEE Journal of Solid-State Circuits*, 43(12):2660–2673, Dec 2008. ISSN 0018-9200. doi: 10.1109/JSSC.2008.2004863.

[54] M. Ju, J. Qian, Y. Li, G. Tan, and X. Li. "Comparison of multiuser MIMO systems with MF, ZF and MMSE receivers". In *2013 IEEE Third International Conference on Information Science and Technology (ICIST)*, pages 1260–1263, March 2013. doi: 10.1109/ICIST.2013.6747766.

[55] S. Khademi, E. DeCorte, G. Leus, and A. J. van der Veen. "Convex optimization for joint zero-forcing and antenna selection in multiuser MISO systems". In *2014 IEEE 15th International Workshop on Signal Processing Advances in Wireless Communications (SPAWC)*, pages 30–34, June 2014. doi: 10.1109/SPAWC.2014.6941311.

[56] F. Khan, Z. Pi, and S. Rajagopal. "Millimeter-wave mobile broadband with large scale spatial processing for 5G mobile communication". In *2012 50th Annual Allerton Conference on Communication, Control, and Computing (Allerton)*, pages 1517–1523, Oct 2012. doi: 10.1109/Allerton.2012.6483399.

[57] Taeyoung Kim, Jeongho Park, Ji-Yun Seol, Suryong Jeong, Jaeweon Cho, and Wonil Roh. "Tens of Gbps support with mmWave beamforming systems for next generation communications". In *2013 IEEE Global Communications Conference (GLOBECOM)*, pages 3685–3690, Dec 2013. doi: 10.1109/GLOCOM.2013.6831646.

[58] S. Kutty and D. Sen. "Beamforming for Millimeter Wave Communications: An Inclusive Survey". *IEEE Communications Surveys Tutorials*, 18(2):949–973, Secondquarter 2016. ISSN 1553-877X. doi: 10.1109/COMST.2015.2504600.

[59] E. G. Larsson, O. Edfors, F. Tufvesson, and T. L. Marzetta. "Massive MIMO for next generation wireless systems". *IEEE Communications Magazine*, 52(2):186–195, February 2014. ISSN 0163-6804. doi: 10.1109/MCOM.2014.6736761.

[60] Byung Moo Lee and Youngok Kim. "Zero-forcing and codebook based beamforming scheme for practical usage of multiuser MIMO-OFDM with uplink channel sounding". *Int. J. Commun. Syst.*, 30, Dec 2014. doi: 10.1002/dac.2918.

[61] E. Lier and R. Melcher. "A Modular and Lightweight Multibeam Active Phased Receiving Array for Satellite Applications: Design and Ground Testing". *IEEE Antennas and Propagation Magazine*, 51(1):80–90, Feb 2009. ISSN 1045-9243. doi: 10.1109/MAP.2009.4939021.

[62] T. L. Marzetta. "Noncooperative Cellular Wireless with Unlimited Numbers of Base Station Antennas". *IEEE Transactions on Wireless Communications*, 9(11):3590–3600, November 2010. ISSN 1536-1276. doi: 10.1109/TWC.2010.092810.091092.

[63] Hien Quoc Ngo. *"Massive MIMO: Fundamentals and System Designs"*. PhD thesis, Linkoping university, Linkoping, Sweden, 2015.

[64] A. Osseiran, F. Boccardi, V. Braun, K. Kusume, P. Marsch, M. Maternia, O. Queseth, M. Schellmann, H. Schotten, H. Taoka, H. Tullberg, M. A. Uusitalo, B. Timus, and M. Fallgren. "Scenarios for 5G mobile and wireless communications: the vision of the METIS project". *IEEE Communications Magazine*, 52(5):26–35, May 2014. ISSN 0163-6804. doi: 10.1109/MCOM.2014.6815890.

[65] D. P. Palomar, J. M. Cioffi, and M. A. Lagunas. Joint tx-rx beamforming design for multicarrier mimo channels: a unified framework for convex optimization. *IEEE Transactions on Signal Processing*, 51(9): 2381–2401, Sept 2003. ISSN 1053-587X. doi: 10.1109/TSP.2003.815393.

[66] Z. Pi and F. Khan. "An introduction to millimeter-wave mobile broadband systems". *IEEE Communications Magazine*, 49(6):101–107, June 2011. ISSN 0163-6804. doi: 10.1109/MCOM.2011.5783993.

[67] Z. Pi and F. Khan. "An introduction to millimeter-wave mobile broadband systems". *IEEE Communications Magazine*, 49(6):101–107, June 2011. ISSN 0163-6804. doi: 10.1109/MCOM.2011.5783993.

[68] D. M. Pozar. *Microwave Engineering*. Wiley, USA, 2005.

[69] J. Puskely, Y. Aslan, A. Roederer, and A. Yarovoy. "SIW based antenna array with power equalization in elevation plane for 5G base stations". *to be published in Proc. 12th EuCAP*, April 2018.

[70] Z. Qingling and J. Li. "Rain Attenuation in Millimeter Wave Ranges". In *2006 7th International Symposium on Antennas, Propagation EM Theory*, pages 1–4, Oct 2006. doi: 10.1109/ISAPE.2006.353538.

[71] T. S. Rappaport, J. N. Murdock, and F. Gutierrez. "State of the Art in 60-GHz Integrated Circuits and Systems for Wireless Communications". *Proceedings of the IEEE*, 99(8):1390–1436, Aug 2011. ISSN 0018-9219. doi: 10.1109/JPROC.2011.2143650.

[72] T. S. Rappaport, S. Sun, R. Mayzus, H. Zhao, Y. Azar, K. Wang, G. N. Wong, J. K. Schulz, M. Samimi, and F. Gutierrez. "Millimeter Wave Mobile Communications for 5G Cellular: It Will Work!". *IEEE Access*, 1: 335–349, 2013. doi: 10.1109/ACCESS.2013.2260813.

[73] T. S. Rappaport, W. Roh, and K. Cheun. "Mobile's millimeter-wave makeover". *IEEE Spectrum*, 51(9): 34–58, Sept 2014. ISSN 0018-9235. doi: 10.1109/MSPEC.2014.6882985.

[74] T. S. Rappaport, Y. Xing, G. R. MacCartney, A. F. Molisch, E. Mellios, and J. Zhang. "Overview of Millimeter Wave Communications for Fifth-Generation (5G) Wireless Networks With a Focus on Propagation Models". *IEEE Transactions on Antennas and Propagation*, 65(12):6213–6230, Dec 2017. ISSN 0018-926X. doi: 10.1109/TAP.2017.2734243.

[75] Theodore S. Rappaport. *Wireless Communications: Principles and Practice*. Prentice Hall, USA, 2002.

[76] W. Roh, J. Y. Seol, J. Park, B. Lee, J. Lee, Y. Kim, J. Cho, K. Cheun, and F. Aryanfar. "Millimeter-wave beamforming as an enabling technology for 5G cellular communications: theoretical feasibility and prototype results". *IEEE Communications Magazine*, 52(2):106–113, February 2014. ISSN 0163-6804. doi: 10.1109/MCOM.2014.6736750.

[77] K. Roth, H. Pirzadeh, A. L. Swindlehurst, and J. A. Nossek. "A Comparison of Hybrid Beamforming and Digital Beamforming With Low-Resolution ADCs for Multiple Users and Imperfect CSI". *IEEE Journal of Selected Topics in Signal Processing*, 12(3):484–498, June 2018. ISSN 1932-4553. doi: 10.1109/JSTSP.2018.2813973.

[78] Antoine Roze, Maryline Hélard, Matthieu Crussière, and Charlotte Langlais. "Millimeter-Wave Digital Beamsteering in Highly Line-Of-Sight Environments for Massive MIMO Systems". In *WWWRF35 Meeting*, Copenhague, Denmark, October 2015. URL `https://hal-univ-rennes1.archives-ouvertes.fr/hal-01252090`.

[79] F. Rusek, D. Persson, B. K. Lau, E. G. Larsson, T. L. Marzetta, O. Edfors, and F. Tufvesson. Scaling up mimo: Opportunities and challenges with very large arrays. *IEEE Signal Processing Magazine*, 30(1):40–60, Jan 2013. ISSN 1053-5888. doi: 10.1109/MSP.2011.2178495.

[80] S. Singh, R. Mudumbai, and U. Madhow. "Interference Analysis for Highly Directional 60-GHz Mesh Networks: The Case for Rethinking Medium Access Control". *IEEE/ACM Transactions on Networking*, 19 (5):1513–1527, Oct 2011. ISSN 1063-6692. doi: 10.1109/TNET.2011.2122343.

[81] P. F. M. Smulders and L. M. Correia. "Characterisation of propagation in 60 GHz radio channels". *Electronics Communication Engineering Journal*, 9(2):73–80, Apr 1997. ISSN 0954-0695. doi: 10.1049/ecej:19970204.

[82] F. Sohrabi and W. Yu. "Hybrid Digital and Analog Beamforming Design for Large-Scale Antenna Arrays". *IEEE Journal of Selected Topics in Signal Processing*, 10(3):501–513, April 2016. ISSN 1932-4553. doi: 10.1109/JSTSP.2016.2520912.

[83] S.Salman, Y.Aslan, J.Puskely, A.Roederer, and A. Yarovoy. "System Modelling and Simulation in 5G: A Hybrid Beamforming Approach With Power Flux Equalization in the Elevation Plane". *IEEE Transaction*, To be submitted.

[84] William Stallings. *Data and Computer Communications*. Prentice Hall, USA, 2006.

[85] F. W. Vook, A. Ghosh, and T. A. Thomas. "MIMO and beamforming solutions for 5G technology". In *2014 IEEE MTT-S International Microwave Symposium (IMS2014)*, pages 1–4, June 2014. doi: 10.1109/MWSYM.2014.6848613.

[86] P. Wongchampa and M. Uthansakul. "Orthogonal Beamforming for Multiuser Wireless Communications: Achieving higher received signal strength and throughput than with conventional beamforming". *IEEE Antennas and Propagation Magazine*, 59(4):38–49, Aug 2017. ISSN 1045-9243. doi: 10.1109/MAP.2017.2706668.

[87] Hao Xu, V. Kukshya, and T. S. Rappaport. "Spatial and temporal characteristics of 60-GHz indoor channels". *IEEE Journal on Selected Areas in Communications*, 20(3):620–630, Apr 2002. ISSN 0733-8716. doi: 10.1109/49.995521.

[88] A. I. Zaghloul, Y. Hwang, R. M. Sorbello, and F. T. Assal. "Advances in multibeam communications satellite antennas". *Proceedings of the IEEE*, 78(7):1214–1232, Jul 1990. ISSN 0018-9219. doi: 10.1109/5.56934.